EIGHTEEN MONTH REPORT

ON

CONTRACT PH-43-67-1136

by

J. W. Melvin, Project Engineer

V. L. Roberts, Project Director

Highway Safety Research Institute

The University of Michigan

Ann Arbor

ACKNOWLEDGMENTS

The authors of this report wish to acknowledge the assistance of the following persons in carrying out the research outlined in this progress report: P. M. Fuller, J. L. Wood, I. Barodawala, G. S. Bahling, A. Engin, and R. Pontius of the Biomechanics-Biomedical Department of the Highway Safety Research Institute; Y. K. Liu and I. K. McIvor of the Department of Engineering Mechanics at The University of Michigan; T. Fallenstein and A. Huntress of Dow-Corning Corporation; D. F. Huelke, Professor, and F. G. Evans, Professor of the Department of Anatomy of The University of Michigan; and P. W. Gikas, Chief of Clinical Laboratory Services at the Veterans Administration Hospital in Ann Arbor, Michigan and R. C. Hendrix, Professor of Pathology at The University of Michigan whose assistance is proving most valuable in obtaining tissues at autopsy.

TABLE OF CONTENTS

(TABLE OF CONTENTS CONTINUED)

APPENDICES

MAIN REPORT

I. INTRODUCTION

The primary object of this eighteen-month progress report on the Head Injury Model Program is to present a complete and concise statement of the methodology, both experimental and analytical, applied by the Biomechanics Group, H.S.R.I. to the program and to present the results obtained to date. In addition, comparison of the experimental results is made, when possible, with the results of the other two contractors.

The experimental determination of the mechanical properties of the tissues of the head (Phase I of the project) is viewed as a basic study in materials science as opposed to a materials testing program. The routine measurement of the mechanical properties of various tissues and gross averaging of the values obtained can be quite misleading in many cases. In view of the goals of this project it is quite necessary to have a basic understanding of the reasons <u>why</u> the tissues behave as they do under load as well as <u>how</u> they behave. A knowledge of the reasons for a particular tissue's behavior will permit a more rational choice of the degree of detail that the model of the tissue should have in the later phases of the project.

The analytical phases of the program are primarily concerned with the development of constitutive equations for the behavior of tissues of the head and with the development of mathematical models of the head. The formulation of constitutive equations is closely related to the experimental program. However, it is necessary that an adequate body of data be available before the present techniques for generating the equations can be meaningfully applied. The analysis of mathematical models of the head is a study in the continuing sophistication of techniques and models.

II. THE EXPERIMENTAL PROGRAM

A. SPECIMEN ACQUISITION

The following are summaries of the procedures used to obtain specimens for testing. Detailed discussions of some of the procedures have appeared in the previous reports.

1. Skull

Fresh human bone specimens are removed at autopsy with a Stryker autopsy saw using either a 3/4-inch or a 1 1/2-inch diameter circular bone plug cutter. The specimens are labeled and then frozen at -10°C until needed.

Whole embalmed calvaria are obtained from the University of Michigan Medical School.

2. Brain

Fresh human brain material is taken at autopsy and placed in plastic bags. Notation is made on the data sheet as to the exact location from which the section is taken. The plastic bags are placed in a mixture of crushed ice and water (3°C) in an insulated container and transported to the Biomechanics laboratory or to Dow-Corning (a 1 3/4-hour drive).

3. Meninges

Dura mater is taken fresh at autopsy and then placed in saline solution. The sealed jars are placed in a refrigerator until the time of testing. This material is normally tested as soon after death as possible.

4. CSF

Samples of CSF are removed prior to autopsy. A long needle is inserted between the intervertebral disks and the CSF is drawn off into a sterile syringe and placed in sterile bottles until it is tested. The tests are performed immediately after the CSF is received.

5. Scalp

A strip of scalp 1.0 to 1.5 cm wide will be taken at autopsy. It will be kept moist with saline solution until it is tested.

6. Blood Vessels

The blood vessels from the base of the brain will be removed at autopsy and placed in saline solution. In the event that an immediate test is not possible, the vessels will be refrigerated in saline solution.

Table I lists the supply of human autopsy materials acquired during the last six months.

B. HARD TISSUE TESTS

1. Tension Tests

The goal of the tension testing of skull bone is to determine the tensile stress-strain behavior of the compact bone of the inner and outer tables of the skull. The initial step in most types of skull fracture is the tensile failure of the table material. In a study of skull penetration currently in progress in the Biomechanics Group for the Ford Motor Company, this, initial tensile failure step is most evident. Circular cylindrical flat-ended steel penetrators approximately 0.4 inches in diameter are driven through embalmed calvaria at various velocities using Instron and Plastech testing machines. Load-time traces are recorded as the penetration occurs. As the tip of the penetrator begins to deform the skull, the load increases monotomically. If the test is stopped before failure and unloaded, the skull regains its initial shape. Testing to failure or peak load produces a sharp fall-off in load as the penetrator fractures the outer table in local tension. If the test is stopped immediately after this initial penetration and the penetrator removed, the failed region exhibits a circular hole in the outer table just slightly larger than the penetrator, with the disk of the outer table at the bottom of the cylindrical puncture. Further penetration of the skull produces a significantly lower load until the entire plug of bone is pushed out through the inner table. Thus, the peak load in what might be considered a localized compression test of an entire skull structure is governed by the tensile properties of the outer table of the skull.

Tensile testing poses two major problems - grips to hold the specimen and a transducer to measure strain. The original gripping scheme (using a pin through the enlarged tabs at the ends of the specimen) has proved to be a good choice. The actual grips have undergone several changes but the technique of pinning the tabs has been very satisfactory through the entire range of strain rates tested to date. In the six-month report, a grip was described that was appropriate for tension, compression and tension-compression testing. By using these grips, it was verified that the initial modulus of elasticity is the same in tension and compression. This grip was followed by another type that made grip alignment less critical. These were used during the second six months. As testing rates increased, a stiffer, lower mass grip was used and it now seems that a still lower mass grip will be required at the very high strain tests.

Two strain gages applied directly to the bone are used to measure strain. Any other extensometer attached to the specimen, or to the grips, is subject to serious errors in measuring the deformation over a given gage length. Applying strain gages to bone was at first difficult but has become a very routine procedure. It is felt that the stress-strain data at failure stress levels now being obtained is better and more reliable than most previous data in the literature.

Tensile testing at high strain rates introduces two new problems - recording techniques and the dynamics of the test set-up. Recording techniques have changed considerably during the test program. In the six-month report, the use of an X-Y plotter to obtain data at testing machine speeds of 0.02 in/min to 0.2 in/min was described. In the twelve-month report, the technique of X-Y plotting with Z-axis modulation on a memory oscilloscope was presented. This method is useful for crosshead rates of 0.2 in/min to 200 in/min. Present testing uses open shutter oscillophotography on a dual beam Tektronix 547 oscilloscope. Simultaneous traces of load and strain versus time are obtained on the Polaroid film. The amplifiers have very fast rise times and are well suited for the short duration, high strain rate tests. Typical data obtained by this method is shown in Figure 1, and the cross-plotted stress-strain data in Figure 2.

The material acquisition, storage, and specimen manufacture procedures have not changed since the twelve-month report.

A total of 115 tensile tests from which good, reliable data was obtained, have been performed. The specimens were taken from 24 skulls, with all but seven obtained from parietal bone. The testing speeds used in these tests are summarized in Table II. It can be seen that the largest body of data is at 20 in/min corresponding to a strain rate of 0.3 in/in/sec. There is a lack of sufficient data at higher strain rates to either report an average stress-strain curve for these strain rates or to conclude anything about strain rate effects in tension in bone. This information should be available in time for the next report. Emphasis in the immediate future will be on testing at speeds of 200 in/min and 30,000 in/min.

From the data obtained so far, there has been no detectable directional variation in the tensile properties of parietal bone. It is much more difficult to establish that there is no regional variation since whole unembalmed skulls are not available. However, if there is a regional variation in a given bone it does not seem to be significant. Through careful testing, it has been observed that all of the stress-strain data from any one bone plug at a single strain rate is consistent with regard to initial modulus. There are differences in breaking loads which must partly reflect differences in the local microstructure of one bone compared with another. The histological examination of the specimens allows the microstructure to be studied as described in the twelve-month report. The conclusions of the histology studies should be available in the next report.

2. Compression Tests

The principal objective of the compression testing of skull bone is the determination of the compressive stress-strain behavior of the diploë layer in the radial direction. It is the radial direction that the diploë layer serves its most important load carrying function in compression. The layer acts as a low density foundation for the compact bone of the outer table. The compact bone and the low density of the diploë layer is due to the web-like arrangement of this material. However, for the purpose of understanding the basic mechanical behavior of the skull, the diploë layer must be treated as a material separate from the compact inner and outer table bone. Thus, the majority of the compression testing to date has been with specimens consisting entirely of diploë layer material loaded in the radial direction. The validity of this approach has been born out in the following two examples:

In the skull penetration study for the Ford Motor Company, as described in the previous section on tension testing, a compression of the diploë layer has been noted following the initial penetration of the penetrator through the outer table of the skull. If the test is stopped immediately after the initial penetration, the depressed region remains, but there is no visible damage to the inner table. Resumption of the penetration results in a final breakthrough of the penetrator by means of a shearing failure of the diploë layer in the form of an expanding cone with a large diameter base of inner table bone many times the diameter of the penetrator. As noted in the tension testing section, the peak load occurs at initial penetration of the outer table and the subsequent processes of progressive penetration occur at significantly reduced loads. Thus, in this particular simulation of a head impact, the diploë layer performs its most important function in radial compression.

The use of the materials science approach of understanding the reasons for the mechanical behavior of a material as well as measuring the pertinent properties is illustrated in Appendix A. Appendix A is a copy of a paper, presently in review, based on some of the results of the compression testing program. Bone plugs from five different skulls were used producing fifty-two individual specimens. The material tested was unembalmed diploë layer from regions 9, 10 and 14. Included in the data analysis were only those plugs whose specimens exhibited the collapse mode of abrupt failure, characteristic of low density diploë layers. The test results, at first glance, appeared to have the wide variation attributed to biological materials as "biological variation." The values of compressive strength σ_c ranged from a low of 1820 lb/in^2 to a high of 11,350 lb/in^2 and the values of the compressive modulus of elasticity E_c ranged from a low of 0.57 x 10^5 lb/in^2 to a high of 3.99 x 10^5 lb/in^2. However, the diploë layer is a porous material and both σ_c and E_c should depend, in the same manner, on the actual amount of load carrying material existing across the cross-section of the specimen. This concept was evaluated by plotting σ_c against E_c as shown in Figure 5 of Appendix A. The result is a linear relationship between compressive strength and compressive modulus of elasticity. The average amount of material present in the specimen cross-section is directly related to the specific weight of the specimen. Thus, the structural features relating σ_c to E_c can be embodied in the specific weight of the diploë layer γ_D. A plot of the averages of the compressive strengths of the specimens from each bone plug versus their average specific weights is shown in Figure 6 of Appendix A. It is evident from Figure 6 that the compressive strength σ_c and therefore the compressive modulus of elasticity E_c are strongly influenced by the specific weight of the diploë layer γ_D.

It is these types of relationships between mechanical properties and material structure that will provide an understanding of the material that would not exist if only averaging of experimental values were performed. This knowledge will be indispensable when construction and evaluation of the head model commences.

The present test apparatus and procedure for the compression tests are the same as described in the twelve-month report and in Appendix A except that the high strain rates now being used demand the use of open shutter oscillophotography with a Tektronix 547 oscilloscope. Tests are currently being run at strain rates of approximtely 200 in/in/sec and testing at 2000 in/in/sec will begin shortly. Table III is a listing of the raw data obtained to date on the compressive behavior of the diploë layer.

A limited amount of compressive testing of compact outer table bone has been performed in the tangential direction. The purpose of this testing has been to develop a modulus of elasticity test for compact bone in regions of the skull where the tensile test is not possible. The compact bone was found to exhibit a ductile stress-strain behavior in compression with a yield stress approximately twice the tensile fracture stress. It is not unusual for a material to have different modes of failure in different states of stress; another common example of exactly such behavior is found in plexiglass (PMMA). Thus, the tangential compression test on compact bone can only be used to determine the modulus of elasticity of the material.

3. Shear Tests

The shear test measures the average shear strength of the diploë layer by subjecting a cylindrical bone plug taken radially from a skull to a transverse shear parallel to the tables. It is the one test where embalmed material as well as fresh material has been used. The present test procedure is the same as described in the twelve-month report. Embalmed calvaria have been used to provide a large number of specimens from one skull so that position effects could be studied statistically. The results of an initial study using a three-way analysis of variances technique were discussed in the twelve-month report. The raw data used in that analysis is shown in Table IV of this report. About 500 additional tests on embalmed calvaria have been run at high strain rates using a modified analysis technique, but the data analysis is not yet complete. The results and the data will be presented in the next report along with additional findings on fresh material tests.

C. SOFT TISSUE TESTS

1. Brain Tests

The most important tissue in the entire experimental program is brain tissue. It's complex structure requires mechanical property determination to begin on a rather gross scale, with subsequent refinements as knowledge is obtained. The initial approach to this problem is summarized in Appendix B which is a paper, presently in review, based on the results of the brain testing program to date.

It would appear that the Dynamic Probe Apparatus (DPA) will definitely allow the correlation of in vitro and in vivo brain testing. This should be confirmed as soon as the analysis of the DPA data is finished. This is presently in progress using a computer technique developed at Dow-Corning. In addition, as noted in Appendix B , there is a good possibility that the DPA will allow calculation of the basic complex shear properties G' and G".

2. Dura Mater Tests

Tension tests on dura mater have been used for general soft tissue test development as well as for obtaining mechanical properties of dura mater. The testing has been performed at static strain rates thus far, but higher strain rates will be incorporated in the near future. The test specimens were cut from the dura using a ASTM Tensile Die C. All specimens have been oriented along the fibrous direction of the tissue. The strain in the specimen was measured by a phototransistorized light extensometer. Two lightweight vanes, attached to the specimen in the test section, block a light beam passing from a source to the phototransistor. As the specimen is elongated, the increasing separation of the vanes allows more of the beam to pass through to the phototransistor. The resulting output of the phototransistor is calibrated against vane separation and permits measurement of the strain in the specimen independent of any gripping distortions or slippages. The results of four such tests are shown in Figures 3, 4, 5 and 6. An aggregate of the four tests is shown in Figure 7. It is evident that the initial moduli of elasticity of the specimens are fairly reproducible but that the ultimate strength is much more variable. The mode of failure is a pronounced necking down of a local region of the specimen with an apparent large scale relative sliding of the fibers of the tissue. Table V shows the ultimate strengths of sixteen specimens. It was found that crosshead motion could not be used in place of the extensometer for determining strain in the specimen. Thus, in twelve of the sixteen tests reported, only the ultimate stress was determined.

D. COMPARISON OF CONTRACTORS' RESULTS

The following comparisons can be made from the results reported in the twelve-month reports:

1. Technology Incorporated Results

The only mechanical tests that can be compared with those of The University of Michigan are the fresh autopsy human skull compression tests. The average values presented by T. I. for compressive strength correspond to the lower end of the range of U. of M. data. This would tend to indicate low density diploë layer material; however, the T. I. method of measuring density includes the table material so that no density comparison can be made.

2. West Virginia University Results

The data reported by W. V. U. was for embalmed skull material and, thus, is strictly comparable to only the U. of M. direct shear tests where it would appear the results are basically the same in range and variability. If a comparison of the compression tests is made for regions 9, 10, 13, 14 and 18 for W. V. U. skulls 227 and 286, the values of modulus of elasticity and strength for the most part lie toward the upper end of the range of U. of M. diploë layer data. This indicates high density diploë layer material, but again no density comparisons are possible due to inclusion of the table material in W. V. U. specimens. The tensile test values of W. V. U. skull 245 indicate ultimate tensile strengths much lower than U. of M. data for the same regions 9, 10, 13, and 14, but with similar moduli of elasticity.

III. ANALYTICAL PROGRAM

The analytical program has been divided into two related parts. One is concerned with the development of constitutive equations and is closely related to the experimental determination of the physical properties of the tissues of the head. The other part is concerned with the analysis of progressively more sophisticated mathematical models of the skull and its contents.

The formulation of constitutive equations is given a high priority in the development of a model of the human head in that they form a necessary part of the mathematical equipment.

The point in time at which realistic constitutive equations can be proposed is necessarily later than the experimental determination of tissue properties because an adequate collection of data must be available before the analytical work can be begun in a meaningful manner.

In order to provide a solid foundation for the equations which will be developed, the literature concerned with experimental determination of tissue properties, formulations of equations describing material properties, and related theoretical considerations in nonlinear continuum mechanics has been searched. In addition, a technique for formulating empirical constitutive equations has been developed.

The experimental work carried out on various soft tissues to determine their mechanical properties are numerous. Among the papers which may be useful in developing meaningful equations for various body tissues are those written by Lawton (1952), Roach and Burton (1957), Sonnenblick (1962, 1964), Apter (1964), Ridge and Wright (1966) and Benedict, Walker, and Harris (1968). Ommaya (1968) presented a review of the literature pertaining to the mechanical properties of the tissues of the nervous system. These papers, as well as many others, are listed in Appendix D of this report.

Most of the soft tissues which have been studied exhibit nonhomogeneous, anisotropic, and nonlinear viscoelastic characteristics making the problem of mechanical property determination exceedingly complex. In the mathematical analysis of these materials, the properties have been expressed either by a series of discrete mechanical elements or by a continuous spectral representation. The work by Jamison, Marangoni, and Glaser (1968) can be mentioned as an example of the former. They discuss an experimental technique for obtaining linear viscoelastic models of individual soft tissues. The application of this experimental technique, using a guinea pig skin as an example, is presented along with numerical values for the various viscoelastic parameters. Wiederhelm, Kobayashi, Stromberg, and Woo (1968) obtained the response of relaxed and constricted arterioles to static pressure loads by applying the numerical method of direct stiffness. This constitutes a finite element analysis and can effectively model nonhomogeneous and anisotropic nonlinear viscoelastic characteristics of the blood vessels. For mesentery, Fung (1967) has proposed a stress-strain relation which can be used in simple elongation. In papers which have not yet appeared in the literature, Frisen, Mägi, Sonnerup, and Viidik propose a mathematical expression for the viscoelastic behavior of soft collagenous tissue along with experimental verification. Also Hildebrandt, Fukaya, and Martin have studied the negative strain, which develops in cases of compression and biaxial stress in tissue sheets, using nonlinear elasticity theory for an incompressible isotropic material undergoing uniform deformation.

A technique for the generation of constitutive equations based on experimental data has been developed during the course of the current research project. A computer program generates a linear equation of the form:

$$Y + Bo + B_1 X_1 + B_2 X_2 + \cdot \cdot \cdot + B_k Y_k$$

using regression analysis from a set of N observations of a set of K independent variables and a single dependent variable. At present, the dependent variable Y represents stress while the independent variables (X_1, X_2 $\cdot \cdot \cdot$, X_k) are various functions of strain and strain rate. This relation has been tested on materials for which considerable data exists and found to model nonlinear material behavior within a few percent.

The preceeding discussion serves to outline the approach to constitutive equations which has been taken up to this time in the course of the research project. It is felt that this approach is necessary in order to develop equations which adequately model material behavior on one hand and are useful for analysis on the other.

A few preliminary conclusions concerning material properties can be drawn at this time. The literature indicates that compact skull bone loaded in tension might be approximated by a nearly linear elastic, brittle material. This may not be true at high strain rates, however. Because of the alignment of collagen fibers, skin exhibits little resistance to force until a certain amount of deformation exists. A bilinear curve is a possible stress-strain law for tension. The brain, when viewed as a homogeneous medium (a logical first step), appears to react in shear as a linear viscoelastic medium at small deformation, with nonlinear behavior developing as deformation is increased beyond a certain limit. These early conclusions are being subjected to continuing tests in order to reach clearly formed conclusions in the form of constitutive equations.

A similar approach has been used in the early development of mathematical models of the head. Literature has been searched and analytical work has been done on increasingly complex and diverse models of human head dynamics. An initial study was carried out on the free vibration of a spherical shell to determine the response of the skull bone. This skull was then subjected to impact loadings. Increasing in complexity, the second model was of the impact of a fluid-filled shell. This analysis was submitted as a doctoral thesis to the Engineering Mechanics Department of The University of Michigan, and is included as Appendix C to this report. Since that time, analysis of a spherical region of linear viscoelastic material subjected to steady state regional force input has been carried out. The transient problem of impact is now being carried out. Nonlinear properties of the viscoelastic region (brain) will be added based on the results of current experimentations. Other models of the skull and contents which involve more complex geometry and considerable computer analysis are being evaluated for feasibility. It is felt that progression from a relatively simple model of the head to increasingly complex material models and geometry is the logical way to progress and the one most likely to result in successful fulfillment of the initial contract objectives.

MECHANICAL PROPERTIES DATA SHEET

SPECIMEN NO. VA 63 TL 2

DATE TESTED January 15, 1969

CROSSHEAD RATE 5.000 in/min

I.M. FREQUENCY

TEST SECTION
DIMENSIONS 0.037 in. x 0.056 in

ADDITIONAL DATA

10 lbs/cm
1,500 $\mu\varepsilon$/cm

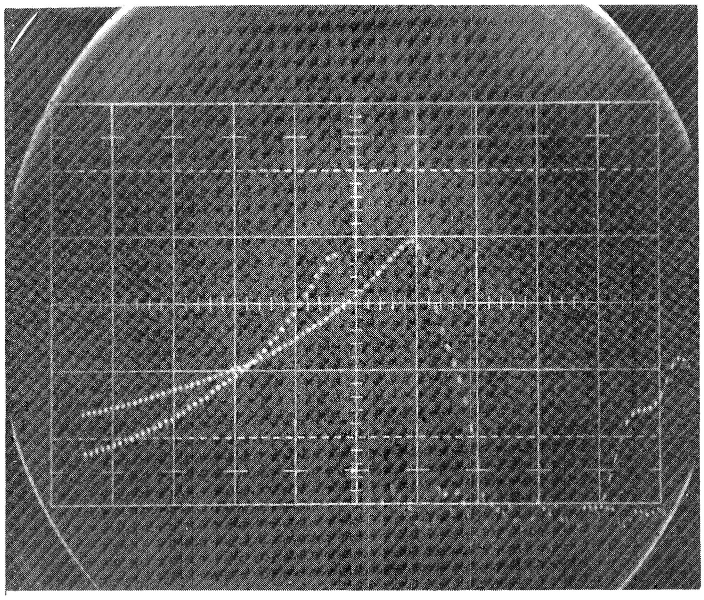

10μ sec/cm

CALCULATED DATA

STRAIN RATE 75 sec^{-1} (Aver.)

MODULUS OF ELASTICITY 2.65×10^6 lb/in^2

ULTIMATE STRESS 14,500 lb/in^2

ULTIMATE STRAIN 0.56%

AREA 0.00204 in^2

HISTOLOGICAL COMMENTS

TEST COMMENTS

Upper trace (at t = 0) represents load (zero level is dashed horizontal line).

Lower trace (at t = 0) represents strain (zero level is lowermost solid horizontal line).

NOTE: Both signals start above their zero levels because of the trigger level used on the oscilloscope.

FIGURE 1. Mechanical Properties Data Sheet

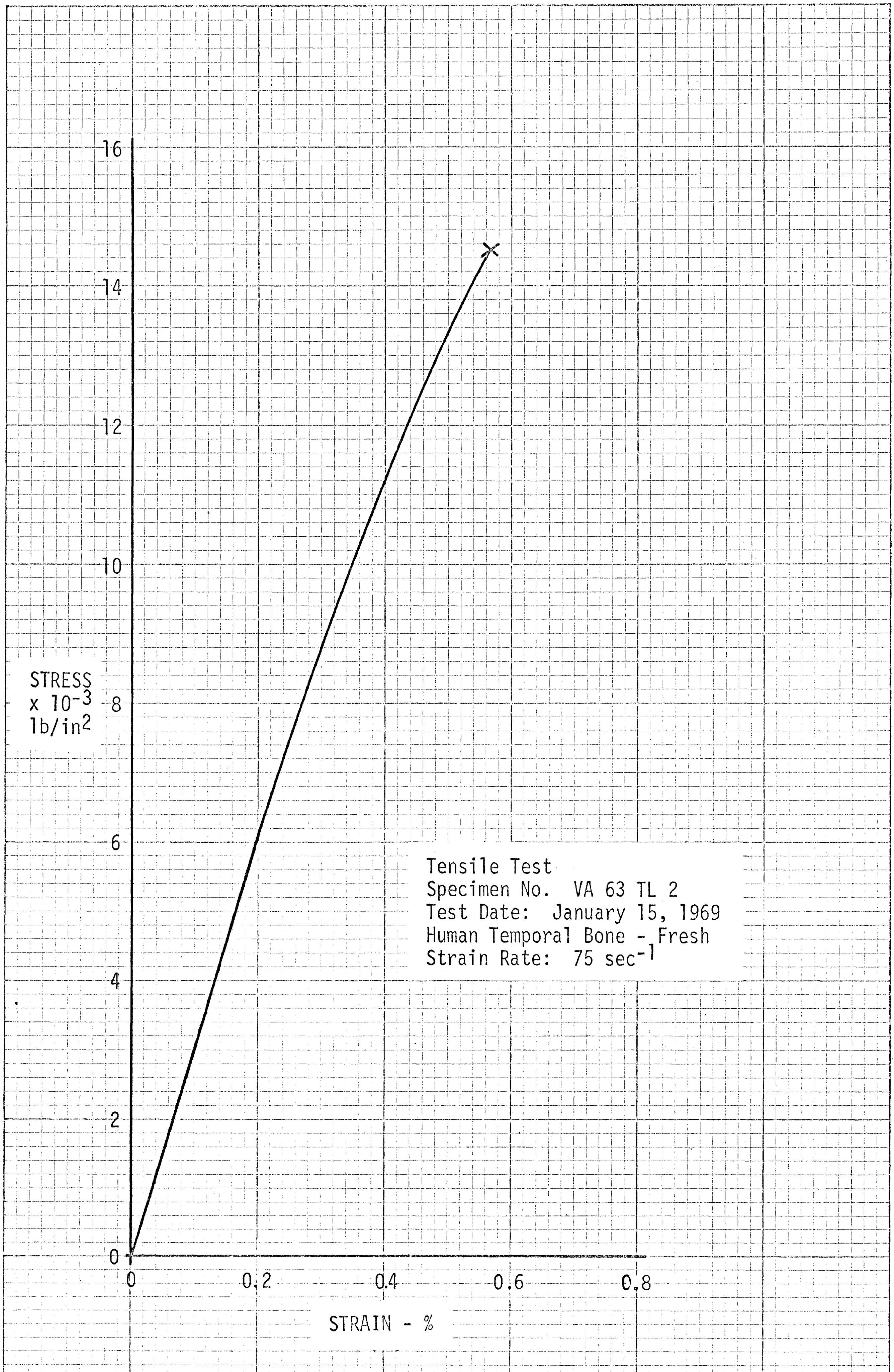

FIGURE 2. Typical Stress-Strain Diagram

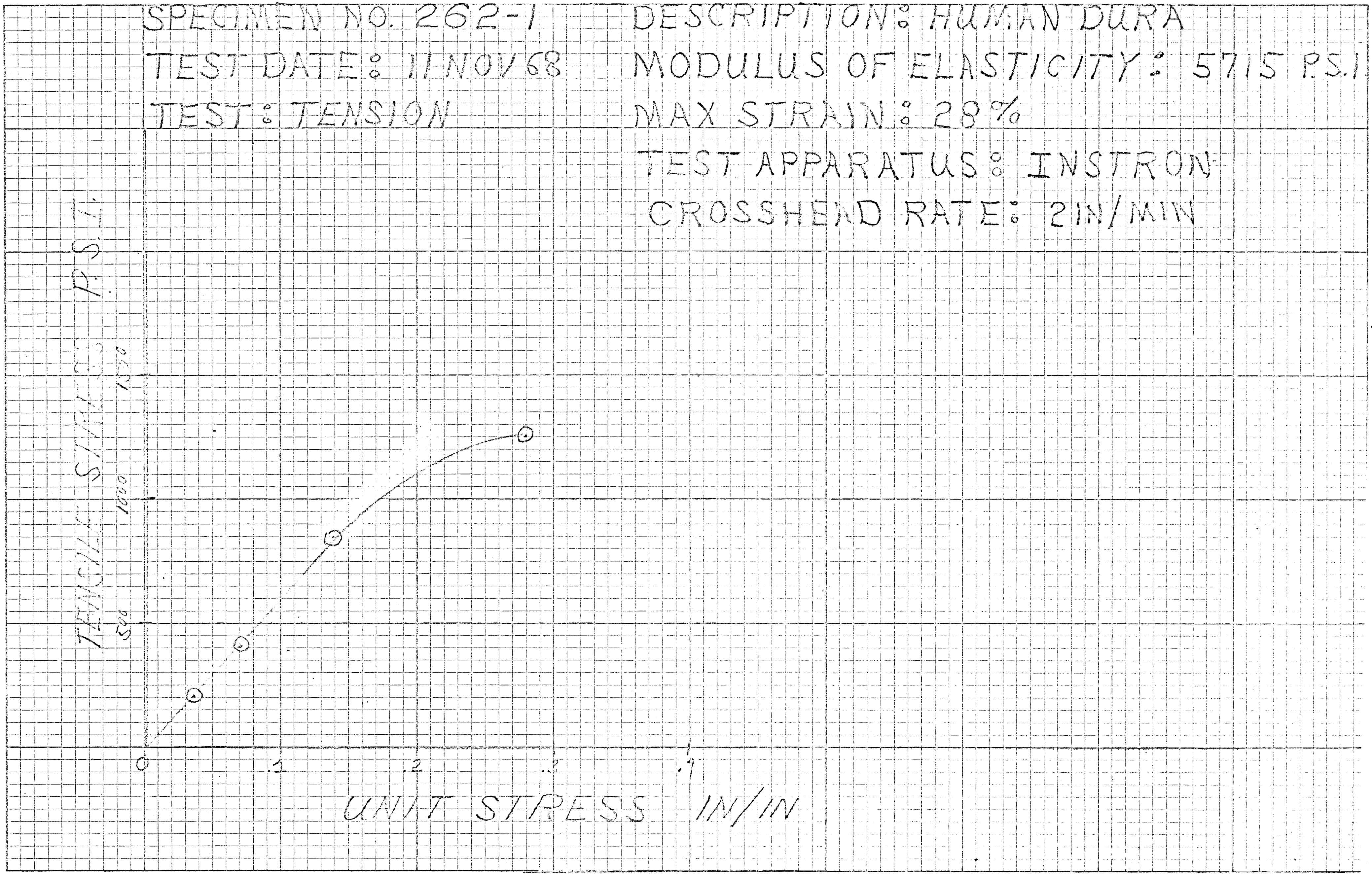

FIGURE 3. Dura Mater Test

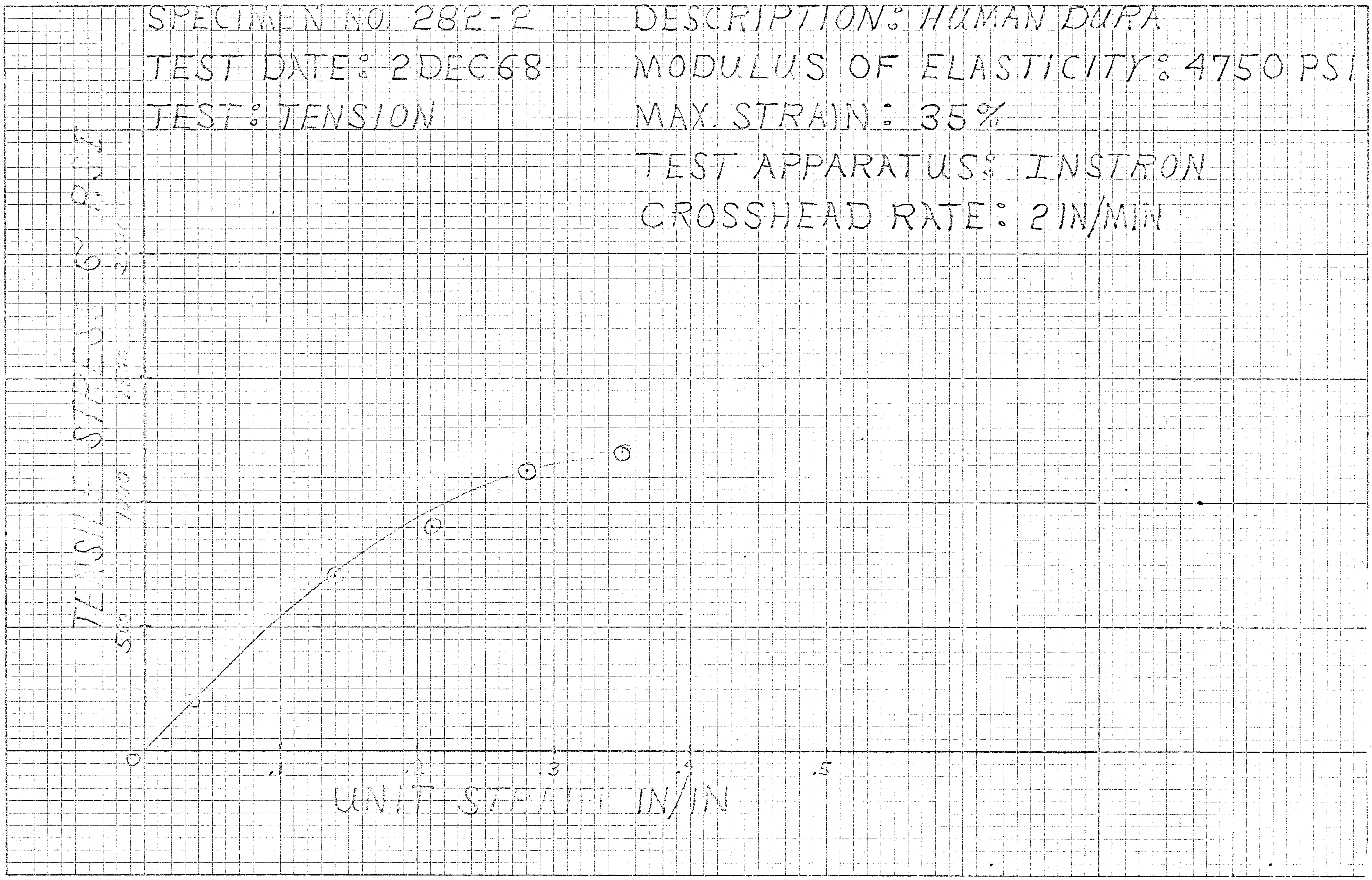

FIGURE 4. Dura Mater Test

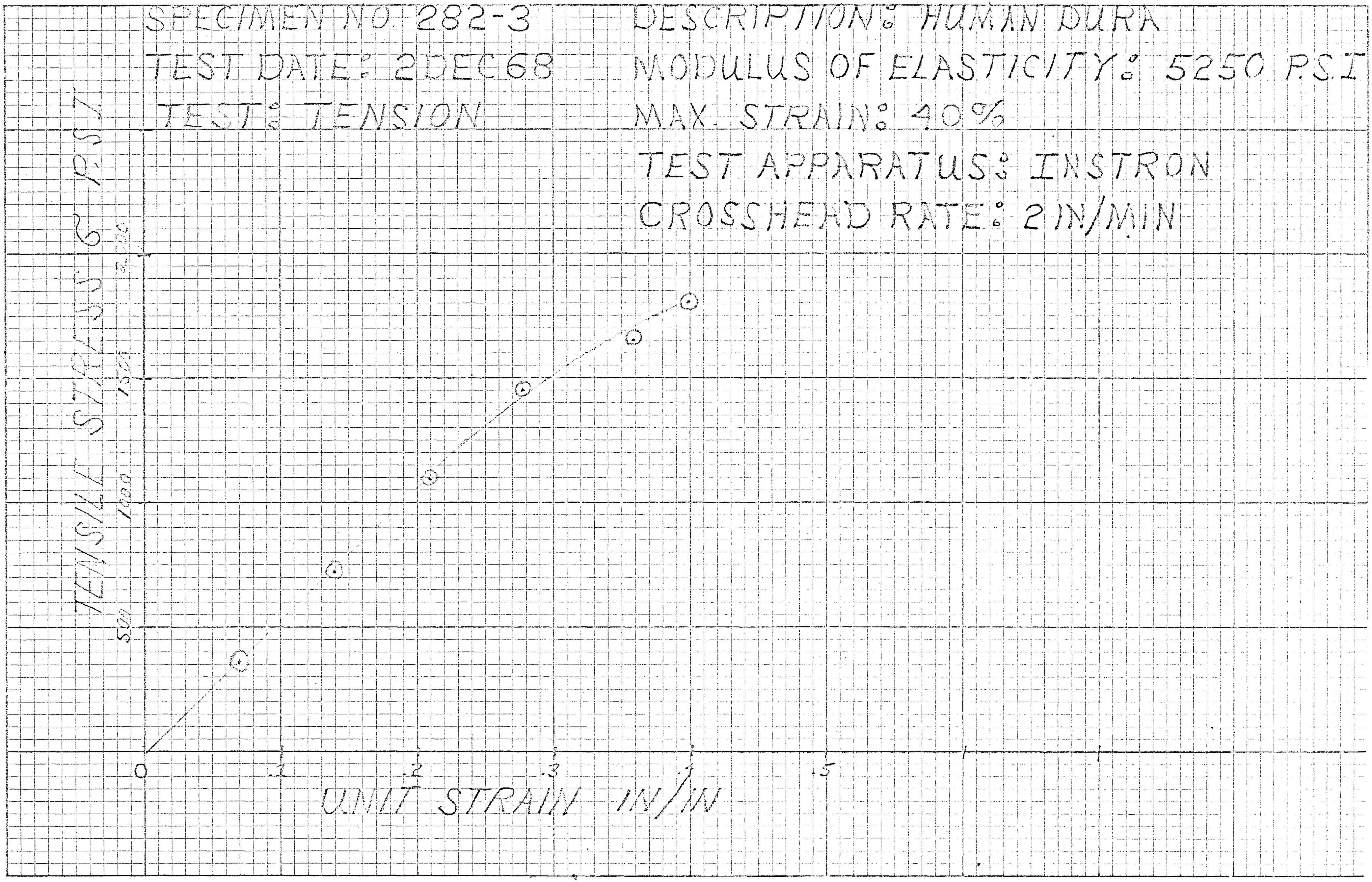

FIGURE 5. Dura Mater Test.

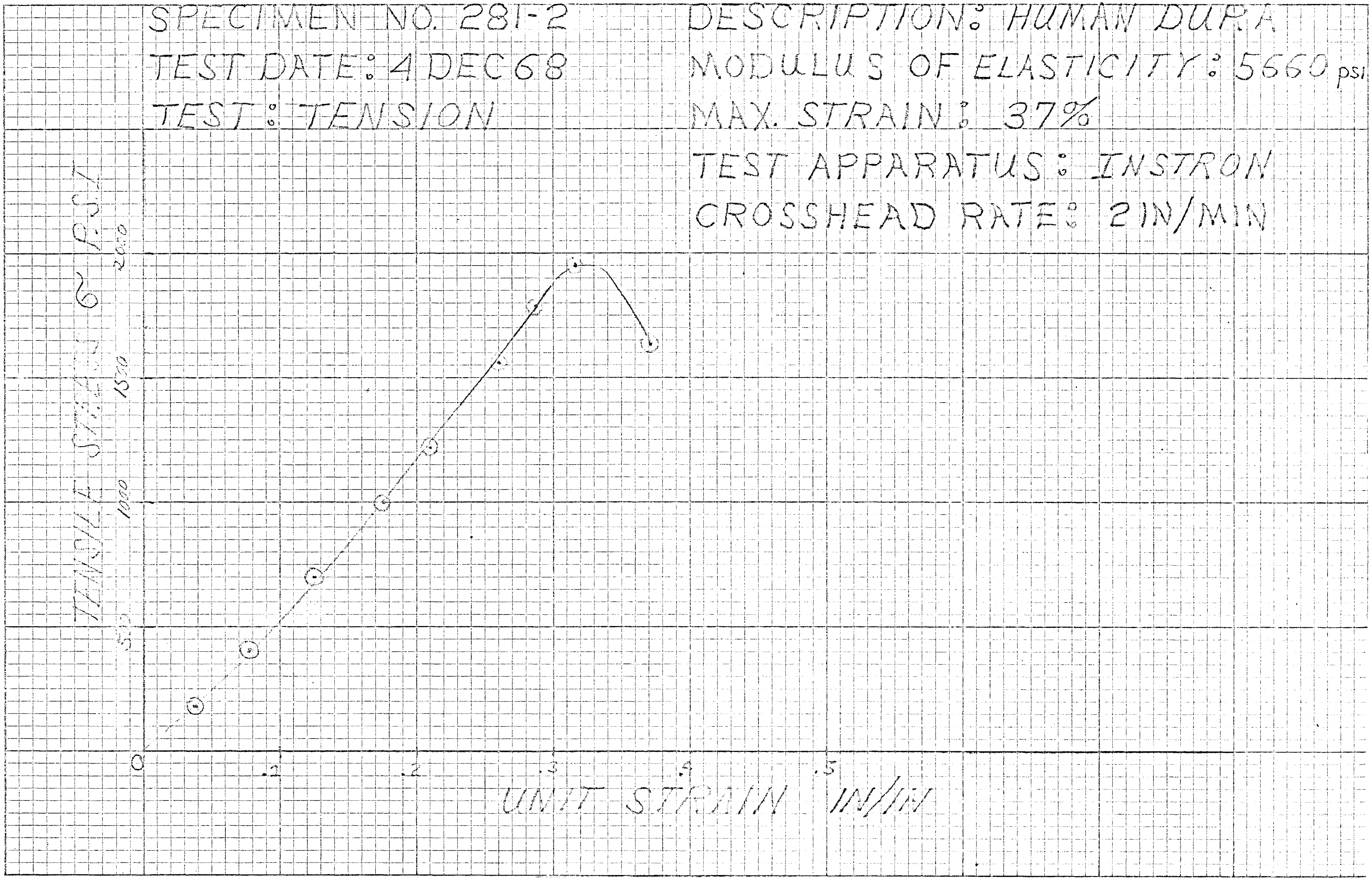

FIGURE 6. Dura Mater Test

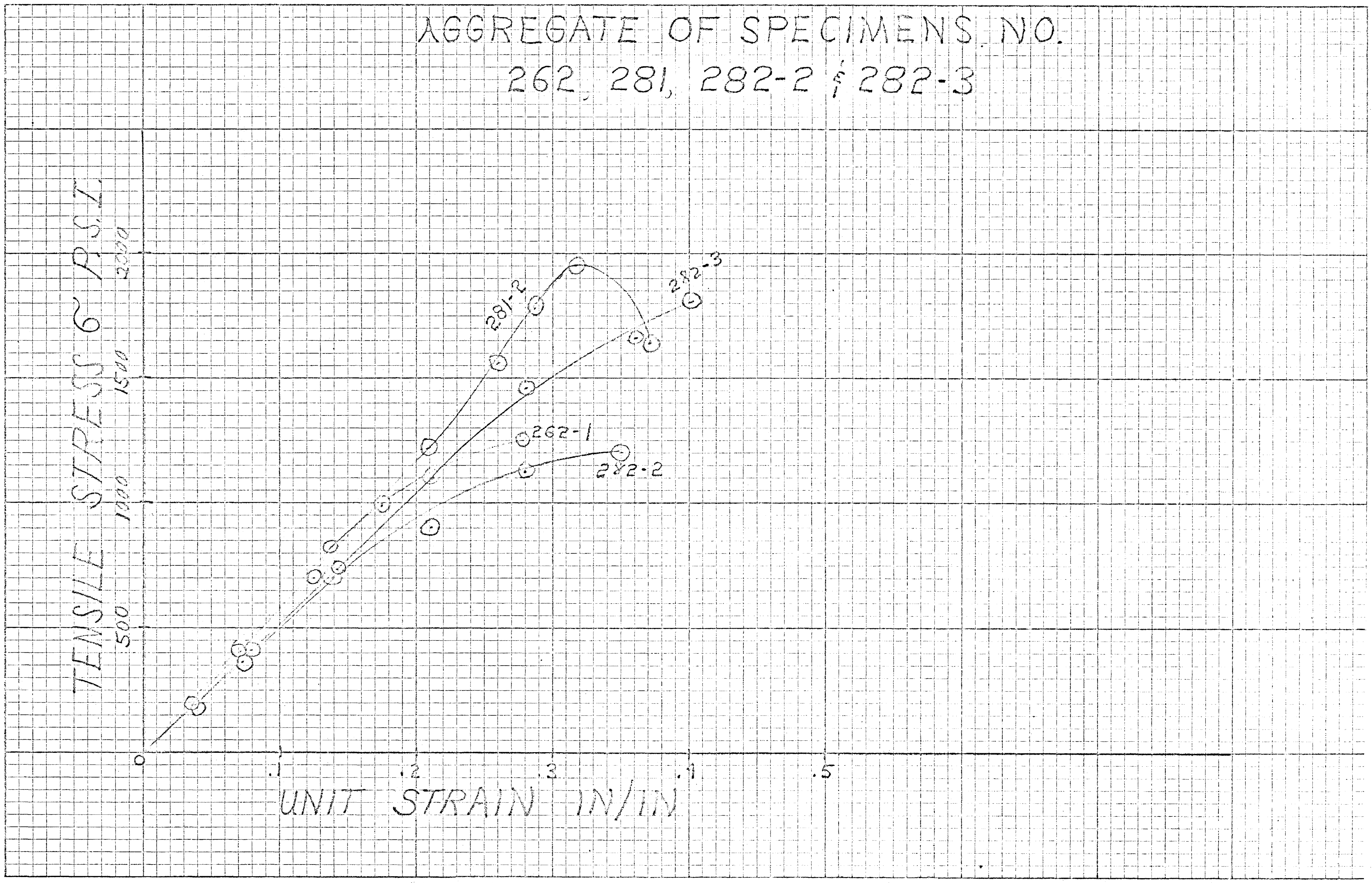

FIGURE 7. Aggregate of Dura Mater Tests

TABLE I. SUMMARY OF HUMAN MATERIAL
June 1968-January 1969

BONE SPECIMEN	AGE	RACE	SEX	CAUSE OF DEATH
UM-36-P (2)	56	C	M	Burns
UM-37-P (2)	13	C	F	Auto Accident
UM-38-P (2)	62	C	F	Aortic Aneurysim
UM-39-P (2)	76	C	M	Pneumonia
UM-40-P (2)	47	C	F	Lung Cancer
UM-41-P (2)	13	N	M	Cardiac arrest
UM-42-P (2)	57	C	F	Cancer
VA-63-TL	73	N	M	Heart attack
VA-64-TL	53	C	M	Cancer of esophagus
VA-65-FL	45	C	M	Heart attack
VA-66-PL	74	C	M	Cancer
VA-67-FR	72	C	M	Cancer
VA-68-TL	60	C	M	Cirrhossis of liver
VA-69-PR	61	C	M	Septirema
VA-70-TL	46	C	M	Cerebral Hemorrhage
VA-71-FL	69	C	M	Cancer & Emphysema
VA-72-FR	73	N	M	Pulmonary embolus
VA-73-FR	53	C	M	Cancer of lung
VA-74-FL	40	C	M	Cancer
DURA MATER SPECIMEN				
260	65	C	M	Myocardial infarct
262	53	C	F	Cancer of breast
270	20	C	M	Lacerated aorta
281	71	C	F	Myocardial infarct
282	51	C	M	Myocardial infarct

TABLE II.

Tension Test Summary.

Test Speed in/min	2.0	20	200	2,000	5,000
Number of Specimens	21	51	14	26	3

TABLE III. COMPRESSION TEST-RAW DATA

Region	Stress p.s.i.	Modulus of Elasticity 10^5 p.s.i.	Specific Wt. lb/in^3	Behavior C=collapse Y=yield
Strain rate=.0022 in/in/sec.				
	10,670	4.05	0.0605	Y
UM-35-PL	11,620	4.17	0.0609	Y
	10,950	4.32	0.0621	Y
	11,770	3.04	0.0610	Y
	10,950	4.06	0.0607	Y
	11,610	4.48	0.0614	Y
	12,200	4.10	0.0622	Y
UM-35-PR	12,200	4.00	0.0592	Y
	14,800	4.63	0.0623	Y
	13,020	3.93	0.0602	Y
	8,750	4.25	0.0565	Y
	10,270	3.57	0.0602	Y
14	1,860	0.835	0.0367	C
VA-52-PR	1,415	0.624	0.0328	C
	1,555	0.845	0.0342	C
	1,590	0.803	0.0343	C
10	7,820	2.70	0.0495	C
VA-59-PR	4,500	1.7	0.0445	C
	6,270	2.34	0.0460	C
	5,010	1.69	0.0413	C
	6,030	2.06	0.0454	C
	4,920	1.53	0.0446	C
Strain rate=0.56 in/in/sec.				
10	6,950	3.05	0.0626	Y
VA-8-PR	10,200	3.93	0.0660	Y
	12,250	3.67	0.0654	Y
	10,100	3.90	0.0648	Y
	9,050	3.52	0.0640	Y
	---	3.39	0.0657	Y
10	7,200	--	0.0471	C
VA-20-PL	6,690	2.23	0.0469	C
	6,010	2.63	0.0440	C
	6,690	2.82	0.0467	C
	5,910	2.64	0.0486	C
	5,743	2.73	0.0467	C
14	2,980	1.105	0.0390	C
VA-55-PR	3,510	1.345	0.0420	C
	6,170	2.185	0.0453	C
	4,440	0.875	0.0440	C
	3,090	1.063	0.0412	C

TABLE III. COMPRESSION TEST-RAW DATA

Strain rate=1.2 in/in/sec.

Region	Stress p.s.i.	Modulus of Elasticity 10^5 p.s.i.	Specific Wt. lb/in^3	Behavior C=collapse Y=yield
9	8,930	2.84	0.0466	C
VA-29-PL	7,360	2.42	0.0457	C
	7,060	2.12	0.0463	C
	8,190	2.64	0.0436	C
13	3,940	2.82		C
UM-23-PL	6,630	1.455	0.0488	Y
	6,780	2.04	0.0199	C
	8,460	2.00	0.0515	Y
	8,220	2.22	0.0477	Y

Strain rate=.022 in/in/sec.

Region	Stress p.s.i.	Modulus of Elasticity 10^5 p.s.i.	Specific Wt. lb/in^3	Behavior C=collapse Y=yield
14	1,451	0.675	0.0344	C
VA-52-PR	1,083	0.493	0.0309	C
	1,848	0.868	0.0367	C
	2,562	1.52	0.0338	C
	1,470	0.447	0.0333	C
	1,780	0.802	0.0376	C

Strain rate=.054 in/in/sec.

Region	Stress p.s.i.	Modulus of Elasticity 10^5 p.s.i.	Specific Wt. lb/in^3	Behavior C=collapse Y=yield
14 VA-55-PR	3,420	1.22	0.0428	C
	3,380	1.420	0.0416	C
	3,260	1.275	0.0411	C
	4,270	1.575	0.0458	C
	4,030	1.63	0.0439	C

TABLE III. COMPRESSION TEST-RAW DATA

Strain rate=0.22 in/in/sec.

Region	Stress p.s.i.	Modulus of Elasticity 10 p.s.i.	Specific Wt. lb/in^3	Behavior C=collapse Y=yield
9 VA-5-PL	3,100	1.27	0.0378	C
	3,230	1.25	0.0394	C
	3,380	1.21	0.0390	C
	5,910	2.12	0.0412	Y
	3,260	1.02	0.0389	C
	5,420	2.27	0.0390	C
9 VA-6-PL	1,940	0.76	0.0368	C
	755	0.24	0.0353	C
	1,990	0.635		C
	1,860	0.59	0.0364	C
	2,260	0.655	0.0384	C
	1,820	0.57	0.0360	C
10 VA-8-PR	9,700	3.39	0.0653	Y
	5,640	2.28	0.0614	Y
	9,240	3.63	0.0650	Y
	11,600	3.72	0.0640	Y
	11,000	3.81	0.0635	Y
	11,800	3.94	0.0668	Y
	5,590	2.49	0.0573	C
				C
10 VA-9-PR	8,550	2.92	0.0473	C
	8,990	3.48	0.0462	C
	10,000	3.91	0.0504	C
	10,700	3.99	0.0473	C
	10,300	3.72	0.0492	C
10 VA-20-PL	7,080	2.35	0.0486	C
	7,260	3.30	0.0492	C
	6,580		0.0487	C
	6,730	2.48	0.0480	C
	6,770	2.45	0.0875	C
	5,650	2.46	0.0461	C
14 VA-55-PR	3,860	1.1215	0.0428	C
	2,880	1.202	0.0414	C
	3,640	1.402	0.0403	C
	3,050	1.275	0.0419	C
	3,020	1.195	0.0400	C
	2,420	0.668	0.0392	C
	4,430	1.738	0.0423	C
10 VA-59-PR	7,380	2.65	0.0463	C
	8,520	2.54	0.0506	C
	6,910	2.22	0.0473	C
	6,430	2.24	0.0442	C
	5,800	2.21	0.0416	C
	5,120	1.63	0.0407	C

TABLE III. COMPRESSION TEST-RAW DATA

Region	Stress p.s.i.	Modulus of Elasticity 10^5 p.s.i.	Specific Wt. lb/in^3	Behavior C=collapse Y=yield
18	10,000	3.83	0.0578	C
UM-22-PR	8,420	3.44	0.0547	C
	7,030	3.92	0.0541	C
13	5,540	2.11	0.0570	C
UM-25-PL	8,280	2.65	0.0595	C
	8,600	2.49	0.0597	C
	12,730	3.27	0.0626	C
10	5,540	2.11	0.0522	C
UM-31-PR	1,972	1.11	0.0492	C
	3,730	1.87	0.0570	C
	1,415	0.780	0.0515	C
	1,425	0.782	0.055	C
10	11,330	3.5	0.0576	C
UM-35-PR	9,940	3.76	0.0592	Y
	13,180	4.57	0.0619	Y
	12,380	4.06	0.0593	Y
	14,320	4.76	0.0615	Y

TABLE III. COMPRESSION TEST-RAW DATA

Region	Stress p.s.i.	Modulus of Elasticity 10^5 p.s.i.	Specific Wt. lb/in^3	Behavior C=collapse Y=yield
Strain rate=2.2 in/in/sec.				
9 VA-5-PL	5,230	1.80	0.0432	C
	4,760	1.85	0.0409	C
	4,850	1.60	0.0397	C
	3,520	1.68	0.0382	C
	5,360	2.24	0.0410	C
9 VA-6-PL	2,060	0.74	0.0374	C
	2,520	0.825	0.0367	C
	2,460	0.84	0.0376	C
	3,190	0.95	0.0397	C
	2,590	0.875	0.0379	C
10 VA-8-PR	11,800	3.98	0.0636	C
	8,130	3.76	0.0644	C
	40,300	12.4	0.0623	Y
	13,080	4.23	0.0652	C
	10,170	3.81	0.0613	Y
	13,050	4.08	0.0647	Y
	6,480	2.98	0.0606	C
10 VA-9-PR	9,070	3.52	0.0465	C
	8,200	3.26	0.0474	C
	11,350	3.54	0.0498	C
	10,400	3.95	0.0478	C
	9,200	3.94	0.0471	C
10 VA-20-PL	7,250	2.99	0.0476	C
	7,080	2.80	0.0451	C
	7,050	2.59	0.0506	C
	7,150	2.86	0.0463	C
	7,880	3.32	0.051	C
	6,980	2.92	0.0470	C
9 VA-29-PL	11,300	--	0.0505	Y
	10,300	2.48	0.0484	C
	8,500	2.82	0.0467	C
	9,950	2.62	0.0454	C
	9,550	1.98	0.0496	Y
	8,600	2.84	0.0451	C
	9,600	2.79	0.0449	C
14 VA-52-PR	2,030	0.925	0.0355	C
	1,925	0.866	0.0359	C
	1,965	0.767	0.0340	C
	1,725	0.732	0.0356	C
	1,525	0.769	0.0370	C
	2,400	0.878	0.0381	C

TABLE III. COMPRESSION TEST-RAW DATA

Region	Stress p.s.i.	Modulus of Elasticity 10^5 p.s.i.	Specific Wt. lb/in^3	Behavior C=collapse Y=yield
14	3,260	1.225	0.0416	C
VA-55-PR	3,800	1.365	0.0433	C
	4,010	1.380	0.0432	C
	3,800	1.085	0.0441	C
	---	1.72	0.0411	C
	4,890	1.790	0.0424	C
	4,280	1.348	0.0417	C
10	7,040	2.62	0.0492	C
VA-59-PR	9,120	2.92	0.0482	C
	7,640	2.66	0.0481	C
	6,580	2.31	0.0427	C
	7,460	2.8	0.0471	C
	6,450	2.15	0.425	C
18	13,400	3.86	0.0568	C
UM-22-PR	11,450	4.2	0.0741	C
	---	1.19	0.057	
13	3,330	1.672	0.0475	C
UM-23-PR	5,580	2.91	0.0557	Y
	5,240	2.25	0.0504	Y
	6,590	3.08	0.0565	Y
	6,370	2.75	0.0542	Y
13	7,730	2.1	0.0584	Y
UM-25-PL	7,380	2.1	0.0592	Y
10	2,720	1.378	0.0506	C
UM-31-PR	2,540	1.275	0.0530	C
	2,290	1.131	0.0525	C
10	14,950	4.72	0.0606	Y
UM-35-PL	15,150	5.08	0.0620	Y
	14,300	4.55	0.0598	Y
	15,640	4.57	0.0609	Y
	15,330	4.75	0.0614	Y
	14,700	4.40	0.0599	Y

TABLE IV. SHEAR TEST RAW DATA

4 Embalmed Calvaria - tested at 4 strain rates
1.66, 6.66, 16.6, 66.6 in/in/sec.
Shear Strength p.s.i. (strain rate in/in/sec)

SKULL NO.	EM95	EM99	EM106	EM108
Region 1		3391 (66.6)	2658 (6.66)	2431 (1.66)
		2697 (1.66)		4858 (1.66)
				3326 (16.6)
				3226 (66.6)
Region 2		5110 (66.6)	2357 (6.66)	4033 (16.6)
		2044 (1.66)	2522 (16.6)	3871 (66.6)
Region 3	2417 (6.66)	3758 (1.66)	4831 (16.6)	3899 (66.6)
	2010 (16.6)	3009 (6.66)	3133 (66.6)	3349 (1.66)
	2765 (1.66)	3440 (66.6)	2417 (6.66)	3841 (16.6)
	1904 (1.66)	2841 (66.6)	2917 (6.66)	3149 (16.6)
		2841 (6.66)	1915 (66.6)	3199 (1.66)
		2741 (16.6)	2841 (1.66)	4357 (6.66)
				4583 (66.6)
	2376 (6.66)	1925 (1.66)	2291 (16.6)	3483 (66.6)
		2291 (16.6)	2291 (1.66)	3899 (6.66)
				4499 (16.6)
		1610 (16.6)	1541 (1.66)	2310 (6.66)
Region 4		3758 (1.66)	4123 (16.6)	3998 (66.6)
	3082 (16.6)	3941 (6.66)	2613 (66.6)	3420 (1.66)
	3536 (1.66)	3091 (66.6)	2146 (6.66)	4766 (16.6)
		2191 (66.6)	2951 (6.66)	2933 (16.6)
	3646 (16.6)	2621 (6.66)	2340 (66.6)	3483 (1.66)
		3758 (16.6)	2592 (1.66)	4371 (6.66)
		1823 (1.66)		4583 (66.6)
	2286 (6.66)		2643 (16.6)	2552 (66.6)
		3195 (16.6)	2567 (1.66)	3369 (6.66)
		2567 (66.6)		4499 (16.6)
		2371 (16.6)	2586 (1.66)	3208 (6.66)
Region 5				5135 (16.6)
				4583 (16.6)
Region 6	3510 (66.6)	4033 (16.6)	3531 (1.66)	3483 (6.66)
		3941 (66.6)	2741 (6.66)	1833 (16.6)
			3581 (66.6)	4332 (1.66)
				3091 (6.66)
	3810 (66.6)	3440 (16.6)	2815 (1.66)	1995 (6.66)
		4358 (66.6)	2542 (6.66)	2765 (16.6)
			3646 (66.6)	3810 (1.66)
				5658 (6.66)
		2537 (1.66)	3091 (16.6)	4267 (66.6)
			3091 (1.66)	4972 (6.66)
		4126 (1.66)	2826 (16.6)	4310 (66.6)
			3291 (1.66)	3717 (6.66)

TABLE IV Continued

SKULL NO.	EM95	EM99	EM106	EM108
Region 7	2044 (1.66)		2910 (6.66)	4216 (16.6)
	2941 (16.6)	4653 (6.66)	3829 (66.6)	3777 (1.66)
	3741 (66.6)	2273 (16.6)	2448 (1.66)	4010 (6.66)
				5331 (1.66)
	4360 (1.66)		5153 (6.66)	4176 (16.6)
	3854 (6.66)	4831 (1.66)	3779 (16.6)	4331 (66.6)
				5774 (6.66)
				3525 (66.6)
			3842 (66.6)	6730 (1.66)
Region 8		5743 (66.6)	2901 (6.66)	4983 (16.6)
	3440 (16.6)	1467 (6.66)	3936 (66.6)	3391 (1.66)
	4357 (66.6)	2986 (16.6)	4813 (1.66)	2933 (6.66)
			1843 (66.6)	2895 (1.66)
			5690 (6.66)	4766 (16.6)
	2390 (6.66)	3420 (1.66)	5045 (16.6)	4792 (66.6)
			4473 (66.6)	5276 (1.66)
Region 9	4863 (6.66)	2537 (1.66)	3483 (16.6)	4228 (66.6)
	3420 (66.6)	2910 (16.6)	2951 (1.66)	2986 (6.66)
	3918 (1.66)	4858 (66.6)	3391 (6.66)	1065 (16.6)
	2510 (16.6)	2481 (6.66)	2542 (66.6)	4933 (1.66)
	4742 (1.66)	3741 (66.6)	2629 (6.66)	5153 (16.6)
	4110 (6.66)	4813 (1.66)	2962 (16.6)	3941 (66.6)
	2273 (1.66)	2189 (66.6)	2291 (6.66)	4583 (16.6)
	2522 (16.6)	5276 (6.66)	2371 (66.6)	5010 (1.66)
	2410 (66.6)	2735 (16.6)	2741 (1.66)	5153 (6.66)
	3041 (6.66)	2188 (1.66)	2592 (16.6)	4424 (66.6)
	2006 (66.6)	3440 (16.6)	2410 (1.66)	5870 (6.66)
	3239 (1.66)	2826 (66.6)	1915 (6.66)	4011 (16.6)
	3010 (66.6)	3941 (16.6)	2567 (1.66)	4243 (6.66)
	2522 (6.66)	2962 (1.66)	3354 (16.6)	3810 (66.6)
	2213 (16.6)	1977 (6.66)	1814 (66.6)	3717 (1.66)
Region 10	3672 (6.66)		3779 (16.6)	3311 (66.6)
	5214 (66.6)	3687 (16.6)	2951 (1.66)	2575 (6.66)
	4260 (1.66)	5210 (66.6)		1649 (16.6)
	2066 (16.6)	2992 (6.66)	3536 (66.6)	3998 (1.66)
	3173 (1.66)	3622 (66.6)	3349 (6.66)	5245 (16.6)
	4217 (6.66)	5410 (1.66)	2962 (16.6)	3391 (66.6)
	2383 (1.66)	2176 (66.6)	2673 (6.66)	3440 (16.6)
	2176 (16.6)	4499 (6.66)	2006 (66.6)	5216 (1.66)
	3694 (66.6)	4858 (16.6)	2191 (1.66)	4331 (6.66)
	2190 (6.66)	2545 (1.66)	2467 (16.6)	5408 (66.6)
	2410 (66.6)	3841 (16.6)	2176 (1.66)	2841 (6.66)
	2673 (1.66)	2950 (66.6)	2861 (6.66)	3391 (16.6)
	6388 (66.6)	2658 (16.6)	2621 (1.66)	4216 (6.66)
	3010 (6.66)	1833 (1.66)	3899 (16.6)	3490 (66.6)
	2542 (16.6)	3082 (6.66)	2951 (66.6)	3440 (1.66)

TABLE IV. Continued

SKULL NO.	EM95	EM99	EM106	EM108
Region 11	4217 (6.66)	4499 (1.66)	2481 (16.6)	2951 (66.6)
	2552 (16.6)		2621 (66.6)	2992 (1.66)
	3281 (1.66)	2901 (66.6)	2861 (6.66)	5280 (16.6)
	3228 (66.6)	4626 (16.6)	2986 (1.66)	4011 (6.66)
	4387 (1.66)	3173 (66.6)	2273 (6.66)	2326 (16.6)
		6041 (6.66)	5673 (66.6)	3349 (1.66)
			2941 (6.66)	2621 (16.6)
			5461 (16.6)	6750 (66.6)
Region 12	4012 (6.66)	2537 (1.66)	4855 (16.6)	1904 (66.6)
	3779 (16.6)	2587 (6.66)	3560 (66.6)	3768 (1.66)
	3291 (1.66)	1833 (66.6)	2552 (6.66)	3941 (16.6)
	5624 (66.6)	3525 (16.6)	4033 (1.66)	5335 (6.66)
	4126 (1.66)	5110 (66.6)	3354 (6.66)	3687 (16.6)
	5295 (16.6)	3627 (6.66)	2481 (66.6)	3941 (1.66)
			4126 (6.66)	5135 (16.6)
	6253 (6.66)	4892 (1.66)	6183 (16.6)	5443 (66.6)
			5245 (1.66)	
Region 13	6090 (16.6)	6730 (6.66)	3009 (66.6)	1649 (1.66)
	5245 (66.6)	2068 (16.6)	3264 (1.66)	3483 (6.66)
	5226 (6.66)	2735 (1.66)	2986 (16.6)	3391 (66.6)
	3560 (66.6)	4331 (16.6)	3208 (1.66)	4653 (6.66)
	3354 (1.66)	2826 (66.6)	2567 (6.66)	3464 (16.6)
	2951 (16.6)	3420 (6.66)	1995 (66.6)	3581 (1.66)
	3027 (6.66)	3461 (1.66)	2191 (16.6)	3091 (66.6)
	2878 (16.6)	2522 (6.66)	2017 (66.6)	2273 (1.66)
	2304 (1.66)	2410 (66.6)	1904 (6.66)	2291 (16.6)
	2371 (16.6)	2291 (6.66)	1977 (66.6)	3025 (1.66)
	2910 (66.6)	2383 (16.6)	2056 (1.66)	2992 (6.66)
	2754 (6.66)	1595 (1.66)	2085 (16.6)	2542 (66.6)
	3354 (1.66)	2613 (66.6)	2080 (6.66)	2992 (16.6)
	2918 (6.66)	3464 (1.66)	2371 (16.6)	2711 (66.6)
	2951 (66.6)	2273 (16.6)	2542 (1.66)	3841 (6.66)
Region 14		6585 (6.66)	3998 (66.6)	2171 (1.66)
	5245 (66.6)	4177 (16.6)	3311 (1.66)	3173 (6.66)
	4863 (6.66)	2895 (1.66)	3445 (16.6)	2410 (66.6)
	2481 (66.6)	4675 (16.6)	3082 (1.66)	2428 (6.66)
	4884 (1.66)	3173 (66.6)	4292 (6.66)	3768 (16.6)
	3666 (1.66)	2962 (6.66)	2176 (66.6)	4151 (1.66)
	2918 (6.66)		2431 (16.6)	3627 (66.6)
	2735 (16.6)	4011 (6.66)	2567 (66.6)	2273 (1.66)
	2815 (1.66)	3841 (66.6)	1644 (6.66)	2986 (16.6)
	2658 (16.6)	3646 (6.66)	2236 (66.6)	3009 (1.66)
	3199 (66.6)	1925 (16.6)	1745 (1.66)	3420 (6.66)
	2613 (6.66)	2575 (1.66)	1732 (16.6)	2085 (66.6)
	3116 (1.66)	2080 (66.6)	2592 (6.66)	2357 (16.6)
	2953 (66.6)	1632 (16.6)	2621 (1.66)	4126 (6.66)
	3450 (6.66)	2467 (1.66)		2410 (66.6)

TABLE IV. Continued

SKULL NO.	EM95	EM99	EM106	EM108
Region 15	4110 (6.66)	2621 (1.66)	3899 (16.6)	5354 (66.6)
		2741 (16.6)		4326 (6.66)
Region 16	5486 (6.66)	2188 (1.66)	2878 (16.6)	6194 (66.6)
			5014 (1.66)	
Region 17	3899 (16.6)	2735 (6.66)	2643 (66.6)	4126 (1.66)
	4856 (1.66)	2189 (66.6)	2962 (6.66)	4972 (16.6)
	4177 (6.66)	2481 (1.66)	3173 (16.6)	3911 (66.6)
	3117 (66.6)	3810 (16.6)	2291 (1.66)	2962 (6.66)
	3091 (6.66)	3025 (1.66)	2371 (16.6)	4151 (66.6)
	5335 (16.6)	2481 (6.66)	3445 (66.6)	5640 (1.66)
	2918 (6.66)	3581 (1.66)	2481 (16.6)	2951 (66.6)
	3552 (66.6)	2279 (16.6)	2592 (1.66)	4331 (6.66)
	2941 (16.6)	2188 (6.66)	2371 (66.6)	3420 (1.66)
	3810 (1.66)	1732 (66.6)	3483 (6.66)	6417 (16.6)
		2552 (1.66)		
	4011 (1.66)	2068 (66.6)	2962 (6.66)	4242 (16.6)
	3464 (16.6)	2279 (16.6)	3445 (66.6)	
	4933 (1.66)	2191 (66.6)	4123 (6.66)	
Region 18	5774 (16.6)	3758 (6.66)	3589 (66.6)	2951 (1.66)
	4563 (1.66)		3091 (6.66)	3779 (16.6)
	4371 (6.66)	2613 (1.66)	3311 (16.6)	4766 (66.6)
	4060 (66.6)	3670 (16.6)	2085 (1.66)	4151 (6.66)
	3842 (6.66)	3009 (1.66)	2371 (16.6)	4675 (66.6)
	5264 (16.6)	2383 (6.66)	3220 (66.6)	6558 (1.66)
	3270 (6.66)	3391 (1.66)	2510 (16.6)	3687 (66.6)
	3379 (66.6)	1833 (16.6)	2552 (1.66)	5774 (6.66)
	4358 (1.66)	2383 (66.6)	3173 (6.66)	5731 (16.6)
	2912 (16.6)	1732 (6.66)	2643 (66.6)	2826 (1.66)
	3420 (1.66)	2279 (66.6)	3116 (6.66)	5774 (16.6)
		2857 (1.66)		
	3829 (1.66)	1745 (66.6)	3354 (6.66)	5317 (16.6)
	4653 (16.6)		3490 (66.6)	4954 (1.66)

TABLE V DURA MATER TENSION TESTS

SPECIMEN NO.	MAX. STRESS (P.S.I.)	RATE IN/MIN
262-1	1250	2
262-2	1120	2
260-1	910	2
270-1	1600	2
260-2	1310	2
260-3	1810	2
282-1	1200	2
282-2	1200	2
282-3	1800	2
281-1	1040	2
281-2	1950	2
288-1	1600	2
288-2	1200	2
288-3	1480	20
325-2	880	2
325-1	1040	2

APPENDIX A

THE MECHANICAL BEHAVIOR OF THE DIPLOË LAYER OF THE HUMAN SKULL IN COMPRESSION

THE MECHANICAL BEHAVIOR OF THE DIPLOË LAYER OF THE HUMAN SKULL IN COMPRESSION

by

J. W. Melvin
D. H. Robbins
V. L. Roberts
Highway Safety Research Institute
University of Michigan
Ann Arbor, Michigan

ABSTRACT

This paper presents an experimental study of the mechanical behavior of the diploë layer of the human skull in compression. Specimens of fresh human skull, obtained at autopsy, were tested at strain rates of 0.22 sec^{-1} and 2.2 sec^{-1} on an Instron testing machine. The modulus of elasticity, the compressive strength and the specific weight of each specimen were determined.

A linear relationship between compressive strength and compressive modulus of elasticity was found empirically for specimens that exhibited a sudden collapse mode of failure. The specific weight of the material was postulated to be the parameter relating the strength to the modulus and an empirical relation between average compressive strength and average specific weight was found. No significant strain rate effect was evident between the two test rates.

INTRODUCTION

The rational design of protective devices for the human body when it is subjected to high loads and accelerations requires a sound knowledge of the mechanical response of the system under such conditions. The human body is a highly complex system both from the viewpoint of the physician and the engineer. This complexity dictates the necessity of careful and thorough investigation when studying topics like the relation of mechanical behavior to injury. Since it is the response of the living human that is of interest, experimental conditions must approach the in vivo state as closely as possible. One of the most important regions of the human body with respect to serious injury is the head. Head injuries account for a large share of traffic fatalities. In the head, two major parts of interest in terms of injury are the brain and the skull. The work presented in this paper is part of a multiphase project directed at the determination of the mechanical properties of the constituent materials of the head. This paper deals with the behavior of unembalmed human skull bone subjected to compressive loading.

The structure of the skull is strikingly analogous to that of the modern day foam core sandwich shell. Like the sandwich shell it has an inner and outer layer of compact bone known as the inner and outer tables of the skull. These layers of dense bone are separated by a porous layer of bone known as the diploë layer of the skull. The porosity and thickness of the diploë layer vary considerably within a single skull ranging from a quite thick, open-structured layer to a layer with little porosity. In some regions it does not exist at all. In general, the diploë layer is quite pronounced in the frontal, parietal and occipital areas of the skull and is quite thin or non-existent in the temporal regions. Wide variations in the layer thicknesses also occur from skull to skull. The basic bone material in both the tables and diploë layer is collagen reinforced by particles of mineral (hydroxyapatite). The diploë layer achieves its porosity by weblike structures of the bone material known as trabeculae. Fig. 1 shows the features of both the tables and the diploë layer (the dark mark near the top of the specimen is an ink mark for identification of the orientation of the specimen in the skull and should not be confused with the structural features of the specimen).

In foam core sandwich shell structures the stiff layers of material on the inner and outer surfaces of the shell play the predominant role in determining the response of the shell to load. However, in many types of loading the overall performance of the shell depends on the core material's ability to perform its functions. Inadequate compressive or shear strength in the core material can significantly effect the total load carrying ability of the shell. Such is the case in the skull. The primary load carrying functions are performed by the tables and indeed, under general compressive impact to the skull the clinical evidence is usually tensile fractures of the outer table or of the entire skull thickness away from the point of impact. If the impacting load is localized, however, conditions can exist such that penetration of the outer table and crushing of the diploë layer occur without total failure to the skull. Thus, it would seem that in the case of compressive failure of skull bone it is most meaningful to talk of the diploë layer.

The purpose of the work reported here is to define the basic mechanical characteristics of the diploë layer in compression and to investigate factors which may influence the characteristics. An initial attempt was made to evaluate strain rate effects.

SPECIMEN ACQUISITION AND PREPARATION

The effectiveness of biomaterials testing programs depend greatly on an adequate supply of material. The fresh bone specimens used in this study were obtained at autopsy from the University of Michigan Medical Center and Veterans Administration Hospital in Ann Arbor. The specimens were removed using a Stryker bone plug cutter and Stryker Autopsy Saw. Special care was taken not to heat the bone during the cutting. The plugs taken at the UM Medical Center were 3/4 inches in diameter and those from the VA Hospital were 1 1/2 inches in diameter. Each bone plug removed has a complete record as to sex, age, cause and time of death, and autopsy number. By recording the autopsy number it is possible to go back into the patient's medical history if necessary. Each plug was given a coding number to indicate the source hospital, the chronological order and region of the skull the plug was located in. The distances and orientation of the plug relative to the sagittal, coronal and/or the lamboidal suture lines were also noted.

The fresh bone plugs were placed in a freezer at -10°C within thirty minutes from the time of removal from the skull. From our experience and data in the literature (1) it was determined that this was the best method to store the specimens. The test specimen developed for this program had a nominally cubical shape 1/8 inches on a side. In the work reported here the specimens consisted entirely of diploë layer material. The reasons for eliminating the upper and lower table material from the specimen were to obtain a constant gage length of the material of interest and to allow determination of the stiffness of the diploë layer without having to consider the stiffness of the tables in series with it. Depending on the curvature of the bone plug and the thickness of the diploë layer the small size of the test specimen allowed as many as twenty-four specimens to be obtained from a 1 1/2 inches diameter bone plug. The test specimens which were machined on a Unimat-SL set up as a milling machine were handled in such a manner that no heating of the material occurred. After fabrication the test specimens were either tested immediately or refrozen until needed.

EXPERIMENTAL PROCEDURE

The first step of the test procedure was to determine the dimensions of the test specimen using a micrometer. Next, the weight of the specimen was obtained using a Voland 640-D balance and the specific weight of the specimen calculated. The specimen was then tested using an Instron floor model testing machine as shown schematically in Fig. 2. A Kistler 937A Force Link was used to measure the load on the specimen. This piezoelectric load cell has a maximum load capacity of 45,000 lbs. in compression with a resolution of 0.1 lbs. and a resonant frequency of 22.5 KHz. Crosshead velocities of 2 inches/minute or 20 inches/minute were used. Initially, a deflectometer consisting of a strain gaged, thin cantilever strip was used to transduce the deformation of the specimen. It was found, due to the very stiff load cell being used and the relatively low stiffness of the specimens, that crosshead travel could be used as an accurate indication of the specimen deformation. The tests were recorded on a Tektronix Type 564 Storage Osiclloscope and then photographed with a Polaroid camera. When the deflectometer was used the load was displayed against the deflection. In the tests without the deflectometer the load was displayed against time. Fig. 1 shows a specimen with the tables present before and after testing. The amount of compressive deflection was controlled in order to allow microscopic examination of the tested specimens.

After the tests, some of the specimens were decalcified, embedded in paraffin and thin sections cut on a microtome for microscopic examination to determine modes of failure.

A total of fifty-two individual tests on specimens from five different skulls are reported in this paper. Half of the tests were conducted at the 2 inches/minute crosshead speed and the other half conducted at 20 inches/minute. The average strain rates corresponding to the two crosshead speeds are 0.22 sec^{-1} and 2.2 sec^{-1} respectively. Approximately half the specimens from each bone plug were run at each strain rate.

RESULTS AND DISCUSSION

In Fig. 3 are shown the two characteristic types of load-deflection curves which were found in this series of experiments. The majority of the specimens showed an abrupt failure at approximately the 4-5% strain level with a corresponding drop in load followed by subsequent build-up of load upon further deformation. The numerical data given in this paper is based on these tests. With this type of behavior the peak load before the unstable collapse was taken as the failure load and the failure stress was calculated using that load and the initial cross-sectional area of the specimen. The initial portion of the load-deformation curve is nonlinear. This is probably the result of the specimen becoming firmly in contact with the loading anvils. This small nonlinear region is followed by a considerable linear region. The linear region was followed by a second nonlinear region with a slope decreasing to zero at failure. Considering the relative magnitude of the linear region, a modulus of elasticity can be defined for the specimen material. The modulus was calculated from the slope using the initial height of the specimen as the gage length and the initial cross-sectional area.

The other type of behavior shown in Fig. 3 is exhibited by specimens with specific weight approaching that of compact bone. The ductile, monotonically increasing load-deformation curve of this type specimen cannot be compared to the rapid collapse behavior of the more porous diploë layer because the basic modes of failure are completely different. The rapid collapse failure exhibited by the specimen shown in Fig. 1 is brought about by tensile tearing and spliting of the trabeculae of the diploë layer. The micrograph shown in Fig. 4 demonstrates this phenomenon clearly. The ductile behavior of the dense diploë layer specimens is associated with yielding of the bone material probably due to shear stresses.

The test results, at first glance, appeared to have the wide variation attributed to biological materials as "biological variation". The values of compressive strength σ_c ranged from a low of 1820 lb/in^2 to a high of 11,350 lb/in^2 and the values of the compressive modulus of elasticity E_c ranged from a low of 0.57×10^5 lb/in^2 to a high of 3.99×10^5 lb/in^2. This range of values for compressive strengths is closely comparable to that of Evans (2). However, the diploë layer is a porous material and both σ_c and E_c should depend, in the same manner, on the actual amount of load carrying material existing across the cross-section of the specimen. This concept can be evaluated by plotting σ_c against E_c as shown in Fig. 5. The result is a linear empirical relationship between compressive strength and compressive modulus of elasticity of the form

$$\sigma_c = 2.9 \times 10^{-2} E_c \tag{1}$$

The average amount of material present in the specimen cross-section is directly related to the specific weight of the specimen. Thus, the structural features relating σ_c to E_c can be embodied in the specific weight of the diploë layer, γ_D. A plot of the averages of the compressive strengths of the specimens from each bone plug versus their average specific weights is shown in Fig. 6. It is evident from Fig. 6 that the compressive strength σ_c and therefore the compressive modulus of elasticity E_c are strongly influenced by the specific weight of the diploë layer γ_D. The relationship of σ_c to γ_D has the form

$$\sigma_c = 8.06 \times 10^{11} \gamma_D^6 \tag{2}$$

No significant strain rate effects were noted in the data. However, both strain rates must be considered quasi-static even though they are an order of magnitude apart. This may also be due to the fact that the collapse failure is a brittle behavior and therefore not subject to marked strain rate effects. In Fig. 5 an indicated extrapolation toward the region of compact bone properties is indicated. Because a transition from the collapse mode of failure to the ductile mode of behavior is occurring, the linear relation of compressive strength to compressive modulus may not hold. Indeed, it depends somewhat on the criteria for determining when failure has occurred. It is expected that strain rate effects such as those found by McElhaney (3) will begin to appear due to ductile behavior as indicated by the bifurcation of the dashed lines. Work is now in progress at higher strain rates up to 2,000 sec^{-1} in order to investigate the findings of this paper in the impact range of strain rates.

CONCLUSIONS

Some conclusions may be drawn from the results which have been reported in this paper:

1. The diploë layer of the skull bone is subject to biological variability leading to a rather wide range of ultimate strengths and elastic moduli.

2. Biological variation in failure stress and elastic modulus are shown to be functions of density and porosity of the material.

3. Compressive strengths for diploë material were found ranging from a low of 1820 lb/in^2 to a high of 11,350 lb/in^2 whereas values for compressive modulus ranged from a low of 0.57×10^5 lb/in^2 to a high of 3.99×10^5 lb/in^2.

4. Due to the weblike structure of diploë a buckling of the trabeculae defines the mode of failure. This mechanism is not observed in specimens of compact bone.

5. A linear-elastic compression modulus may be defined for the diploë layer of the skull bone.

6. No strain rate effects were observed at 0.22 sec^{-1} and 2.2 sec^{-1}.

ACKNOWLEDGMENTS

The authors acknowledge the assistance of I. Barodawala in performing the experiments and data analysis in this test program. This project has been carried out under Contract No. PH 43-67-1136 with the National Institute of Neurological Diseases and Blindness of NIH.

REFERENCES

1. Frankel, V. H., "The Femoral Neck," Almquist and Wiksells, Uppsala, Sweden.
2. Evans, F. G. and Lissner, H. R., "Tensile and Compressive Strength of Human Parietal Bone," Journal of Applied Physiology, Vol. 10, No. 3, 1957, p. 494.
3. McElhaney, J. H., "Dynamic Response of Bone and Muscle Tissue," Journal of Applied Physiology, Vol. 20, No. 4, July 1966, pp. 1231-1236.

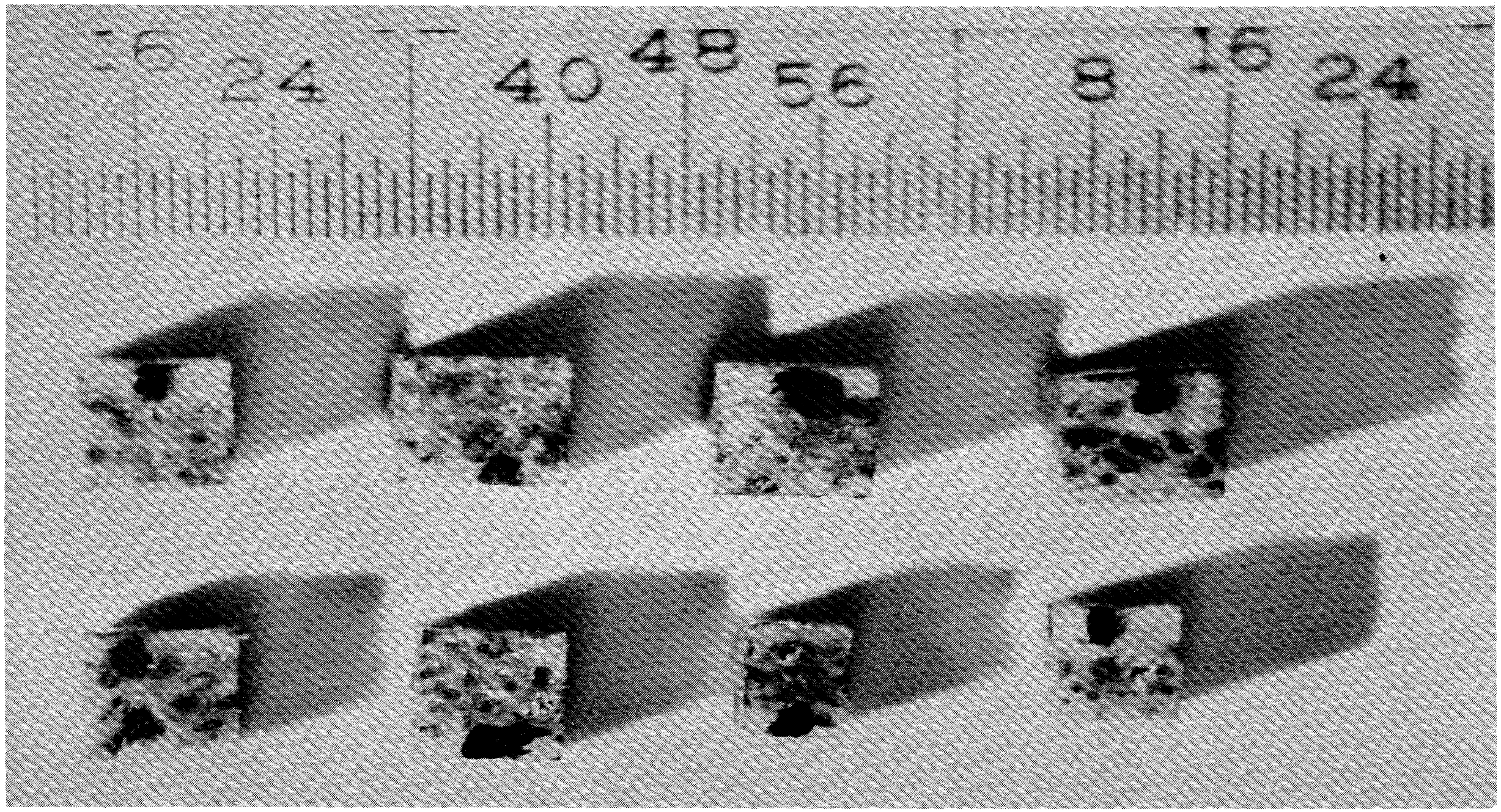

FIGURE 1. Typical Specimens Before Testing

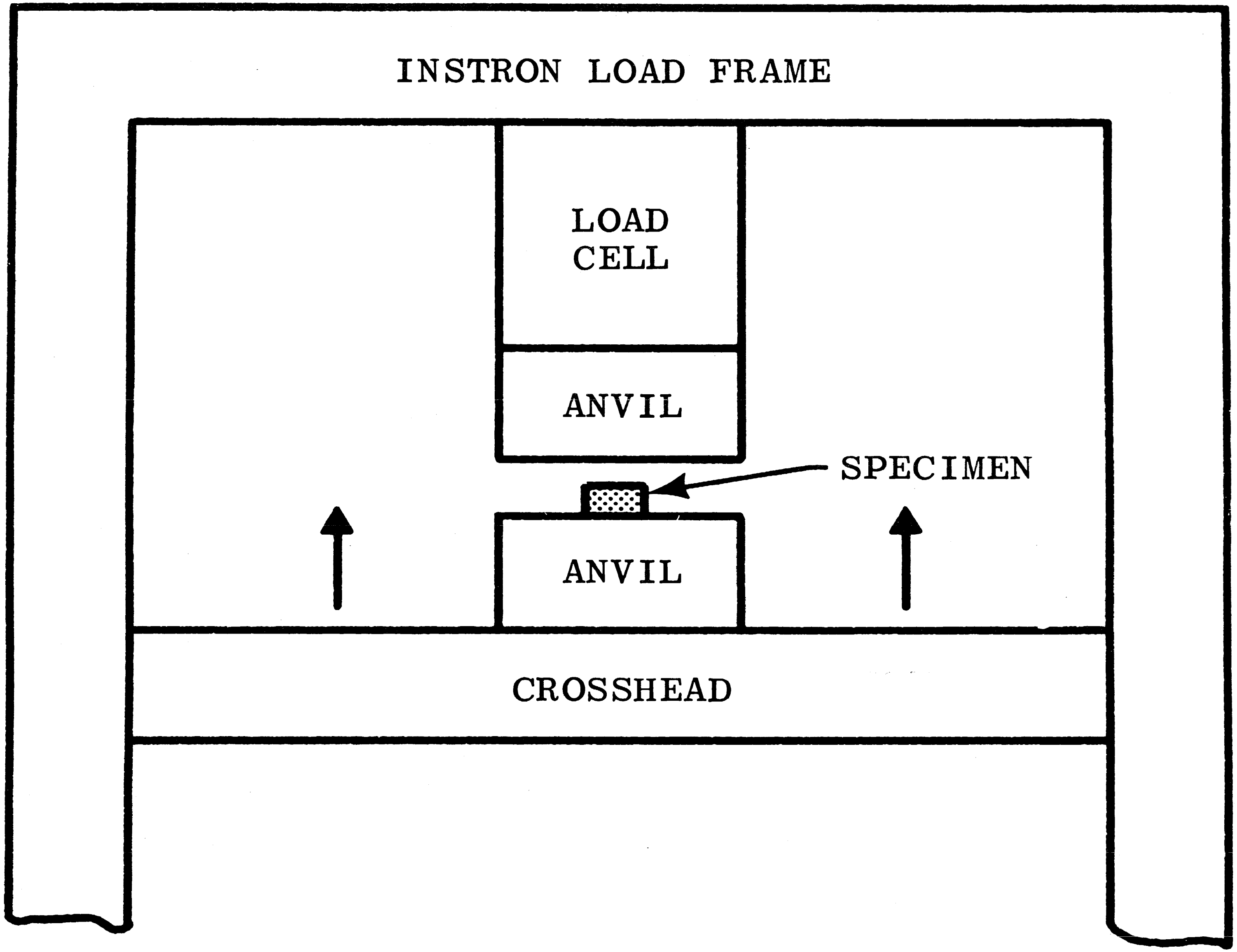

FIGURE 2. Schematic of Test Layout

TYPICAL BEHAVIOR
OF A POROUS
DIPLOË LAYER
SPECIMEN

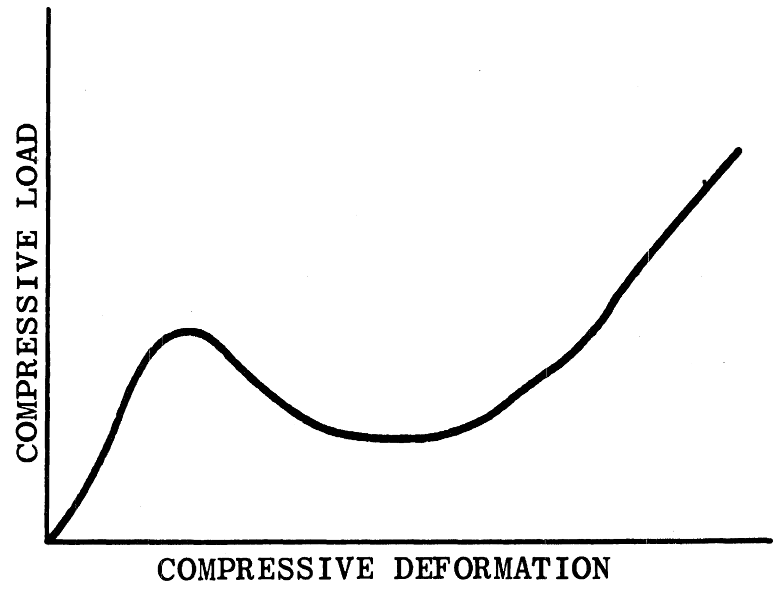

TYPICAL BEHAVIOR
OF A SLIGHTLY
POROUS DIPLOË
LAYER SPECIMEN

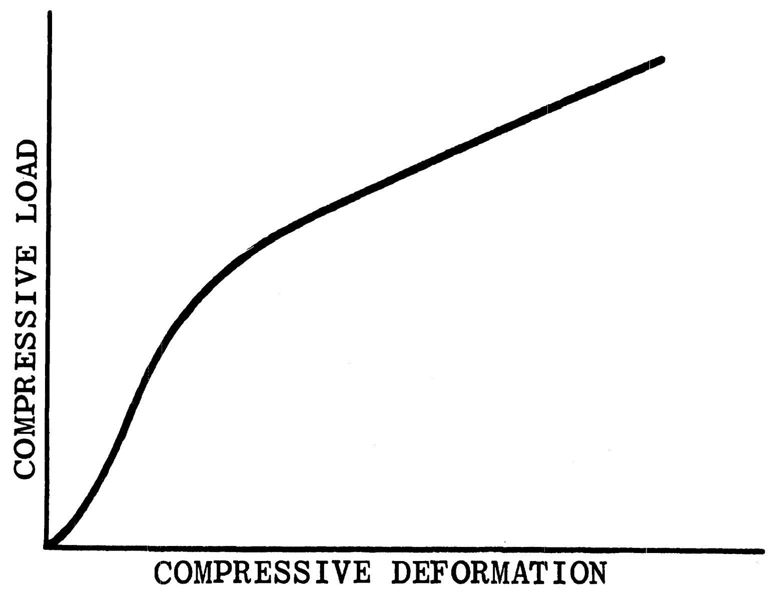

FIGURE 3. Types of Characteristic Load-Deformation Behavior

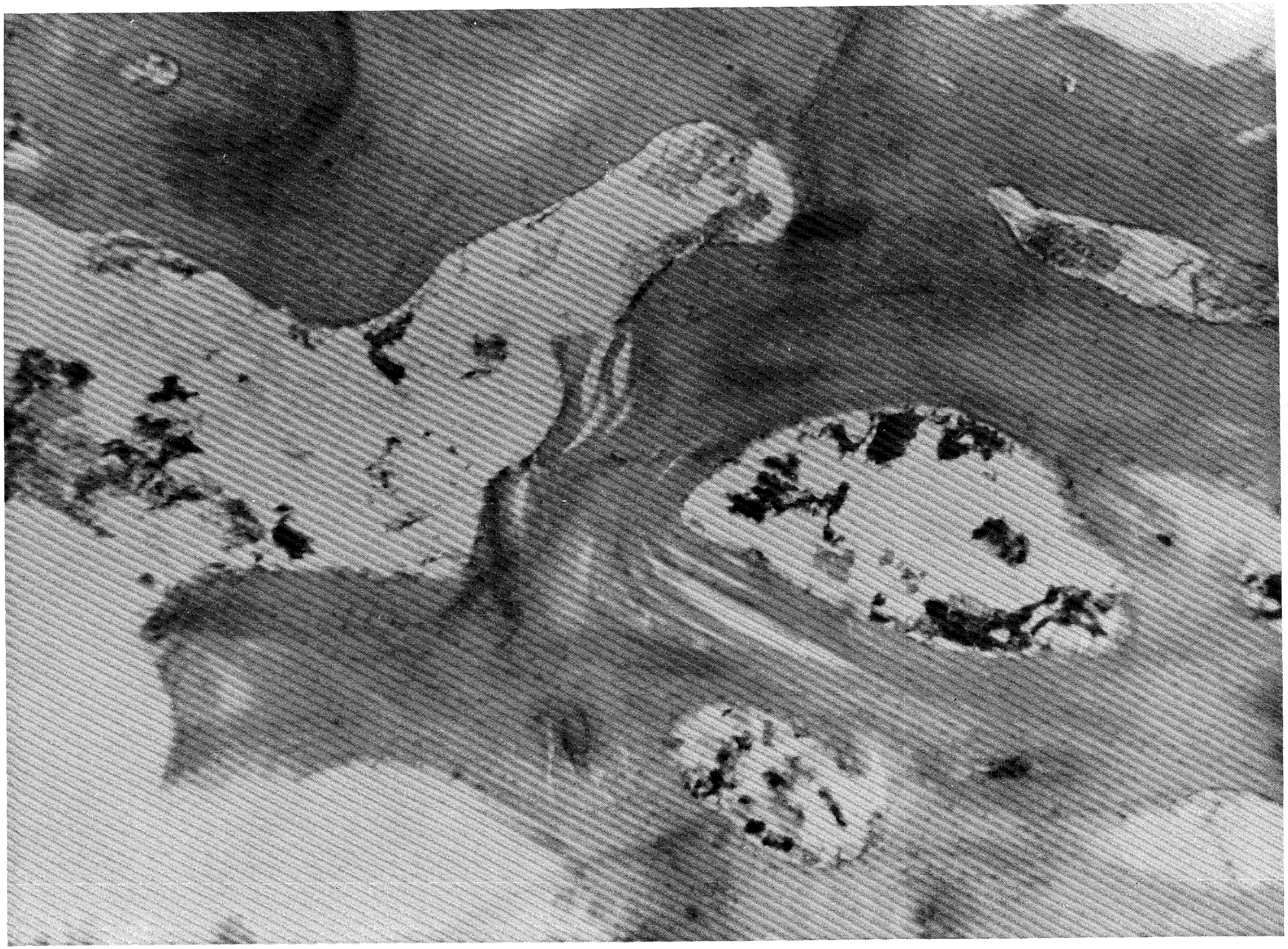

FIGURE 4. Micrograph of Failed Region of Diploë Layer

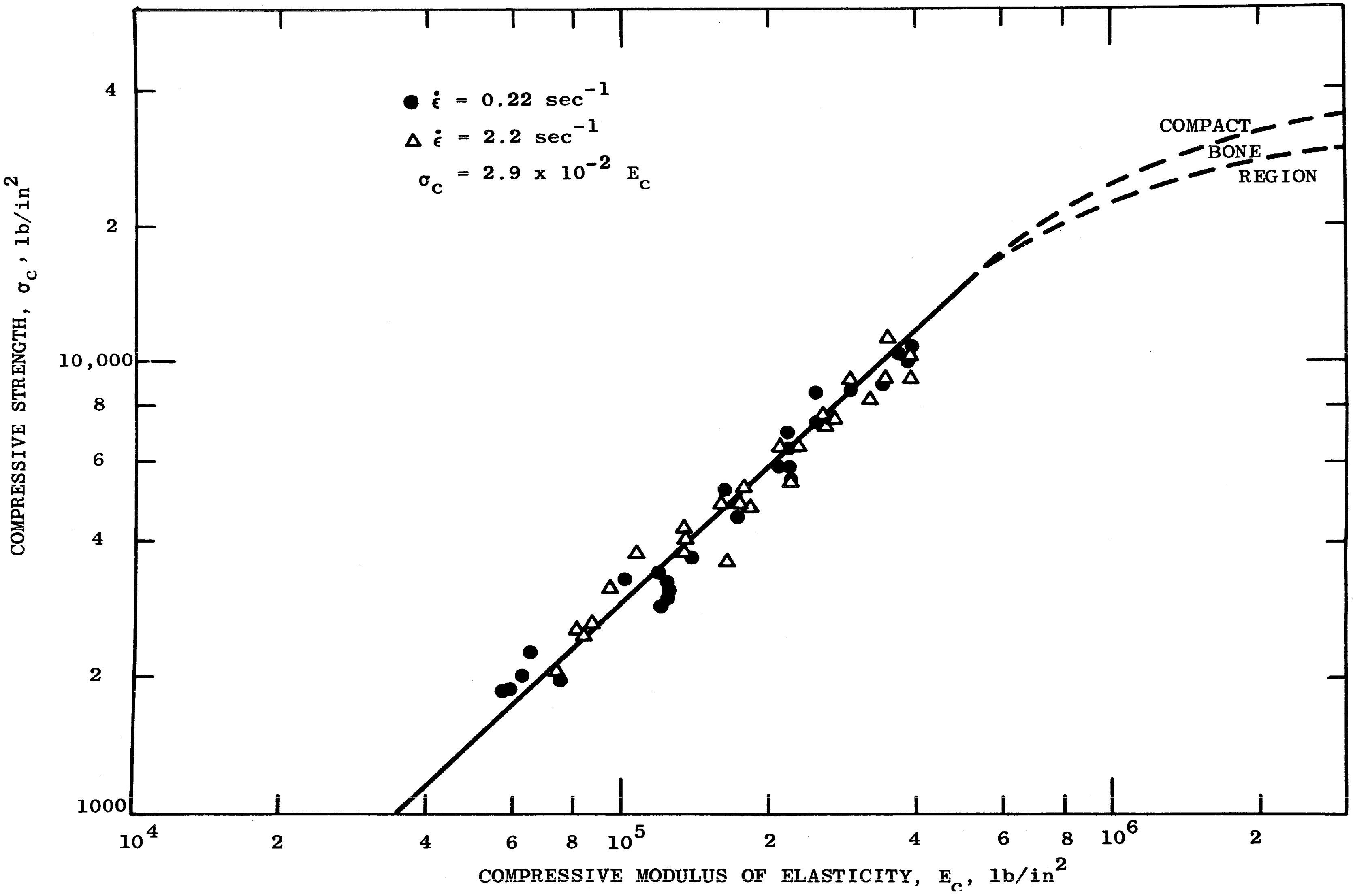

FIGURE 5. Compressive Strength Versus Compressive Modulus of Elasticity

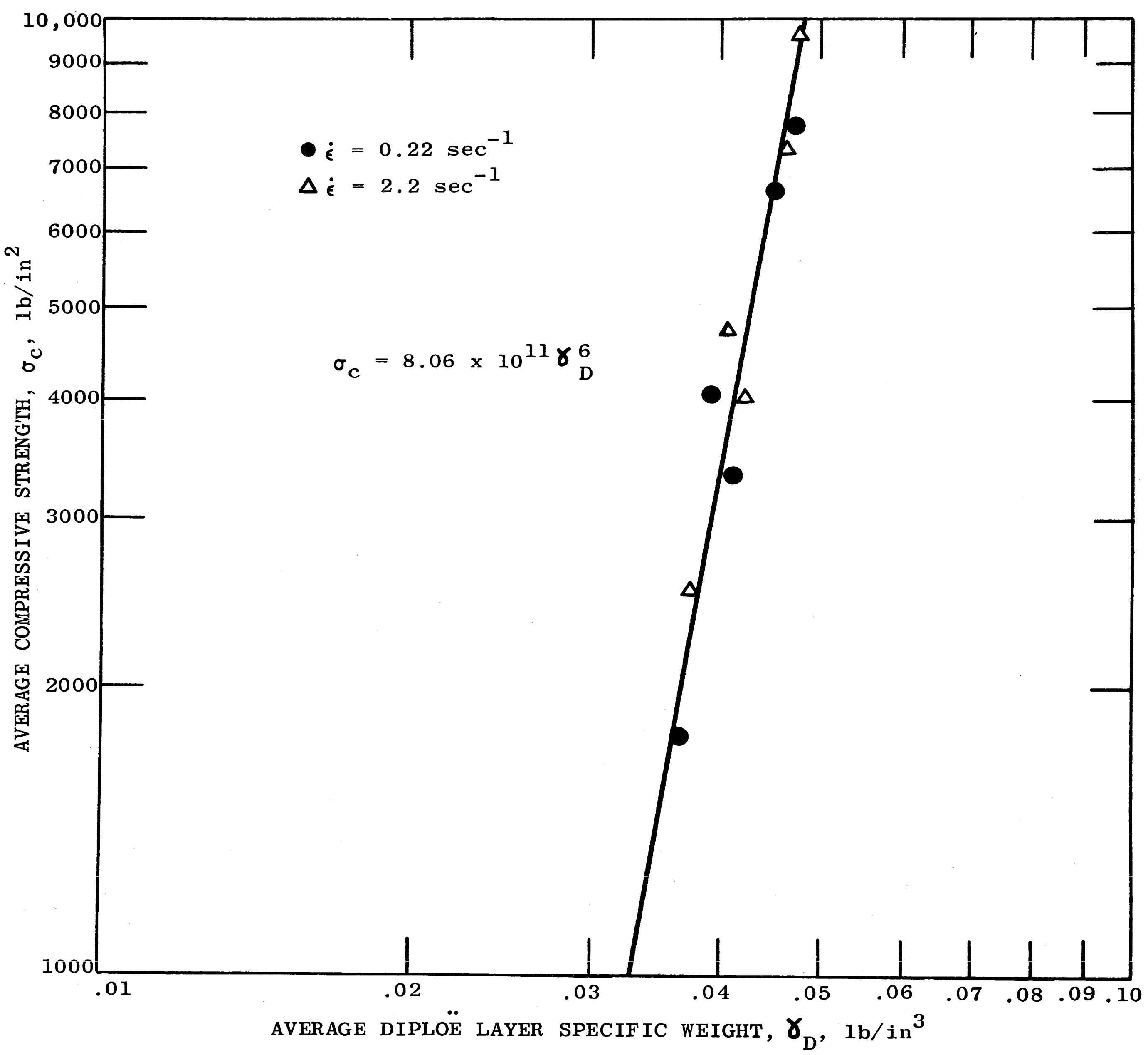

FIGURE 6. Average Compressive Strength Versus. Average Diploe Layer Specific Weight

APPENDIX B

DYNAMIC MECHANICAL PROPERTIES OF HUMAN BRAIN TISSUE

DYNAMIC MECHANICAL PROPERTIES OF HUMAN BRAIN TISSUE

G. T. Fallenstein
V. D. Hulce
Dow-Corning Corporation
Midland, Michigan

and

J. W. Melvin
Highway Safety Research Institute
The University of Michigan
Ann Arbor, Michigan

ABSTRACT

Investigators have been studying the mechanical phenomena associated with impact to the head for many years. Several theories on the behavior of the brain during head impact have come from these studies but there has been a notable lack of information on the bulk mechanical properties of the brain which are necessary for the evaluation of these theories. This paper represents an initial attempt at providing such information.

The dynamic complex shear modulus of in vitro samples of human brain have been measured. Specimens from eight brains have been subjected to a sinusoidal shear stress input under resonant conditions in an electro-mechanical test device. Tests were conducted to determine the effects of time after death, refrigeration of material and shear strain dependence. A device to measure the dynamic properties of brain in vivo is described and preliminary data on in vivo tests on Rhesus monkeys is presented.

The results of the dynamic shear testing on in vitro human brain indicate that the storage modulus G' lies between 6-11 x 10^3 dynes/cm^2 the loss modulus G" lies between 3.5-6.0 x 10^3 dynes/cm^2 and the loss tangent tan δ is in the range 0.40-0.55.

INTRODUCTION

The mechanical phenomena associated with accelerations and impacts to the head have been studied by a number of investigators over the years. The prime interest in these studies has been the motions of the brain and its subsequent damage or malfunction. Holbourn (1943) proposed on theoretical grounds that injury to the brain is caused by shear strains. These shear strains can be produced in the brain at the point of impact due to severe deformation or fracture of the skull resulting in contact of the brain, or they can be produced remotely from the impact point due to the rotations of the brain within the skull. Holbourn also proposed that concussion is uniquely the result of rotation. Pudenz and Sheldon (1946) and Ommaya (1966) reported on experiments in which Rhesus monkeys were fitted with transparent plastic calvaria and subjected to head impact. The motions of the brain during impact were easily visible and tended to confirm Holbourn's predictions of brain rotational movement. Martinez (1963) has shown that brain injury in rabbits can be produced by the rotational motions of severe whiplash alone without impact to the head.

Other theories of brain injury being proposed at the present time are based on the idea of a hydrostatic tension being produced in regions of the brain during impact. Goldsmith (1966) discussed the concept of a compressive wave in the brain caused by an impact being reflected from the inner surface of the skull back into the brain as a tensile wave which could result in damaging cavitation phenomena. Unterharnscheidt (1966) also proposed a caviation phenomena but attributes its formation to an inertia process wherein the brain tries to separate from the skull as the skull accelerates upon impact.

The final correlation of head injury theories with head injury experiments has not been forthcoming because of the almost complete lack of knowledge of the mechanical properties of brain tissue. Goldsmith (1966) has pointed out this problem and has suggested some of the pertinent properties to be determined. Ommaya (1968) has reviewed the scientific literature pertaining to the mechanical properties of the tissues of the nervous system. In the case of brain tissue, only three papers on the mechanical properties of brain were found. Franke (1954) determined the coefficient of shear viscosity from calculations made on data from driving point impedance measurements of a glass sphere vibrating within whole, fresh pig brain and pig brain homogenates at frequencies of 150 to 500 Hz. The viscosity was reported to be similar to that of room temperature glycerin. Creep experiments were performed by Dodgson (1962) on fresh mouse brain in an attempt to determine the Mises-Hencky flow condition under static compression. Koeneman (1966) studied creep and dynamic cyclic properties from rabbits, rats and pigs. Again, the loading condition was compression. All of the above methods have been in vitro tests on species other than primates. Ommaya emphasized the importance of future studies including in vivo experiments to check the validity of the in vitro work and the use of animals suitable for scaling the data for extrapolation to human brain.

The purpose of this paper is to report the results of the initial phase of a program to provide information on the mechanical properties of human brain pertinent to the problem of head injury. Both in vitro and in vivo techniques were used. In accordance with the concepts of shear strain mechanisms of brain injury, the dynamic shear properties of in vitro human

MATERIALS AND METHODS

A. In Vitro Testing

The complex dynamic shear modulus (G^*) of a viscoelastic material is defined as the vector sum of G' and iG'', with G'' normal to G'. G' is the dynamic elastic modulus and is a measure of the spring stiffness of the test material under shear stress. G'', the dynamic loss modulus, is a measure of the damping ability of the material and represents viscous losses in the material. The relative damping ability of the material, $\tan \delta$, is defined as G''/G'.

G^* is determined by applying a dynamic shear stress to the visco-elastic test material and measuring the resulting strain. The Dynamic Mechanical Apparatus (DMA) consists of a sinusoidally actuated mechanism for shearing the sample and electronic equipment to monitor input force, strain level (output) and the phase angle between them. See Figure 1. The sample shear mechanism is centrally located on a magnesium-aluminum alloy rod which connects twin electro-mechanical transducers. The driving signal, from a function generator operating in the sine mode, is connected to one transducer. The other transducer provides an output signal, operating as a velocity transducer. The input force is determined by the current to the driving transducer; strain and strain rate are measured by the output voltage and amplitude. The driving amperage and output voltage are measured on a vacuum tube voltmeter. (The amperage is measured as a voltage across a shunt resistor on the driving transducer.) The input and output signals are displayed as an x-y (Lissajous) plot on an oscilloscope to aid the operator in placing the system in resonance. The input frequency is read directly from the function generator control. Input force is adjustable by means of the function generator signal level control. An auxiliary amplifier is provided for increased signal strength, if needed.

The sample shearing mechanism consists of a horizontal aluminum base plate rigidly attached to the magnesium-aluminum rod and a clear plastic plate which is positioned above, and parallel to, the aluminum base plate. This plastic plate is rigidly attached to the main structure of the DMA and is vertically adjustable. The test sample is sandwiched between these two plates. The sample section, between the twin transducers, is enclosed in a chamber heated by a small electrical heater-fan system. The temperature is controlled by means of a temperature potentiometer which utilizes an iron-constantan thermocouple placed adjacent to the sample.

The DMA operates as a subtractive impedance device, i.e., the impedance of the unloaded system must be subtracted from that of the system with the sample in place. This is accomplished by obtaining a master curve of input amperage (I_0) and resonant frequency (f_0) as functions of test amplitude and then subtracting these values from the raw test data for corresponding amplitudes. All measurements are obtained with the system in resonance. Briefly stated, the data reduction consists of the following equations:

$$G' = q(\omega^2 M - \omega_0{}^2 M) \qquad (1)$$

$$G'' = \omega q C \left(\frac{I - I_0}{E}\right) \qquad (2)$$

$$|G^*| = [(G')^2 + (G'')^2]^{1/2} \qquad (3)$$

$$\tan \delta = G''/G'$$

where: q = Sample shape factor, height/area,

$\omega = 2\pi f$,

M = Vibrating mass of DMA, 243 grams,

C_2 = Force constant of DMA, 1.53×10^6 gm-ohm-sec^{-1},

I = Driving amperage,

E = Output voltage,

Subscript zero indicates values for the DMA without sample and at corresponding amplitude.

The apparatus and data reduction are based on the work of Fitzgerald and Ferry (1953). The dynamic viscosity (η_0) and spring (k) constants are obtained from the relations

$$\eta_0 = G''/\omega \tag{4}$$

$$k = G'/q \tag{5}$$

The test procedure includes the following operations:

(1) The sinusoidal input amperage and frequency are adjusted to yield resonance at the desired strain level.

(2) The resonant frequency (f), input amperage (I), and output voltage (E) are recorded.

(3) Steps (1) and (2) are repeated for each desired strain level.

(4) A photograph of the sample is taken vertically from the overhead position. The sample area (A) is determined by using a planimeter.

(5) The sample height (h) is determined by a vernier micrometer.

(6) Steps (1) and (2) are repeated without a sample (i.e., unloaded), in order to obtain master curves of (f_0) and (I_0) versus strain level.

Human brain sections, taken at autopsy, were obtained from the Veterans Administration and University of Michigan Hospitals in Ann Arbor. The sections were packed in polyethylene bags and placed on ice and water within 10 minutes after removal from the skull. They were then transferred to Dow Corning within 2.5 hours. Initial tests were run immediately upon receipt. Subsequent storage was at 3°C., since early tests on Rhesus brain confirmed that gross change occurs in the modulus upon freezing the tissue. Freezing lowered the storage modulus approximately an order of magnitude and the loss modulus by a factor of three.

Rectangular solid test specimens with the approximate dimensions of 2 cm x 3 cm and 0.4 to 0.7 cm in height were used. Both of the sample-holder plates contacting the specimen were scored with a cross-hatch pattern to reduce slippage. An aerosol adhesive was sprayed on both plates to further reduce slippage. The test specimen was placed on the base plate and the cover plate was then allowed to rest in light contact with the upper specimen surface before being rigidly secured to the DMA frame. A plastic cover was placed over the sample section to form the test chamber and the temperature was adjusted to test specifications. Testing was begun after a 15-minute equilibration period.

A total of 13 samples of human brain tissue from eight individuals has been tested in vitro utilizing the DMA. All of the samples were cerebral white matter and were tested at 37°C. The tests were conducted at 9 to 10 Hz.

In order to describe the specific test procedure for each sample, two terms are employed. A scan consists of approximately six individual measurements conducted in rapid sequence, generally moving from low to high strain levels. Strains approaching 0.37 were achieved during the testing, though not for all samples. A series consists of a number of scans conducted in rapid sequence. Each test was numbered to identify it as to type of brain, specific brain, and specific scan.

(B) In Vivo Testing

The Dynamic Mechanical Apparatus, though suitable for in vitro testing, can not be used in in vivo testing. To meet the need of an in vivo test, a small driving point impedance device was constructed. Termed the Dynamic Probe

Apparatus (DPA), it consists of a sinusoidally-driven probe attached to an impedance head, and associated electronic equipment for signal conditioning and display.

The output shaft of a small electrodynamic vibrator (shaker) is connected to the impedance head. A flat-ended, cylindrical probe of 0.1 cm^2 cross-sectional area, mounted on the impedance head, transmits the sinusoidal motion of the shaker output to the test material and measures the transmitted force. An accelerometer mounted on the impedance head measures the acceleration of the probe. See Figure 2.

The apparatus functions as a driving point impedance device. The output consists of the force transferred from the probe to the test material and the dynamic displacement of the probe. The force transducer measures a composite signal consisting of the force transferred to the test material and the force caused by the acceleration of the probe mass. This latter force component is subtracted from the composite signal in order to obtain the desired transfer force function. This is accomplished with the acceleration transducer, by electronically subtracting an acceleration signal, equal in magnitude to the mass acceleration of the probe, from the composite signal. The accelerometer output is also utilized to measure dynamic displacement by electronically shifting it 180° out of phase (i.e., inverting it). The resultant signal is proportional to displacement, at a given frequency.

The transferred force and dynamic displacement signals are displayed on a dual-beam oscilloscope. Both linear and x-y (Lissajous) plots are possible. The Lissajous figures are recorded with a Polaroid camera mounted on the oscilloscope. A complete test record is recorded on magnetic tape.

Subjects tested in initial experiments using the DPA were young adult Rhesus monkeys (Macaca mulatta) ranging from 4.5 to 5.5 Kg and anesthetized with phencyclidine hydrochloride and sodium pentobarbital. The right internal carotid artery was cannulated for blood pressure monitoring and the right internal jugular vein was cannulated for saline infusion and drug administration. Subjects were mounted in a primate chair and the head secured with a surgical head holder through an intra-orbital to dental clamp. The cranial test sites were prepared after a midsagittal incision in the scalp and separation of the overlying skin and the galea aponeurotica. At a point located according to coarse stereotaxic position over the medial area of the precentral gyrus, a burr hole was made in the calavarium and enlarged with a 3/8 inch trephine. Upon attaining hemostasis the dura mater under the test site was removed. Either one test site or two contralateral sites were prepared.

The DPA was then positioned over the monkey's head so that the probe tip would be able to contact the exposed cerebral cortex. After positioning, the probe could be pressed into the brain surface through a screw drive mechanism on its crosslide mount and the static brain deformation measured with an attached dial indicator. The pia-arachnoid was not punctured during the tests.

While at a specified static deformation the probe was driven with a small sinusoidal amplitude and the force and acceleration signals from the probe recorded. These signals were displayed on an oscilloscope and also recorded on magnetic tape. The oscilloscope display permits a simple analysis of tan δ and the recorded data will be digitized and used to solve a model of the brain-probe system.

In tests where the dynamic mechanical properties were measured as a function of blood pressure, the arterial pressure was controlled by intravenous infusion of a 0.1% solution of trimethaphan camphorsulfonate in Ringer-Locke solution. The infusion rate was adjusted to get the desired blood pressure depression, which could be restored to normal values by stopping the administration.

RESULTS

A. In Vitro Tests

Initial tests yielded modulus values which increased with time as the test series progressed. This increase has been attributed to sample drying. Subsequent tests were conducted in a high-humidity environment and generally with a very thin coating of a silicone adhesive on the sample surface. Values of G' and G" for a typical test (HBM-6-20) are shown in Figures 2 and 3. The first scan of a series yields a strain-dependent modulus whereas the second and third scans do not give a determinable indication of strain independence. Repeated series following a period with the specimen at rest yield similar results, with the modulus returning to the same level as in the previous series during the first scan and remaining so through subsequent scans. This repeatability indicates that there is no rapid irreversible change occurring as a result of the test environment. It is concluded that the change in modulus during the first scan shows not a strain dependence, but a conditioning caused by shear. Stiffening of the specimen edge while at rest is likely, relieved by shear or redistribution of moisture under shear. Thixotropy has not been ruled out, however.

Table I summarizes the modulus values obtained from all tests conducted on the eight brains, listing the steady-state values from shear-conditioned samples. Based on the above interpretation, these tests indicate that G' lies between 6-11 x 10^3 dynes/cm^2, G" lies between 3.5-6.0 x 10^3 dynes/cm^2, and tan δ is in the range 0.40 to 0.55.

B. In Vivo Tests

Using the DPA and the experimental procedure discussed above, Lissajous figures of force versus deformation have been obtained on eight Rhesus monkeys. The experiments were designed to examine the effects of static probe deformation, dynamic amplitude, frequency and systemic blood pressure on the in vivo dynamic behavior of the brain. The animals were sacrificed during the experiments and postmortem effects were studied. In vitro tests on Rhesus monkey brain were also performed.

Figure 5a shows a typical high amplitude (30×10^{-3} cm) test result demonstrating a highly asymmetric Lissajous figure. This type of figure can not be analyzed by present techniques. The symmetric Lissajous plot in Figure 5b is typical of the lower amplitude tests (2.5×10^{-3} cm). The symmetry of this type of sinusoidal force Lissajous pattern allows certain dynamic constants to be calculated (Gehman, 1957) after suitable analysis but allows the loss tangent tan δ to be calculated directly as indicated in Figure 5b.

A complete analysis of the test results in terms of the basic dynamic shear moduli depends on a mathematical analysis of the DPA-brain system now in progress. This analysis will allow direct comparison with the in vitro results of the previous section. It is possible, however, to present values of tan δ for in vivo Rhesus monkey cerebral cortex as a function of blood pressure as shown in Figure 6. These results for a single amplitude test (2.5×10^{-3} cm) show a decreasing tan δ with decreasing blood pressure.

DISCUSSION

In view of the very soft nature of brain tissue, the values of the in vitro dynamic shear moduli are not surprising. The lowness of these values is emphasized when they are compared to soft engineering materials as shown in Figure 7.

Approximate values of the shear elasticity and shear viscosity of soft human body tissue have been calculated by von Gierke et al. (1952) from impedance measurements. The value of the shear elasticity was found to be 2.5×10^4 dynes/cm^2 and the shear viscosity was 150P for in vivo muscular tissues. Comparison of G' values from the in vitro brain test ($6\text{-}11 \times 10^3$ dynes/cm^2) with this approximate shear elasticity coefficient places the in vitro human brain stiffness just below that of in vivo human muscular tissue. Equation (4) can be used to calculate the dynamic shear viscosity η_0 for the in vitro human brain giving a range of 56 to 96P, which again places it just below that of in vivo human muscular tissue. Koeneman (1966) found the dynamic elastic compression modulus of in vitro brain white matter of rabbits, rats and pigs to lie in the range from 0.8 to 1.5×10^5 dynes/cm^2. The compression modulus is approximately three times the shear modulus for a linear viscoelastic material of this type, thus his values are equivalent to a G' range of 2.7 to 5×10^4 dynes/cm^2, somewhat higher than von Gierke's values for muscular tissue. Koeneman reported a dynamic viscosity of 43.5P while Franke (1954) reported a shear viscosity of 14.9P calculated from impedance measurements on in vitro pig brain. Dividing Koeneman's value by three gives a dynamic shear viscosity of 14.5P, in close agreement with Franke. Both of these values were calculated from data obtained in the frequency range of 100 to 500 Hz. Since the in vitro tests reported in this paper were performed at 9 to 10 Hz, the differences between the shear viscosity coefficients could very well be due to variation of the dynamic properties with frequency, a situation found in most viscoelastic materials. The possibility of differences between the mechanical properties of the brain in lower animals and those of primate brain cannot be ruled out, however. Ommaya (1966) discussed the high impact tolerance of small animals with their compact brains which are not as deformable as larger brains.

The high values of tan δ (Table I)obtained in the in vitro testing characterize the brain tissue as a material with high internal damping. These high values correlate with the in vivo test as shown in Figure 6 where the tan δ for zero blood pressure approaches the range found for in vitro human brain. The indications from this initial in vivo to in vitro correlation are that the test will provide the means for resolving the questions of postmortem changes, blood pressure effects and frequency effects on the dynamic properties of brain tissue. Von Gierke (1966) showed that for this type of material being tested and for the frequency range being employed, that the probe test is basically a shear test. Thus, the possibility of calculating G' and G" from the data using the proper mathematical techniques is quite good.

TABLE I

SUMMARY OF IN VITRO DYNAMIC MECHANICAL PROPERTIES OF HUMAN BRAINS

BRAIN	AGE	Hours Post-Mortem	G' (dynes/cm^2)	G' (dynes/cm^2)	tan δ
1	48	10	$11.1\text{x}10^3$	$5.1\text{x}10^3$	0.4.6
		33	9.8	5.2	.53
2	77	10	6-9	5.5-6.5	.65-1.00
3	44	33	7.7	3.9	.51
		51	9.0	5.0	.55
4	92	20	14.1	6.0	.42
5	80	28	9.7	4.8	.50
6	50	20	10.0	4.5	.45
7	49	47	7.5	3.0	.35
		62	10.5	4.5	.43
8	71	25	7.7	4.0	.52

ACKNOWLEDGMENT

This work was supported by National Institute for Neurological Diseases and Blindness Contract No. PH-43-67-1136.

REFERENCES

Dodgson, M. C. H. (1962) Colloidal Structure of Brain. Biorheology. 1 21-30.

Fitzgerald, E. R. and Ferry, J. D. (1953) Methods for determining the dynamic mechanical behavior of gels and solids at audio frequencies: Comparison of mechanical and electrical properties. J. Colloid Sci. 8 1-34.

Franke, E. K. (1954) The response of the human skull to mechanical vibrations. Wright-Patterson Air Force Base, Ohio, WADC Tech. Rept. 54-24.

Franke, E. K. (1951) Mechanical Impedance of the Surface of the Human Body. J. Appl. Physiol. 3 582-590.

Gehman, S. D. (1957) Dynamic Properties of Elastomers. Rubber Chem and Tech. 30 1202-1250.

von Gierke, H. E., Oestreicher, H. L., Franke, E. K., Parrack, H. O. and von Wittern, W. W. (1952) Physics of Vibrations in Living Tissues. J. Appl. Physiol. 4 886-900.

von Gierke, H. E. (1966) On the Dynamics of Some Head Injury Mechanisms. In Head Injury (Edited by W. F. Caveness and A. E. Walker) pp. 383-396. Lippincott, Philadelphia.

Goldsmith, W. (1966) The Physical Processes Producing Head Injuries. In Head Injury (Edited by W. F. Caveness and A. E. Walker) pp. 350-382. Lippincott, Philadelphia.

Holbourn, A. H. S. (1943) Mechanics of Head Injury. Lancet 2 438-441.

Koeneman, J. B. (1966) Viscoelastic Properties of Brain Tissue. Unpublished M.S. Thesis, Case Institute of Technology.

Martinez, J. L. (1963) Study of Whiplash Injuries in Animals. The American Society of Mechanical Engineers Paper No. 63-WA-281, New York.

Pudenz, R. H. and Sheldon, C. H. (1946) The Lucite Calvarium - A Method for Direct Observation of the Brain. II. Cranial Trauma and Brain Movement. J. Neurosurg. 3, 487-505.

Ommaya, A. K. (1966) Experimental Head Injury in the Monkey. In Head Injury (Edited by W. F. Caveness and A. E. Walker) pp. 260-275. Lippincott, Philadelphia.

Ommaya, A. K. (1968) Mechanical Properties of Tissues of the Nervous System. J. Biomechanics 1 79-88.

Unterharnscheidt, F. and Sellier, K. (1966) Mechanics and Pathomorphology of Closed Brain Injuries. In Head Injury (Edited by W. F. Caveness and A. E. Walker) pp. 321-341. Lippincott, Philadelphia.

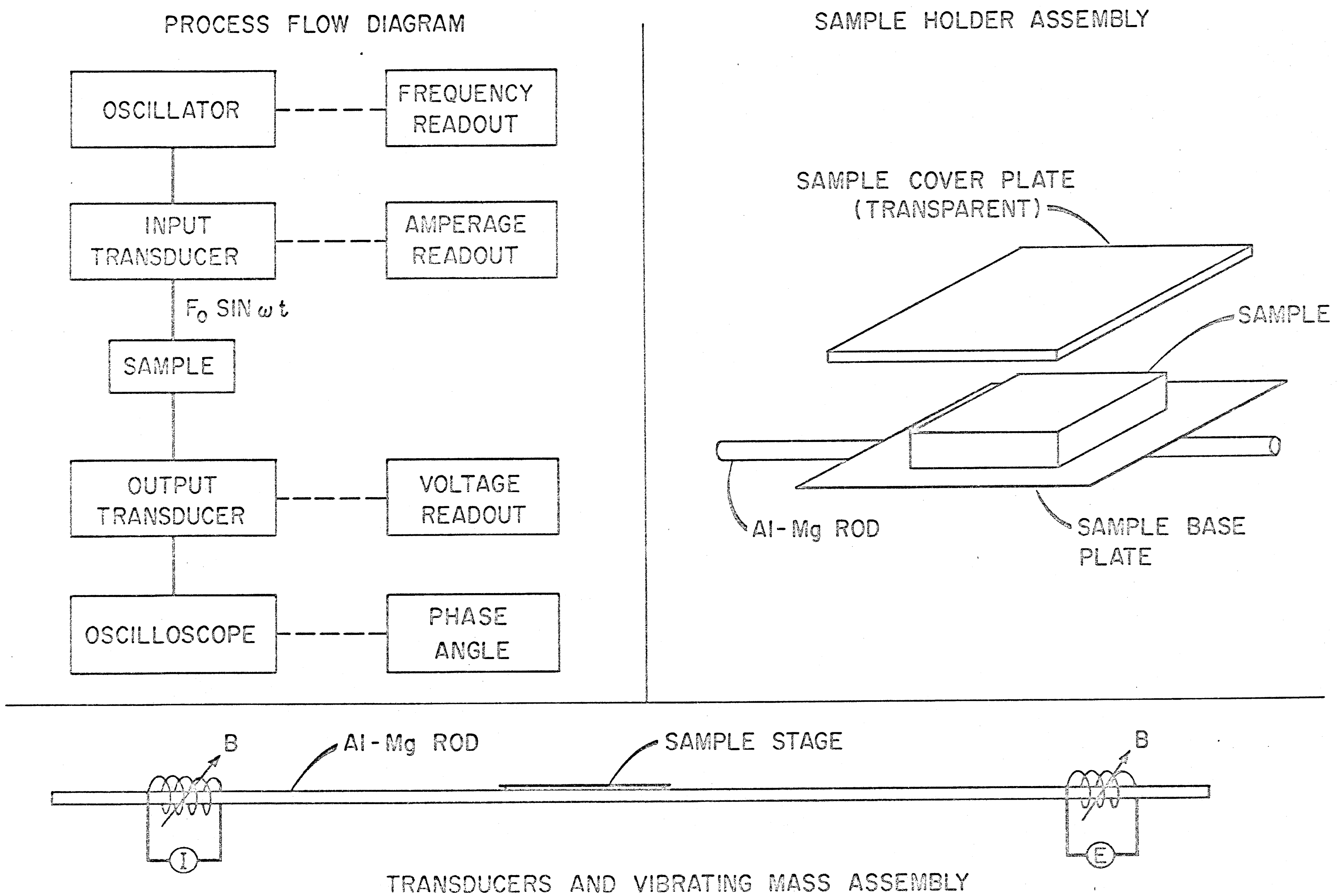

FIGURE 1. Schematic Views of the Dynamic Mechanical Apparatus

DYNAMIC PROBE APPARATUS

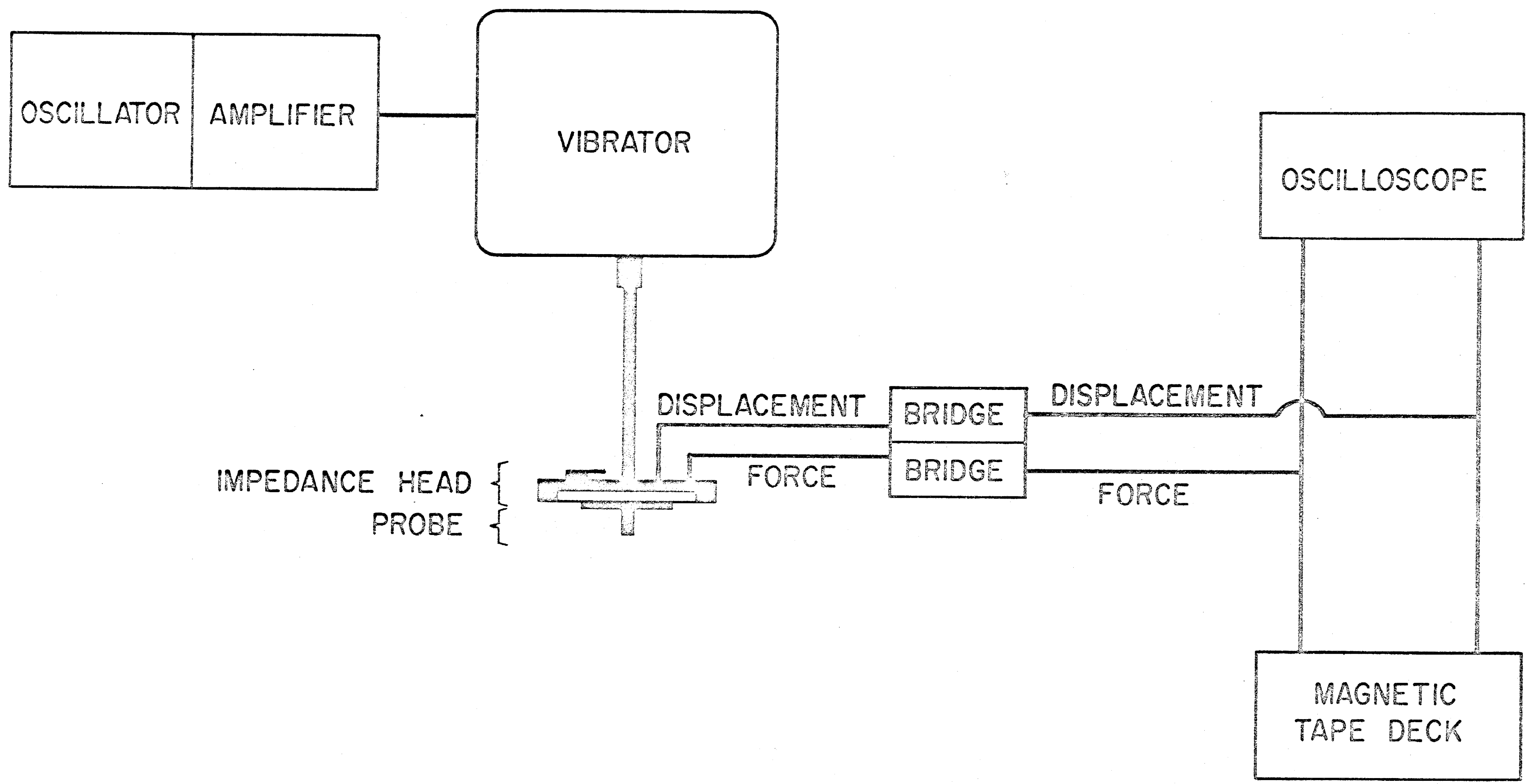

FIGURE 2. Dynamic Probe Apparatus

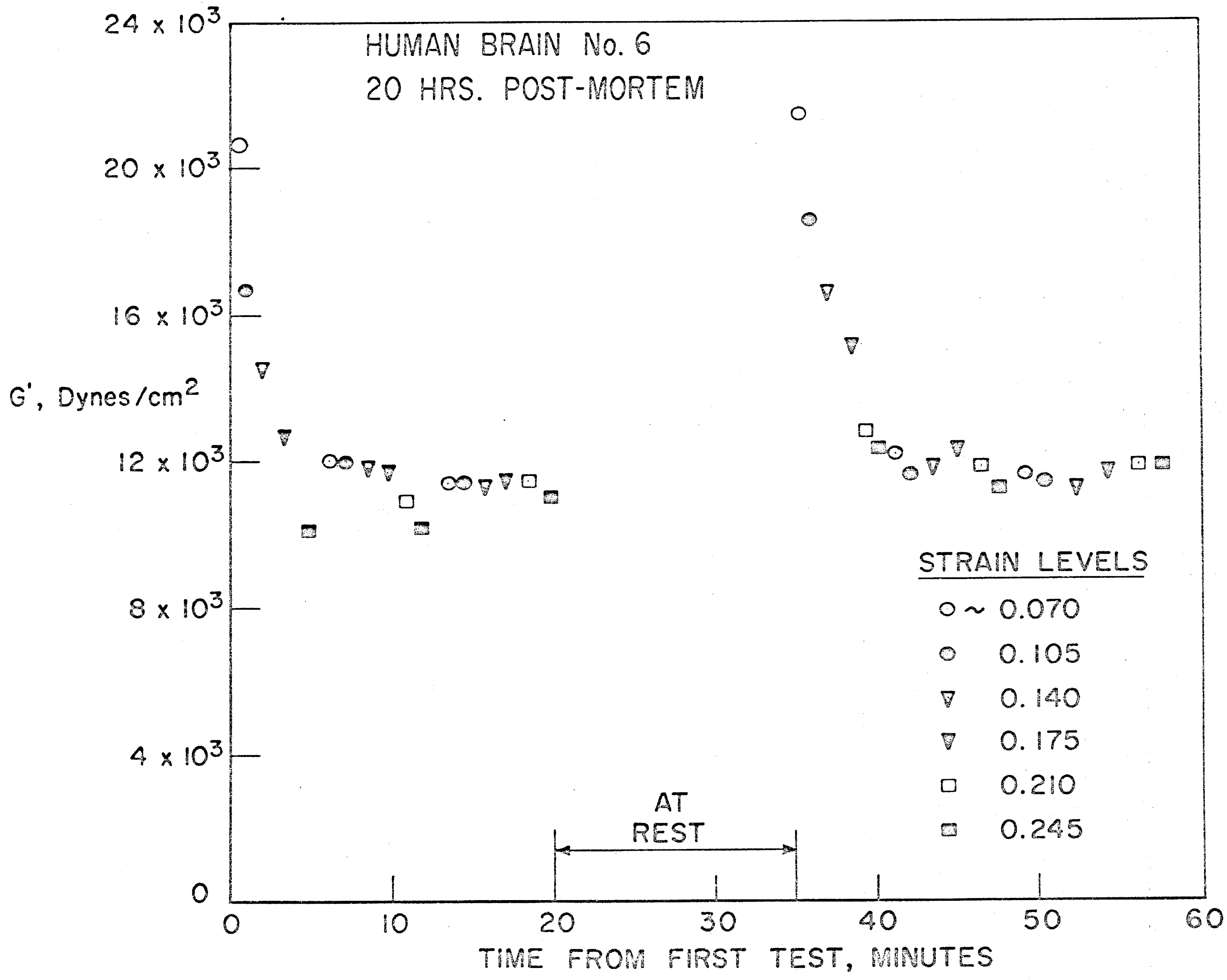

FIGURE 3. Dynamic Elastic Modulus of Human Brain No. 6, 20 Hours Post-Mortem

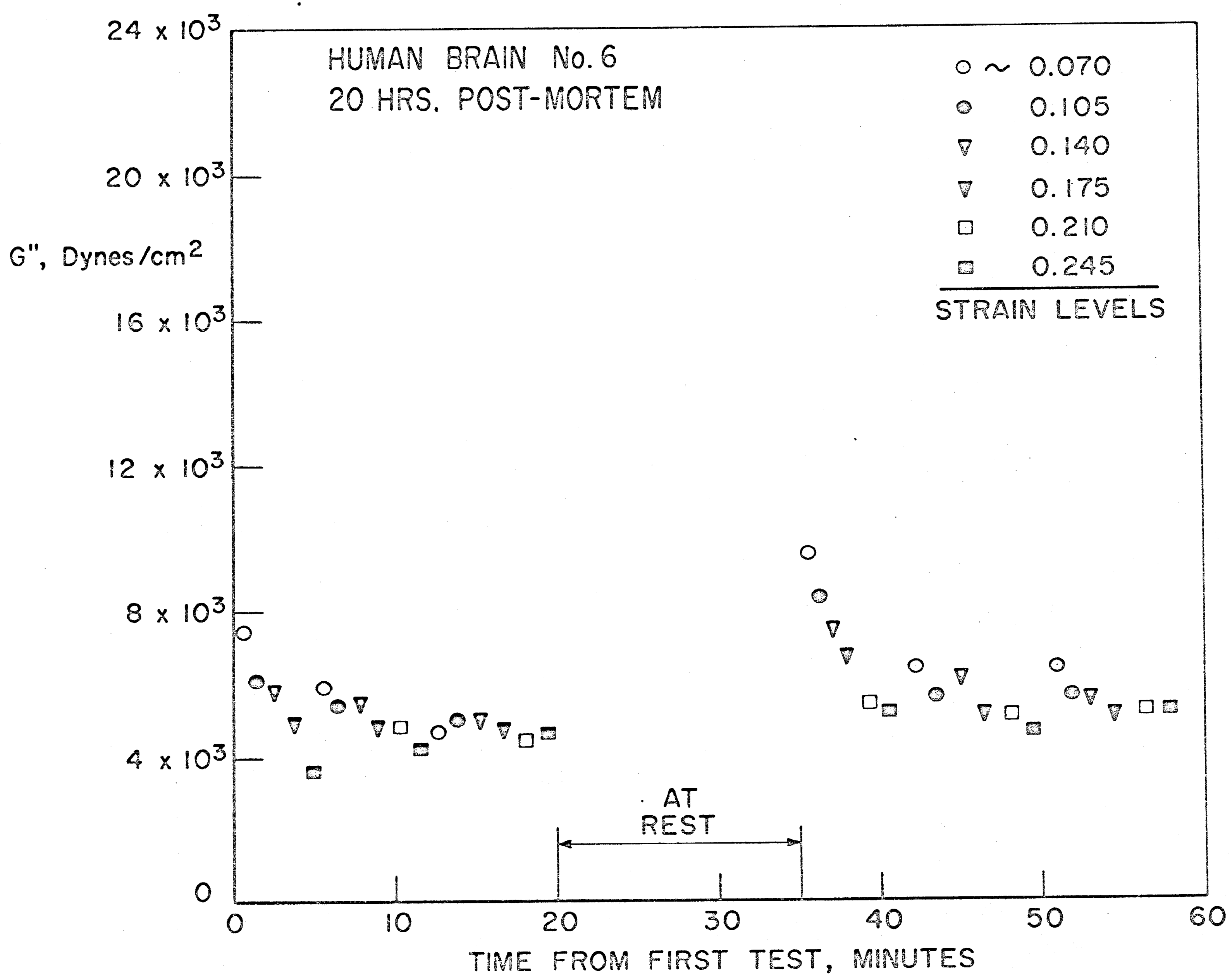

FIGURE 4. Dynamic Loss Modulus of Human Brain No. 6, 20 Hours Post-Mortem

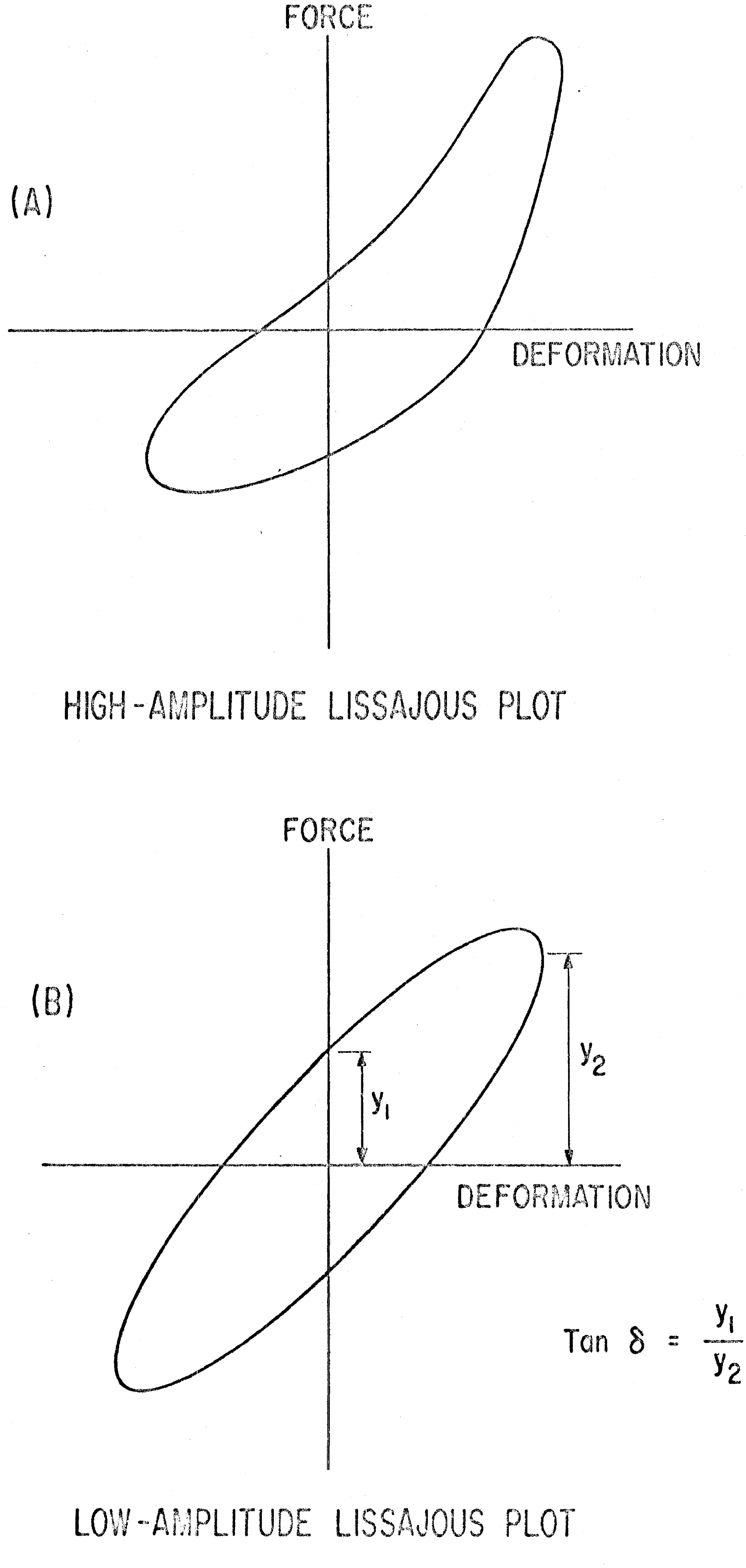

FIGURE 5. DPA Lissajous Plots

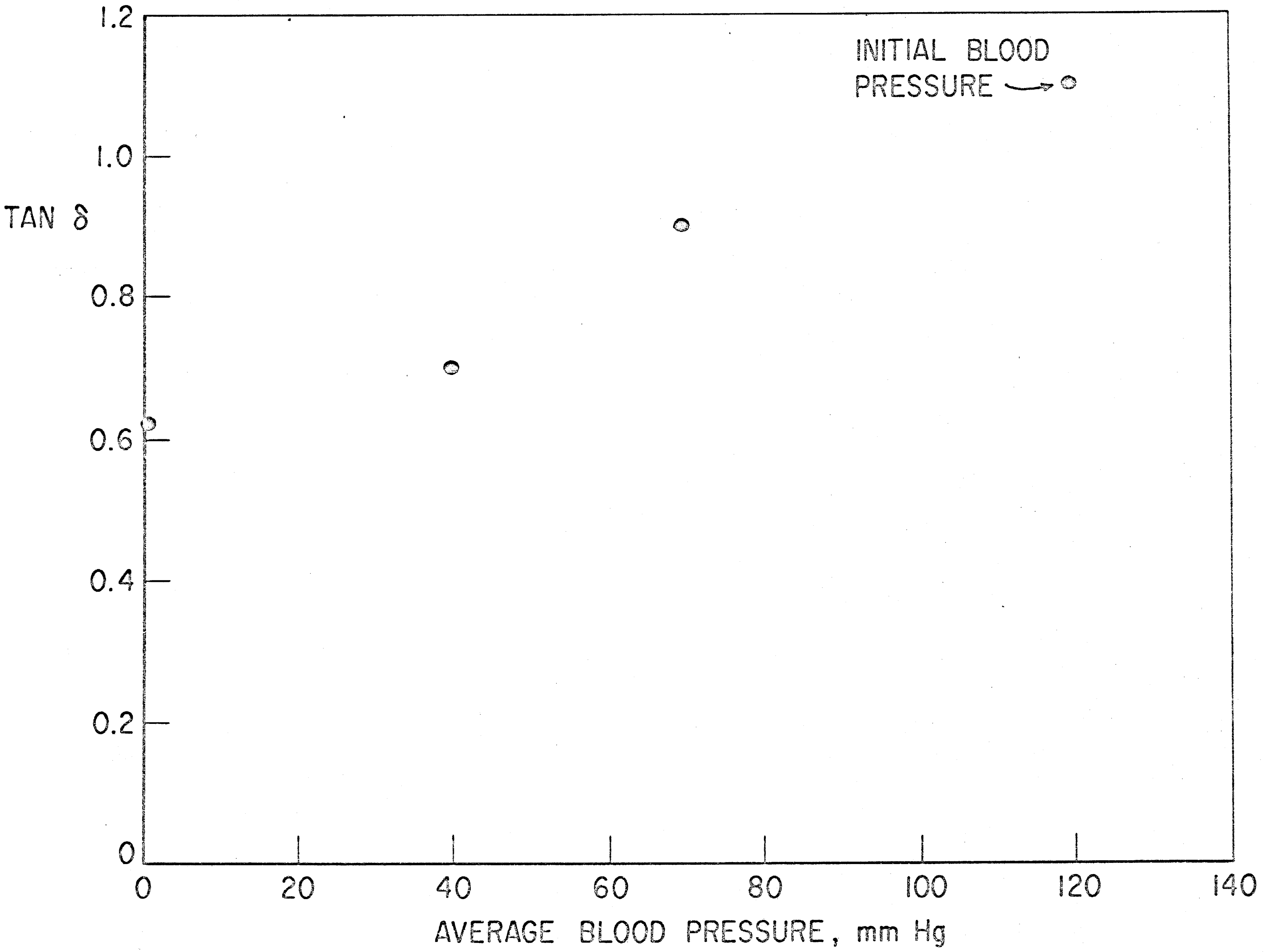

FIGURE 6. Tan δ vs. Average Systemic Blood Pressure

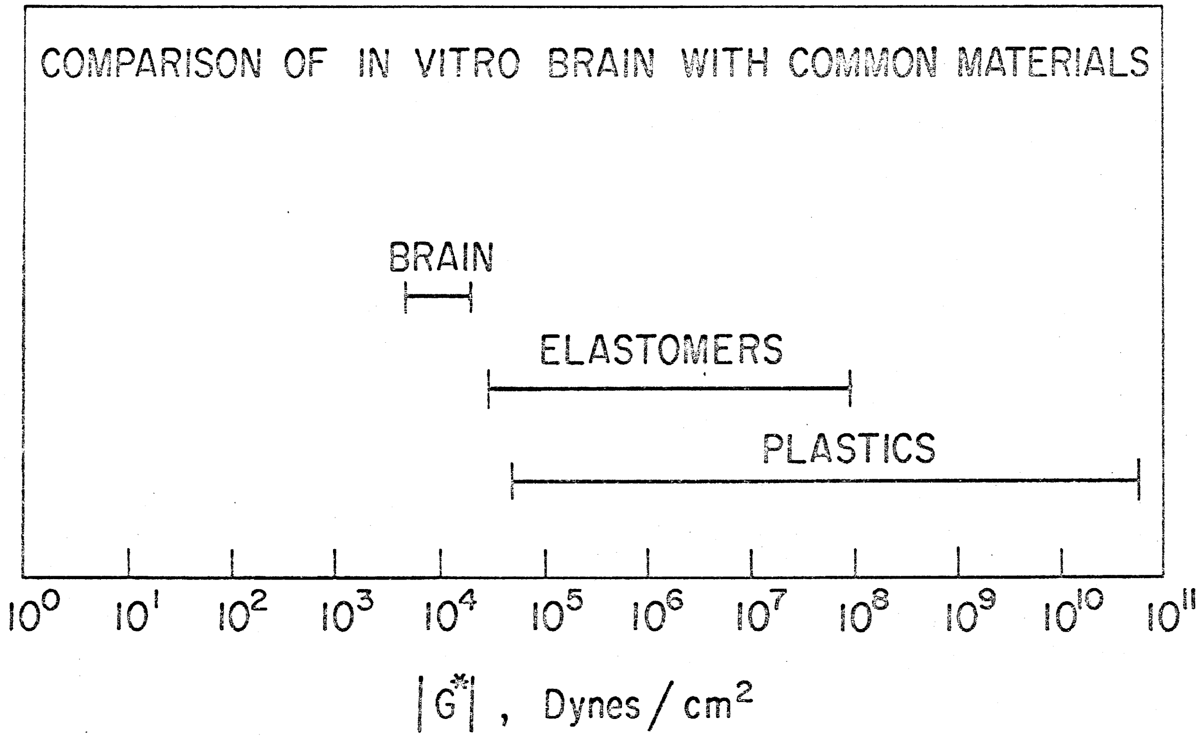

FIGURE 7. Comparison of Brain with Common Materials

APPENDIX C

THE AXISYMMETRIC RESPONSE OF A FLUID-FILLED SPHERICAL SHELL

THE AXISYMMETRIC RESPONSE OF A FLUID-FILLED
SPHERICAL SHELL

by

Ali Erkan Engin

THE AXISYMMETRIC RESPONSE OF A FLUID-FILLED SPHERICAL SHELL

by
Ali Erkan Engin

A dissertation submitted in partial fulfillment
of the requirements for the degree of
Doctor of Philosophy in
The University of Michigan
1968

Doctoral Committee:

Associate Professor Roger D. Low, Co-Chairman
Assistant Professor Y. King Liu, Co-Chairman
Professor Vedat S. Arpacı
Associate Professor Ivor K. McIvor
Professor Chia-Shun Yih

A B S T R A C T

THE AXISYMMETRIC RESPONSE OF A FLUID-FILLED SPHERICAL SHELL

by

Ali Erkan Engin

Co-Chairmen: Roger D. Low, Y. King Liu

This investigation is concerned with the free vibration analysis of a fluid-filled spherical shell and the determination of the dynamic response of such a fluid-shell system when subjected to a local radial impulsive load. From the application point of view, a fluid-filled spherical shell is considered to be a simple, but to date, the most improved theoretical model representing the human head when subjected to impulsive external loads.

Utilizing linear shell theory, which includes both membrane and bending effects, the differential equations for the axisymmetric, nontorsional motion of a fluid-filled thin spherical shell are obtained by means of Hamilton's principle. The motion of the fluid is assumed to be governed by the linear wave equation. It is shown that appropriate limiting cases of the frequency equation for the above system agree with those of the simpler models previously investigated. We use the Laplace transform technique in determining the transient response of the system to a local radial impulsive load. The solution thus obtained for the velocity potential of the fluid and the displacement components of the shell mid-surface is the Green's function of the problem with respect to time.

Some numerical results for the theoretical model are obtained for a set of appropriate data. We compare the stress distributions at various times in the shell for both the empty and the fluid-filled cases. In the fluid-filled case the excess pressure propagation in the fluid is also discussed. The possible locations of brain damage and skull injury are indicated on the basis of the numerical computations.

ACKNOWLEDGMENTS

I would like to express my gratitude to Professor Y. K. Liu who has suggested this area of research and Professor R. D. Low for his very valuable suggestions and assistance in carrying out the mathematical aspects of the investigation. I would also like to thank all committee members for their interest and helpful criticisms.

This thesis was primarily supported by the Highway Safety Research Institute of The University of Michigan under Contract No. 43-67-1136 sponsored by the National Institute for Neurological Diseases and Blindness.

Finally, I would like to thank Mr. J. E. Tuttle for his assistance in programming to obtain the numerical results.

TABLE OF CONTENTS

LIST OF FIGURES

NOMENCLATURE

A_1, A_2	Lamé parameters
E	Young's modulus
F_e	External force distribution on the shell
$H(t)$	Heaviside unit step function
M	Total mass of the system, $m_o + m_s$
M_φ, M_θ	Moment resultants
N_φ, N_θ	Stress resultants
$P_n(\cos\varphi)$	Legendre polynomials of the first kind
$P'_n(\cos\varphi)$	Associated Legendre polynomials of the first kind and first order
R_1, R_2	Principal radii of curvatures
S	Mid-surface of the shell
T	Kinetic energy
V	Potential energy
V_c	Velocity imparted to the mass center
$\mathcal{V}_o, \mathcal{V}_s$	Volumes of fluid and shell respectively
U	Strain energy density for the shell
Φ	Velocity potential for the fluid
Φ_1	Nondimensional velocity potential for the fluic, Φ/ac_s
Ω	Nondimensional frequency, $\omega a/c$
$\bar{\Omega}$	Nondimensional frequency, $\omega a/c_s$
a	Radius of spherical shell
a_o, a_n	Coefficients of Legendre polynomial expansion of ζ
b_n	Coefficients of Legendre polynomial expansion of ψ

c_o, c_n	Coefficients of velocity potential
c	Compressional wave speed in the fluid
c_s	Apparent wave speed in the shell, $[E/\rho_s(1-\nu^2)]^{1/2}$
f	Shell-fluid parameter, $\rho_o a/\rho_s h$
h	Shell thickness
$j_n(z)$	Spherical Bessel function, $(\pi/2z)^{1/2} J_{n+1/2}(z)$
k	Wave number, ω/c
m_o, m_s	Masses of fluid and shell respectively
p	Complex variable for the Laplace Transform or pressure
p_a	Fluid pressure on the surface of the shell
p_1	Nondimensional pressure, $p/\rho_o c_s^2$
r, θ, φ	Spherical coordinates
r_1	Nondimensional radius, r/a
s	Speed ratio, c/c_s
t	Time
u	Meridional displacement with respect to center of mass of the system
w	Radial displacement with respect to center of mass of the system
x, y, z	Cartesian coordinates
v_r, v_φ	Radial and tangential components of velocity of fluid particles
z	Distance from the mid-surface, or complex variable
α^2	Thickness parameter, $h^2/12a^2$
α_1, α_2	Curvilinear coordinates of the shell mid-surface
γ	Mid-surface shear strain
δ	Variation symbol

$\delta(t)$ Dirac delta function

$\epsilon_\varphi, \epsilon_\theta$ Mid-surface normal strains, in general ϵ_1, ϵ_2

$\epsilon_\varphi^{(z)}, \epsilon_\theta^{(z)}$ z-surface normal strains

ζ Nondimensional radial displacement, w/a

ψ Nondimensional meridional displacement, u/a

$\kappa_\varphi, \kappa_\theta$ Mid-surface curvatures, in generak κ_1, κ_2

λ_n $n(n+1)$

ν Poisson's ratio

ρ_o, ρ_s Mass density of fluid and shell respectively

$\sigma_\varphi, \sigma_\theta$ Normal stresses for the mid-surface

$\sigma_\varphi^{(z)}, \sigma_\theta^{(z)}$ Normal stresses for the z-surface

τ Nondimensional time, ct/a

ω Angular frequency

CHAPTER 1

INTRODUCTION

The subject matter of this investigation received its stimulus from the following two considerations. First of all, the complete determination of the dynamic response of a fluid-filled shell subjected to a local radial impulsive load is a point of interest in theoretical mechanics due to the fluid-solid interaction nature of the problem. Secondly, it is hoped that a fluid-filled spherical shell will serve as a simple but improved theoretical model representing the human head when subjected to impulsive external loads. The previous studies can be put into three categories:

(1) Studies on the response of an inviscid and irrotational fluid contained in a rigid, closed spherical shell or container.

(2) Studies on the dynamic analysis of various elastic shells.

(3) Studies involving shells in contact externally and/or internally with fluids.

In the first category the major contributions were made by Anzelius[1] and Güttinger.[7] Their formulation, motivated by investigations of the response of the brain to a sudden blow on the skull, are essentially identical and involve an axisymmetric solution of the wave equation in spherical coordinates. In the papers of both authors the eigenvalues of the problem are determined by requiring the radial component of the fluid velocity to vanish at the interior surface of the rigid spherical shell surrounding the fluid. In the analysis of Anzelius the spherical vessel containing the fluid has constant translational velocity for $t < 0$. At $t = 0$ the vessel is brought to a sudden stop. From this physical situation he gets one initial condition for the velocity potential, Φ, of the fluid and assumes the initial pressure distribution which supplies the second initial condition on the time derivative of Φ. In Guttinger's analysis the fluid-filled spherical vessel is initially at rest. At $t = 0$ a "momentary impact" force instantaneously accelerates the vessel to a constant velocity which the vessel retains for all $t > 0$. Again from the physical situation the first initial condition on Φ can be written down immediately and the second initial condition on the time derivative of Φ is equal to zero since the initial dynamic pressure distribution in this case is zero. Both authors concluded that an initial compression wave arises from the pole of impact, and due to the rigidity of the shell, instantaneously a tension (rarefaction) wave is emitted from the counterpole, both traveling towards the geometric center of the system. The super-position of the two waves at the center produces large changes in the fluid pressure and this phenomena was considered to be the cause of brain trauma. It should be remarked that the assumption of rigidity of the shell causes an infinite speed of wave propagation in the container and, as a direct consequence of this, every point of the interior surface of the container instantaneously becomes a source of varying strength which transmits energy into the fluid. The obvious shortcomings of the fluid-filled rigid shell model led Goldsmith[4] to suggest the construction of a fluid-filled elastic shell model and its analytical or numerical solution. Goldsmith's paper was primarily addressed to those who are outside of the discipline of mechanics; however, a thorough review of previously employed theoretical and experimental methods describing the formation of brain trauma and head injury has been given.

The investigations belonging to the second category are numerous. Only a few representative ones will be mentioned here. Dynamic analysis of shells dates back as early as 1882 when Lamb[13] used an extensional formulation in the study of closed spherical shells. A few years later a famous dispute took place between Rayleigh[23] and Love[15] in an endeavor to construct a theory for the vibration of bells. Rayleigh's treatment was inextensional, i.e., he assumed that no stretching of the mid-surface of the shell takes place during deformation, whereas Love[16] included both flexural and extensional effects. Love's formulation of the problem has become the classical bending theory of shells now known as Love's first approximation. Based on the extensional theory of Love, Silbiger[26] studied free and forced vibrations of spherical shells and Baker[2] obtained some experimental results. Naghdi and Kalnins,[20] using classical bending theory, investigated axisymmetric as well as asymmetric vibrations of thin spherical shells and obtained some numerical results for the natural frequencies (of 4 lowest circumferential wave numbers) and mode shapes. Kalnins,[11] using linear bending theory, made vibration analyses of spherical shells closed at one pole and open at other and determined natural frequencies and mode shapes for opening angles ranging from shallow to closed shells. He also explained certain paradoxial situations which occurred at the lower branch of Love's frequency spectrum in terms of the effects of bending. Klein[12] applied the finite element approach to the dynamic analysis of multilayer shells with special emphasis on the computational aspects and obtained a solution for a shallow spherical cap under a time dependent axisymmetric pressure load. Medick,[18] within the framework of modified shallow shell theory, obtained the initial response of a restricted class of thin shells which are essentially spherical and shallow in the neighborhood of loading. Based on the linear classical shell theory Long[14] investigated the effect of radial preload on the natural frequencies of thin closed spherical shells and found that pure radial and torsional modes are virtually independent of the radial preload. Using linearized small deformation theory Humphreys and Winter[9] obtained solutions in the form of infinite series for an infinitely long cylindrical shell under a transverse pressure pulse. Recently, McIvor and Sonstegard[17] studied the axisymmetric response of a closed spherical shell to a nearly uniform radial impulse and the associated stability problem of the breathing mode.

The problems in the third category received some attention especially by those in the field of acoustics. Junger[10] investigated the effect of the fluid on the natural frequencies of cylindrical and spherical shells freely suspended in a compressible fluid medium. Free and forced oscillations of infinitely long, (thick as well as thin) cylindrical shells surrounded by water were studied by Greenspon[6] who treated unpressurized shells by exact elasticity theory and cylindrical shells with internal fluid by approximate shell theory. Goodman and Stern,[5] using elasticity theory and numerical integration of a system of ordinary differential equations, investigated the steady state response of a fluid-filled spherical shell submerged in another fluid. Shklyarchuk[25] made approximate calculations to obtain lower frequencies and mode shapes of the axisymmetric oscillations of liquid-filled shells of revolution. Assuming "flat surface motion" for the free surface of the liquid and applying Ritz method he carried out the calculations for a liquid-filled cylinder and a half-sphere. Recently, Rand and Dimaggio[22] obtained frequency equations and mode shapes for the axisymmetric, extensional, nontorsional oscillations of fluid-filled elastic spherical shells and rigid prolate spheroidal shells.

As it was pointed out in Goldsmith's paper, the various mechanisms of skull and brain damage proposed by previous investigators are of little practical value in _quantitative_ determinations of the _location_ and _magnitude_ of brain trauma and head injury. In the literature there are no rigorous mathematical treatments of the theoretical head injury models except for the fluid-filled _rigid_ shell model analyzed by Anzelius and Güttinger. It should be emphasized that a continuum model is much superior to a lumped-parameter model due to the nature of the skull and brain matter. In the lumped-parameter model the criterion of damage is based on maximum acceleration whereas in the continuum model on maximum stress, which is clearly established from the experimental data to be the cause of injury. Therefore any theoretical model representing the human head when subjected to a time-dependent force must be constructed on the basis of continuum mechanics, which allows deformations depending both on location within the body and on time.

The theoretical model for the present investigation consists of a thin _elastic_ spherical shell filled with inviscid compressible fluid. In Chapter 2 the governing differential equations of a fluid-filled spherical shell are obtained by means of Hamilton's principle. Since one of the major problems of the dynamic analysis of continuous elastic systems is the proper description of the natural frequencies, the frequency equation for the model under consideration is determined for axisymmetric and nontorsional motion from the combined theory which includes membrane and bending effects of the shell. It is also shown that various limiting cases of the frequency equation agree with the frequency equations of the simpler models previously investigated. Chapter 2 is concluded with delineation of some of the salient features of the frequency spectrum in view of the frequency spectra of the limiting cases. In Chapter 3, the response of a fluid-filled elastic spherical shell subjected to a local, radial impulsive load is determined by means of the Laplace transformation. The solutions obtained for the nondimensional velocity potential of the fluid and nondimensional radial and tangential displacements of the shell mid-surface essentially is the Green's function of the problem with respect to nondimensional time. Thus the response of the system to any arbitrary time-dependent external load of finite duration is obtained by making use of the convolution integral. The last chapter of the thesis is devoted to some numerical results and their discussion.

CHAPTER 2

A LINEAR FORMULATION

In this chapter the frequency equation of a closed, fluid-filled elastic spherical shell for axisymmetric, nontorsional motion is obtained from the combined linear theory which includes membrane (extensional) and bending (inextensional) effects of the shell.

2.1 REPRESENTATION OF SHELL DEFORMATION

Deformation of a given shell can be analyzed in terms of the deformation of its mid-surface. The mid-surface of a shell is defined to be a surface which lies midway between the two bounding surfaces of the shell. In the following analysis any surface which is equidistance from the mid-surface will be called a z-surface. A set of Cartesian axes is chosen with origin at the center of the shell. A spherical coordinate system can then be set up, as shown in Figure 1.

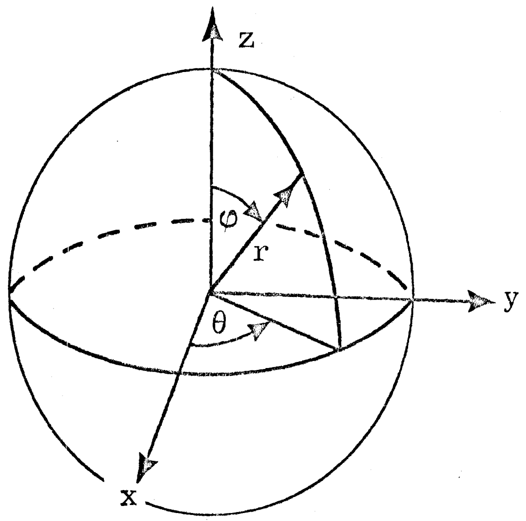

Figure 1. Coordinate system for the shell and its interior.

2.2 STRAIN-DISPLACEMENT-STRESS RELATIONS

Deformation of the mid-surface is completely determined by the strain quantities ϵ_1, ϵ_2, γ, κ_1, κ_2, τ. The first three characterize the variations of the dimensions of a small element of the surface and the other three characterize the distortion of the element. These strain quantities are given, in general, in terms of the components u, v, w, of the displacement vector, the Lamé parameters A_1, A_2 and the principal radii of curvature R_1, R_2. If one takes the curvilinear coordinates α_1, α_2 of the mid-surface to be the principal coordinates, then these strain quantities are[21]

$$\begin{aligned}
\epsilon_1 &= \frac{1}{A_1}\frac{\partial u}{\partial \alpha_1} + \frac{1}{A_1A_2}\frac{\partial A_1}{\partial \alpha_2}v + \frac{w}{R_1}, \\
\epsilon_2 &= \frac{1}{A_2}\frac{\partial v}{\partial \alpha_2} + \frac{1}{A_1A_2}\frac{\partial A_2}{\partial \alpha_1}u + \frac{w}{R_2}, \\
\gamma &= \frac{A_2}{A_1}\frac{\partial}{\partial \alpha_1}\left(\frac{v}{A_2}\right) + \frac{A_1}{A_2}\frac{\partial}{\partial \alpha_2}\left(\frac{u}{A_1}\right), \\
\kappa_1 &= -\frac{1}{A_1}\frac{\partial}{\partial \alpha_1}\left(\frac{1}{A_1}\frac{\partial w}{\partial \alpha_1} - \frac{u}{R_1}\right) - \frac{1}{A_1A_2}\frac{\partial A_1}{\partial \alpha_2}\left(\frac{1}{A_2}\frac{\partial w}{\partial \alpha_2} - \frac{v}{R_2}\right), \qquad (2.2.1) \\
\kappa_2 &= -\frac{1}{A_2}\frac{\partial}{\partial \alpha_2}\left(\frac{1}{A_2}\frac{\partial w}{\partial \alpha_2} - \frac{v}{R_2}\right) - \frac{1}{A_1A_2}\frac{\partial A_2}{\partial \alpha_1}\left(\frac{1}{A_1}\frac{\partial w}{\partial \alpha_1} - \frac{u}{R_1}\right), \\
\tau &= -\frac{1}{A_1A_2}\left(\frac{\partial^2 w}{\partial \alpha_1 \partial \alpha_2} - \frac{1}{A_1}\frac{\partial A_1}{\partial \alpha_2}\frac{\partial w}{\partial \alpha_1} - \frac{1}{A_2}\frac{\partial A_2}{\partial \alpha_1}\frac{\partial w}{\partial \alpha_2}\right) + \\
&\quad \frac{1}{R_1}\left(\frac{1}{A_2}\frac{\partial u}{\partial \alpha_2} - \frac{1}{A_1A_2}\frac{\partial A_1}{\partial \alpha_2}u\right) + \frac{1}{R_2}\left(\frac{1}{A_1}\frac{\partial v}{\partial \alpha_1} - \frac{1}{A_1A_2}\frac{\partial A_2}{\partial \alpha_1}v\right).
\end{aligned}$$

For a spherical surface of radius a, $A_1 = R_1 = R_2 = a$, and $A_2 = a \sin \varphi$. Introduction of axisymmetry and precluding torsional displacements mean

$$\frac{\partial \square}{\partial \alpha_2} = \frac{\partial \square}{\partial \theta} = 0 , \qquad (2.2.2)$$

$$v = 0 , \qquad (2.2.3)$$

where v is the displacement component in the θ (α_2) direction. The remaining displacement components of the mid-surface are along $\varphi(\alpha_1)$ and along the outward normal to the surface. These are

$$u = u(\varphi,t) \ ,$$

and (2.2.4)

$$w = w(\varphi,t) \ .$$

Imposing the conditions (2.2.2) and (2.2.3) on (2.2.1) yields the following mid-surface strain-displacement expressions:

$$\begin{aligned} \epsilon_\varphi &= \frac{1}{a}\left(\frac{\partial u}{\partial \varphi} + w\right) , & \kappa_\varphi &= \frac{1}{a^2}\left(-\frac{\partial^2 w}{\partial \varphi^2} + \frac{\partial u}{\partial \varphi}\right) , \\ \epsilon_\theta &= \frac{1}{a}\,(u \cot\varphi + w) \ , & \kappa_\theta &= \frac{\cot\varphi}{a^2}\left(-\frac{\partial w}{\partial \varphi} + u\right) , \\ \gamma &= 0 \ , & \tau &= 0 \ . \end{aligned} \qquad (2.2.5)$$

In (2.2.5) ϵ_φ and ϵ_θ are the tangential strains, whereas κ_φ and κ_θ can be viewed as the variations of the curvature of the mid-surface of the shell during deformation. It can be shown[21] that the z-surface strains are related to those of the mid-surface in the following manner:

$$\begin{aligned} \epsilon_\varphi^{(z)} &= \frac{1}{1+z/a}\,(\epsilon_\varphi + z\,\kappa_\varphi) \ , \\ \epsilon_\theta^{(z)} &= \frac{1}{1+z/a}\,(\epsilon_\theta + z\,\kappa_\theta) \ . \end{aligned} \qquad (2.2.6)$$

By Hooke's law and the second hypothesis of Kirchoff,* one has for a homogeneous

*The hypotheses of Kirchoff can be stated as:

(1) The normals to the undeformed mid-surface remain normal after deformation and do not stretch.

(2) The normal stresses acting on planes parallel to the mid-surface are neglected.

and isotropic shell the following stress-strain relations.

$$\sigma_{\varphi}^{(z)} = \frac{E}{1-\nu^2}\left(\epsilon_{\varphi}^{(z)} + \nu\epsilon_{\theta}^{(z)}\right) ,$$
$$\sigma_{\theta}^{(z)} = \frac{E}{1-\nu^2}\left(\epsilon_{\theta}^{(z)} + \nu\epsilon_{\varphi}^{(z)}\right) , \tag{2.2.7}$$

where E is Young's modulus and ν is Poisson's ratio.

2.3 EQUATIONS OF MOTION

The equations of motion of a closed, fluid-filled spherical shell can be derived by use of Hamilton's Principle. In order to apply this principle to the problem under consideration, it is necessary to calculate the potential and kinetic energies of the thin spherical shell surrounding the fluid.

The potential energy of the shell is

$$V = \int_S \bar{U} dS - \int_S p_a w dS - \int_S F_e w dS , \tag{2.3.1}$$

where the first integral represents the strain energy of the shell during deformation; $\bar{U}$ is the strain energy density per unit mid-surface of the shell and is given as

$$\bar{U} = \frac{Eh}{2(1-\nu^2)}\left[(\epsilon_{\varphi}+\epsilon_{\theta})^2 - 2(1-\nu)(\epsilon_{\varphi}\epsilon_{\theta} - \frac{\gamma^2}{4})\right] + \frac{Eh^3}{24(1-\nu^2)}\left[(\kappa_{\varphi}+\kappa_{\theta})^2 - 2(1-\nu)(\kappa_{\varphi}\kappa_{\theta} - \tau^2)\right] . \tag{2.3.2}$$

In (2.3.2) the first term gives the strain energy density of stretching and shearing of the mid-surface, the second that of bending and torsion. The second and the third integrals in (2.3.1) represent the potential energy due to the effects of internal fluid pressure p_a and any external surface force

F_e on the shell. S is the area of the mid-surface of the shell.

The kinetic energy of the shell is

$$T = \frac{1}{2} \int_{\forall_s} \rho_s \left[\left(\frac{\partial u}{\partial t} \right)^2 + \left(\frac{\partial w}{\partial t} \right)^2 \right] d\forall_s \; , \tag{2.3.3}$$

where ρ_s and $\forall_s$ are mass density and volume of the shell material respectively. In (2.3.3) the effect of rotary inertia of the shell is neglected.

According to Hamilton's Principle the actual path followed by a dynamical process is that particular one for which the time integral of the function (T-V) assumes a stationary value. The analytical statement of this principle is

$$\delta \int_{t_1}^{t_2} (T-V) dt = 0 \; , \tag{2.3.4}$$

where t_1 and t_2 are two distinct, arbitrary but fixed times, and δ denotes the usual variational operation.

Substitution of (2.2.5) into (2.3.2) gives the strain energy density in terms of displacements u and w of the mid-surface. Using (2.3.1) and (2.3.3) in (2.3.4) along with some concepts* of calculus of variations yields the following variational expression

$$\delta \int_{t_1}^{t_2} (T-V) dt = \int_{t_1}^{t_2} 2\pi dt \Big\langle \int_0^{\pi} \Big\{ \Big[\Big[-a^2 \rho_s h \frac{\partial^2 u}{\partial t^2} - K \Big(u \cot^2\varphi - \frac{\partial^2 u}{\partial \varphi^2} - \cot\varphi \, \frac{\partial u}{\partial \varphi} - \frac{\partial w}{\partial \varphi}$$

$$+ \nu \Big(u - \frac{\partial w}{\partial \varphi} \Big) \Big) - \frac{D}{a^2} \Big(-\cot^2\varphi \, \frac{\partial w}{\partial \varphi} + u \cot^2\varphi + \frac{\partial^3 w}{\partial \varphi^3} + \cot\varphi \, \frac{\partial^2 w}{\partial \varphi^2} - \cot\varphi \, \frac{\partial u}{\partial \varphi} - \frac{\partial^2 u}{\partial \varphi^2}$$

(equation continues on next page)

*See, for example, Hildebrand,(8) pp. 119-181; H. Bateman,(3) p. 152.

$$+ \nu\left(u - \frac{\partial w}{\partial\varphi}\right)\Big)\Big]\delta u + \Big[+a^2\rho_s h\frac{\partial^2 w}{\partial t^2} + K\Big(\frac{\partial u}{\partial\varphi} + u\cot\varphi + 2w + \nu\Big(\frac{\partial u}{\partial\varphi} + u\cot\varphi + 2w\Big)\Big)$$

$$- \frac{D}{a^2}\Big(\cot\varphi\Big(-\frac{\partial w}{\partial\varphi} + u\Big)(2+\cot^2\varphi) - (1+\cot^2\varphi)\Big(-\frac{\partial^2 w}{\partial\varphi^2} + \frac{\partial u}{\partial\varphi}\Big) - \frac{\partial^4 w}{\partial\varphi^4} + \frac{\partial^3 u}{\partial\varphi^3}$$

$$+ 2\cot\varphi\Big(\frac{\partial^2 u}{\partial\varphi^2} - \frac{\partial^3 w}{\partial\varphi^3}\Big) + \nu\Big(\frac{\partial^2 w}{\partial\varphi^2} - \frac{\partial u}{\partial\varphi} - u\cot\varphi + \cot\varphi\frac{\partial w}{\partial\varphi}\Big)\Big) + a^2\rho_o h\frac{\partial\Phi(a,\varphi,t)}{\partial t}$$

$$- F_e\Big]\delta w\Big\}\sin\varphi\, d\varphi - \Big\{K\Big[\frac{\partial u}{\partial\varphi} + w + \nu(u\cot\varphi + w)\Big]\sin\varphi + \frac{D}{a^2}\Big[-\frac{\partial^2 w}{\partial\varphi^2} + \frac{\partial u}{\partial\varphi}$$

$$+ \nu\cot\varphi\Big(-\frac{\partial w}{\partial\varphi} + u\Big)\Big]\sin\varphi\Big\}\delta u\Big|_0^\pi - \Big\{\frac{D}{a^2}\Big[\cot^2\varphi\Big(-\frac{\partial w}{\partial\varphi} + u\Big) + \frac{\partial^3 w}{\partial\varphi^3} + \cot\varphi\frac{\partial^2 w}{\partial\varphi^2}$$

$$- \frac{\partial^2 u}{\partial\varphi^2} - \cot\varphi\frac{\partial u}{\partial\varphi} + \nu\Big(-\frac{\partial w}{\partial\varphi} + u\Big)\Big]\sin\varphi\Big\}\delta w\Big|_0^\pi - \Big\{\frac{D}{a^2}\Big[-\frac{\partial^2 w}{\partial\varphi^2} + \frac{\partial u}{\partial\varphi}$$

$$+ \nu\cot\varphi\Big(-\frac{\partial w}{\partial\varphi} + u\Big)\Big]\sin\varphi\Big\}\delta\Big(\frac{\partial w}{\partial\varphi}\Big)\Big|_0^\pi\Big\rangle = 0\,. \qquad (2.3.5)$$

In (2.3.5) $K = Eh/1-\nu^2$, $D = Eh^3/12(1-\nu^2)$; also let $\alpha^2 = D/a^2K = h^2/12a^2$ be a thickness parameter.

From (2.3.5) one gets the differential equations of motion of the shell and natural boundary conditions on u and w at $\varphi = 0$ and π. These are:

$$(1+\alpha^2)\Big[-\frac{\partial^2 u}{\partial\varphi^2} - \cot\varphi\frac{\partial u}{\partial\varphi} + (\nu+\cot^2\varphi)u\Big] + \alpha^2\frac{\partial^3 w}{\partial\varphi^3} + \alpha^2\cot\varphi\frac{\partial^2 w}{\partial\varphi^2}$$

$$- [\alpha^2(\cot^2\varphi+\nu) + (1+\nu)]\frac{\partial w}{\partial\varphi} + \frac{1-\nu^2}{E}\rho_s a^2\frac{\partial^2 u}{\partial t^2} = 0\,, \qquad (2.3.6)$$

$$\alpha^2\frac{\partial^3 u}{\partial\varphi^3} + 2\alpha^2\cot\varphi\frac{\partial^2 u}{\partial\varphi^2} - [(1+\nu)(1+\alpha^2) + \alpha^2\cot^2\varphi]\frac{\partial u}{\partial\varphi} + [\alpha^2\cot^3\varphi + 3\alpha^2\cot\varphi$$

$$- (1+\nu)(1+\alpha^2)\cot\varphi\,]u - \alpha^2\Big[\frac{\partial^4 w}{\partial\varphi^4} + 2\cot\varphi\frac{\partial^3 w}{\partial\varphi^3} - (1+\nu+\cot^2\varphi)\frac{\partial^2 w}{\partial\varphi^2}$$

(equation continues on next page)

$$+(2\cot\varphi+\cot^3\varphi-\nu\cot\varphi)\,\frac{\partial w}{\partial\varphi}\Bigg] - 2(1+\nu)w - \frac{1-\nu^2}{E}\,\rho_s a^2\,\frac{\partial^2 w}{\partial t^2}$$

$$-\frac{1-\nu^2}{Eh}\,a^2\left[\rho_o\,\frac{\partial\Phi(a,\varphi,t)}{\partial t} - F_e(\varphi,t)\right] = 0 \qquad (2.3.7)$$

where Φ and ρ_o are velocity potential and density of the ideal fluid filling the interior space of the shell,

$$\left\{K\left[\frac{\partial u}{\partial\varphi} + w + \nu(u\cot\varphi + w)\right]\sin\varphi + \frac{D}{a^2}\left[-\frac{\partial^2 w}{\partial\varphi^2} + \frac{\partial u}{\partial\varphi} + \nu\cot\varphi\left(-\frac{\partial w}{\partial\varphi} + u\right)\right]\sin\varphi\right\}\delta u\Bigg|_0^\pi = 0\,, \qquad (2.3.8)$$

$$\left\{\frac{D}{a^2}\left[\cot^2\varphi\left(-\frac{\partial w}{\partial\varphi} + u\right) + \frac{\partial^3 w}{\partial\varphi^3} + \cot\varphi\,\frac{\partial^2 w}{\partial\varphi^2} - \frac{\partial^2 u}{\partial\varphi^2} - \cot\varphi\,\frac{\partial u}{\partial\varphi} + \nu\left(-\frac{\partial w}{\partial\varphi} + u\right)\right]\sin\varphi\right\}\delta w\Bigg|_0^\pi = 0, \qquad (2.3.9)$$

$$\left\{\frac{D}{a^2}\left[-\frac{\partial^2 w}{\partial\varphi^2} + \frac{\partial u}{\partial\varphi} + \nu\cot\varphi\left(-\frac{\partial w}{\partial\varphi} + u\right)\right]\sin\varphi\right\}\delta\left(\frac{\partial w}{\partial\varphi}\right)\Bigg|_0^\pi = 0\,. \qquad (2.3.10)$$

(2.3.6) and (2.3.7) are the partial differential equations of motion and they have been obtained from (2.3.5) as a result of equating the coefficients of δu and δw under the time and spacial integral to zero. The previous operation is valid if one also sets the remaining terms in (2.3.5) equal to zero and this yields the natural boundary conditions (2.3.8), (2.3.9) and (2.3.10). The motion of the inviscid and irrotational fluid for small oscillations is governed by the wave equation

$$\frac{1}{r^2}\frac{\partial}{\partial r}\left(r^2\,\frac{\partial\Phi}{\partial r}\right) + \frac{1}{r^2\sin\varphi}\,\frac{\partial}{\partial\varphi}\left(\sin\varphi\,\frac{\partial\Phi}{\partial\varphi}\right) - \frac{1}{c^2}\,\frac{\partial^2\Phi}{\partial t^2} = 0 \qquad (2.3.11)$$

where c is the compressional wave speed in the fluid. Inspection of (2.3.6) and (2.3.7) shows rather strong coupling among the shell displacement components u and w. The effect of the fluid is only seen in (2.3.7) which contains the radial inertia term.

2.4 FREE VIBRATION, THE FREQUENCY EQUATION

In this section the solutions of the partial differential equations (2.3.6), (2.3.7) and (2.3.8) will be given and the frequency equation of a closed, fluid-filled spherical shell for axisymmetric and nontorsional motion will be determined. For the free vibration the external forces must be absent, i.e. $F_e(\varphi,t) = 0$.

Equations (2.3.6) and (2.3.7) are put in nondimensional form by the introduction of a nondimensional time τ, a nondimensional radial displacement ζ, and tangential displacement ψ. These are defined as

$$\psi = \frac{u}{a} \quad , \; \zeta = \frac{w}{a} \quad , \; \tau = \frac{c_s}{a}\, t \tag{2.4.1}$$

where $c_s = [E/\rho_s(1-\nu^2)]^{1/2}$ is the apparent wave speed* in the shell. The non-dimensionalized form of equations (2.3.6) and (2.3.7) are:

$$\alpha^2\left[\frac{\partial^2\psi}{\partial\varphi^2} + \cot\varphi\ \frac{\partial\psi}{\partial\varphi} - (\nu+\cot^2\varphi)\psi - \frac{\partial^3\zeta}{\partial\varphi^3} - \cot\varphi\ \frac{\partial^2\zeta}{\partial\varphi^2} + (\nu+\cot^2\varphi)\ \frac{\partial\zeta}{\partial\varphi}\right]$$

$$+ \frac{\partial^2\psi}{\partial\varphi^2} + \cot\varphi\ \frac{\partial\psi}{\partial\varphi} - (\nu+\cot^2\varphi)\psi + (1+\nu)\ \frac{\partial\zeta}{\partial\varphi} - \frac{\partial^2\psi}{\partial\tau^2} = 0 \ , \tag{2.4.2}$$

---

*The wave speed, c_s, corresponds to the speed of compressional waves in an infinite plate for the limiting case of symmetrical waves of long wavelength.

$$\alpha^2\left[\frac{\partial^3\psi}{\partial\varphi^3} + 2\cot\varphi\ \frac{\partial^2\psi}{\partial\varphi^2} - (1+\nu+\cot^2\varphi)\ \frac{\partial\psi}{\partial\varphi} + (\cot^2\varphi-\nu+2)\psi\cot\varphi\right.$$

$$\left. - \frac{\partial^4\zeta}{\partial\varphi^4} - 2\cot\varphi\ \frac{\partial^3\zeta}{\partial\varphi^3} + (1+\nu+\cot^2\varphi)\ \frac{\partial^2\zeta}{\partial\varphi^2} - (2-\nu+\cot^2\varphi)\cot\varphi\ \frac{\partial\zeta}{\partial\varphi}\right]$$

$$-(1+\nu)\left(\frac{\partial\psi}{\partial\varphi} + \psi\cot\varphi + 2\zeta\right) - \frac{\partial^2\zeta}{\partial\tau^2} - \frac{a\rho_o}{h\rho_s}\ \frac{\partial\Phi_1(1,\varphi,\tau)}{\partial\tau} = 0\ , \qquad (2.4.3)$$

where Φ_1 is the nondimensional velocity potential for the fluid, defined as $\Phi_1 = \Phi/ac_s$. For the nondimensional radial and tangential displacements of the shell mid-surface the following expansions in series of Legendre polynomials of the first kind is considered;

$$\zeta(\varphi,\tau) = \sum_{n=0}^{\infty} a_n(\tau)P_n(\cos\varphi)\ , \qquad (2.4.4)$$

$$\psi(\varphi,\tau) = \sum_{n=1}^{\infty} b_n(\tau)P_n'(\cos\varphi)\ , \qquad (2.4.5)$$

where $P_n(\cos\varphi)$ are Legendre polynomials of the first kind and $P_n'(\cos\varphi)$ are associated Legendre polynomials of the first order, first kind. Since the second solutions of the Legendre equations are singular at the poles they are not included in the expansions (2.4.4) and (2.4.5).

From (2.3.11) the form of the velocity potential Φ_1 can be determined as

$$\Phi_1(r_1,\varphi,\tau) = \sum_{n=0}^{\infty} c_n(\tau)j_n(kar_1)P_n(\cos\varphi)\ , \qquad (2.4.6)$$

where $j_n(kar_1)$ is spherical Bessel function, $k = \omega/c$ is the wave number, ω is the circular frequency, c is the compressional wave speed in the fluid and r_1

is the nondimensional radial coordinate defined to be r/a.

The boundary condition between the fluid and shell can be stated as the continuity of normal velocities for all φ and τ i.e.

$$\frac{\partial\zeta(\varphi,\tau)}{\partial\tau} = \frac{\partial\Phi_1(1,\varphi,\tau)}{\partial r_1} . \tag{2.4.7}$$

Substitution of (2.4.4) and (2.4.6) into (2.4.7) yields the following relationship between $a_n(\tau)$ and $c_n(\tau)$ for each n,

$$c_n(\tau) = \frac{1}{ka j_n'(ka)} \frac{da_n(\tau)}{d\tau} , \tag{2.4.8}$$

where $j_n'(ka)$ is the first derivative of $j_n(kar_1)$ with respect to its argument evaluated at $r_1 = 1$.

It can be shown that substitution of (2.4.4), (2.4.5) and (2.4.6) along with (2.4.8) into the coupled partial differential equations (2.4.2) and (2.4.3) yields the following system of equations for the determination of $a_n(\tau)$ and $b_n(\tau)$:

for n = 0

$$\left[1+f\frac{j_o(\Omega)}{\Omega j_o'(\Omega)}\right]\frac{d^2a_o(\tau)}{d\tau^2} +2(1+\nu)a_o(\tau) = 0 , \tag{2.4.9}$$

for $n \geq 1$

$$\frac{d^2b_n(\tau)}{d\tau^2} -[1+\nu-\alpha^2(1-\nu-\lambda_n)]a_n(\tau)-(1-\nu-\lambda_n)(1+\alpha^2)b_n(\tau) = 0 , \tag{2.4.10}$$

for $n \geq 1$

$$\left[1+f\frac{j_n(\Omega)}{\Omega j_n'(\Omega)}\right]\frac{d^2a_n(\tau)}{d\tau^2} -\{(1+\nu)\lambda_n+\alpha^2[\lambda_n^2-\lambda_n(1-\nu)]\}b_n(\tau)$$

$$+\{2(1+\nu)+\alpha^2[\lambda_n^2-\lambda_n(1-\nu)]\}a_n(\tau) = 0 , \tag{2.4.11}$$

where $f = \rho_o a/\rho_s h$ = nondimensional fluid-shell parameter, $\Omega = ka = \omega a/c$, and $\lambda_n = n(n+1)$. In obtaining equations (2.4.9), (2.4.10) and (2.4.11) the differential equations satisfied by P_n and P'_n were used repeatedly.

Equations (2.4.9), (2.4.10) and (2.4.11) are linear differential equations with constant coefficients, the solutions of which are of the form

$$a_n(\tau) = A_n e^{i\Omega s\tau} ,$$
$$b_n(\tau) = B_n e^{i\Omega s\tau} , \tag{2.4.12}$$

where A_n, B_n are constants and $s = c/c_s$ is the ratio of the compressional wave speed in the fluid to the wave speed c_s defined previously.

Substitution of $a_o(\tau) = A_o e^{i\Omega s\tau}$ into (2.4.9) with the condition $A_o \neq 0$ gives the following frequency equation for n = 0

$$\left[1+f\,\frac{j_o(\Omega)}{\Omega j_o'(\Omega)}\right]s^2\Omega^2-2(1+\nu) = 0 . \tag{2.4.13}$$

Substituting (2.4.12) in (2.4.10) and (2.4.11) and factoring out $e^{i\Omega s\tau}$, one gets for $n \geq 1$

$$[(1+\nu)-\alpha^2(1-\nu-\lambda_n)]A_n+[(1+\alpha^2)(1-\nu-\lambda_n)+s^2\Omega^2]B_n = 0 ,$$
$$\left\{2(1+\nu)+\alpha^2[\lambda_n^2-\lambda_n(1-\nu)]-\left[1+f\,\frac{j_n(\Omega)}{\Omega j_n'(\Omega)}\right]s^2\Omega^2\right\}A_n-\{(1+\nu)\lambda_n+\alpha^2[\lambda_n^2-\lambda_n(1-\nu)]\}B_n = 0 , \tag{2.4.14}$$

which are homogeneous linear algebraic equations in A_n and B_n. This set of equations has a solution other than the trivial one, $A_n = B_n = 0$, only if the determinant $\Delta(\Omega)$ of the coefficients of A_n and B_n vanishes. Expansion of this determinant yields the frequency equation for $n \geq 1$

$$\left[1+f\,\frac{j_n(\Omega)}{\Omega j_n'(\Omega)}\right]s^4\Omega^4+\left\{\left[1+f\,\frac{j_n(\Omega)}{\Omega j_n'(\Omega)}\right](1-\nu-\lambda_n)(1+\alpha^2)-2(1+\nu)-\alpha^2[\lambda_n^2-\lambda_n(1-\nu)]\right\}s^2\Omega^2 \tag{2.4.15}$$

$$-(1+\nu)\{2(1-\nu-\lambda_n)(1+\alpha^2)+\lambda_n[1+\nu-\alpha^2(1-\nu-\lambda_n)]\}-\alpha^2(2-\lambda_n)[\lambda_n^2-\lambda_n(1-\nu)] = 0 .$$

It is interesting to note that appropriate limiting cases of the above frequency equations agree with results obtained by other authors.

Case 1

$f = 0$ corresponds to the absence of fluid. Introduction of values of s and Ω into (2.4.13) gives the dimensional angular frequency of pure radial motion as

$$\omega_o = \frac{1}{a}\left[\frac{2E}{\rho_s(1-\nu)}\right]^{1/2} \tag{2.4.16}$$

which was first obtained by Lamb.[13] Setting $f = 0$ and defining a new nondimensional frequency $\bar{\Omega} = \Omega s = \omega a/c_s$ in (2.4.15) yields the following frequency equation of the empty shell which was recently obtained by McIvor and Sonstegard.[17]

$$\bar{\Omega}^4-[1+3\nu-\alpha^2(1-\nu)+\lambda_n(1+\nu\alpha^2)+\alpha^2\lambda_n^2]\bar{\Omega}^2$$

$$+[\alpha^2\lambda_n^3-4\alpha^2\lambda_n^2+\alpha^2\lambda_n(5-\nu^2)+\lambda_n(1-\nu^2)-2(1+\alpha^2)(1-\nu^2)] = 0 . \tag{2.4.17}$$

Case 2

$f > 0$ and $s \to 0$ corresponds to a rigid shell containing a fluid. For this case the frequency equations (2.4.13) and (2.4.15) for an ideal fluid degenerate to

$$j'_n(\Omega) = 0 \tag{2.4.18}$$

which is easily shown to be the same as

$$2\Omega J'_{n+1/2}(\Omega) = J_{n+1/2}(\Omega) \tag{2.4.19}$$

where $J_{n+1/2}(\Omega)$ is the Bessel function of the indicated order. The frequency equation (2.4.19) was obtained by Guttinger.[7]

Case 3

$\alpha^2 = 0$ yields the frequency equation corresponding to the membrane (extensional) theory for both the empty shell ($f = 0$) and fluid-filled shell ($f > 0$) cases. The frequency equations for vibrations of a fluid-filled spherical membrane possessing infinite bulk modulus ($\nu = 1/2$) were given by Morse and Feshbach,[19] and their results agree with (2.4.13) and (2.4.15) when α^2, f and ν are given the above values.

Figure 2 is a plot of the frequency spectrum for a spherical shell *in vacuo* obtained from (2.4.17), using $\nu = .3$ and $a/h = 20$. It is to be parenthetically stated that throughout this thesis all the plots which have abscissas involving the mode number n are discrete, i.e., only those points corresponding to the integer values of n are physically meaningful. In figure 2 both the composite* (lower branch) and the membrane mode (higher branch) frequencies are

*This type of classification was first used in Ref. 17.

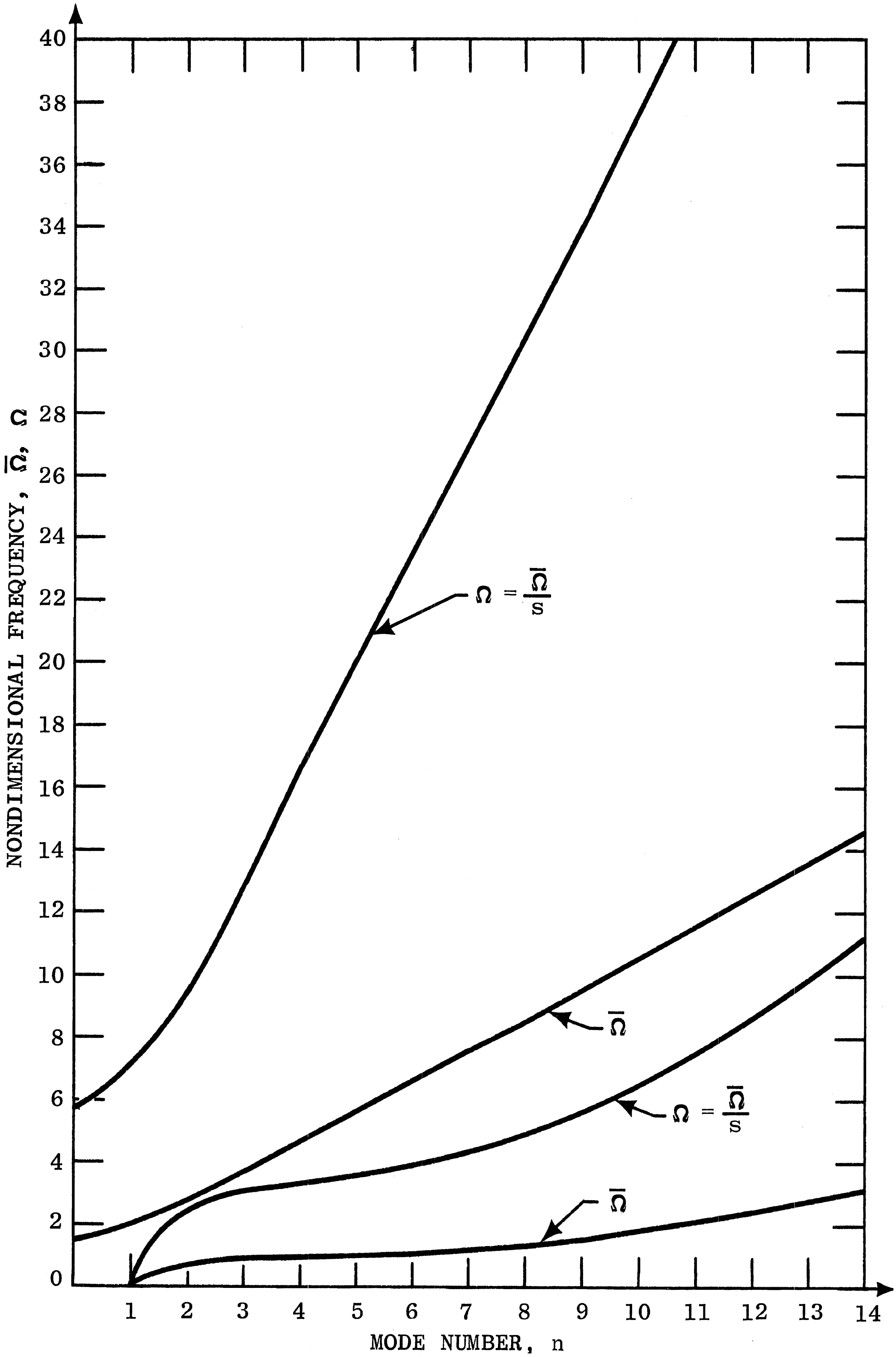

Figure 2. Frequency spectrum for an elastic spherical shell in vacuo.

plotted using the nondimensional frequency $\bar{\Omega} = \omega a/c_s$, and also $\Omega = \bar{\Omega}/s = \omega a/c$. The reason for plotting the same frequency spectrum in terms of two nondimensional frequency parameters, namely, $\bar{\Omega}$ and Ω will be readily seen after the explaination of Figures 3 and 4.

Equation (2.4.18), which gives the frequency spectrum for any ideal fluid in a rigid spherical shell, is plotted in Figure 3. In Figure 4, the spectrum of equations (2.4.13) and (2.4.15) is plotted for $\nu = .3$, $a/h = 20$ and $f = 2.56$ which corresponds to steel shell filled with water.

A close study of Figures 2, 3 and 4 reveals the following results:

(a) In Figures 2 and 3 the frequency spectra represent the natural frequencies of an empty shell and a fluid filled rigid shell, respectively. For Figure 4 one can no longer say that a particular frequency of the spectrum belongs to the shell or to the fluid since each frequency in that figure represents a natural frequency of the system composed of an elastic spherical shell and the fluid occupying the interior space of the shell.

(b) When the shell containing the fluid becomes elastic, certain portions of the spectrum become distorted. This author will name the above-mentioned phenomenon as "The higher branch distortion" since the membrane behavior of the shell, serving as an elastic boundary for the fluid, is responsible for this phenomenon. It is to be noted that if Figures 2 and 4 are compared the higher branch of the frequency spectrum for spherical shell in vacuo, passes through the distorted portion of the spectrum in Figure 4. Due to predominately membrane behavior of the modes corresponding to the frequencies located on the "higher branch" of the spectrum shown in Figure 2, it is reasonable to seek the cause of "the higher branch distortion" appearing in Figure 4 in the membrane

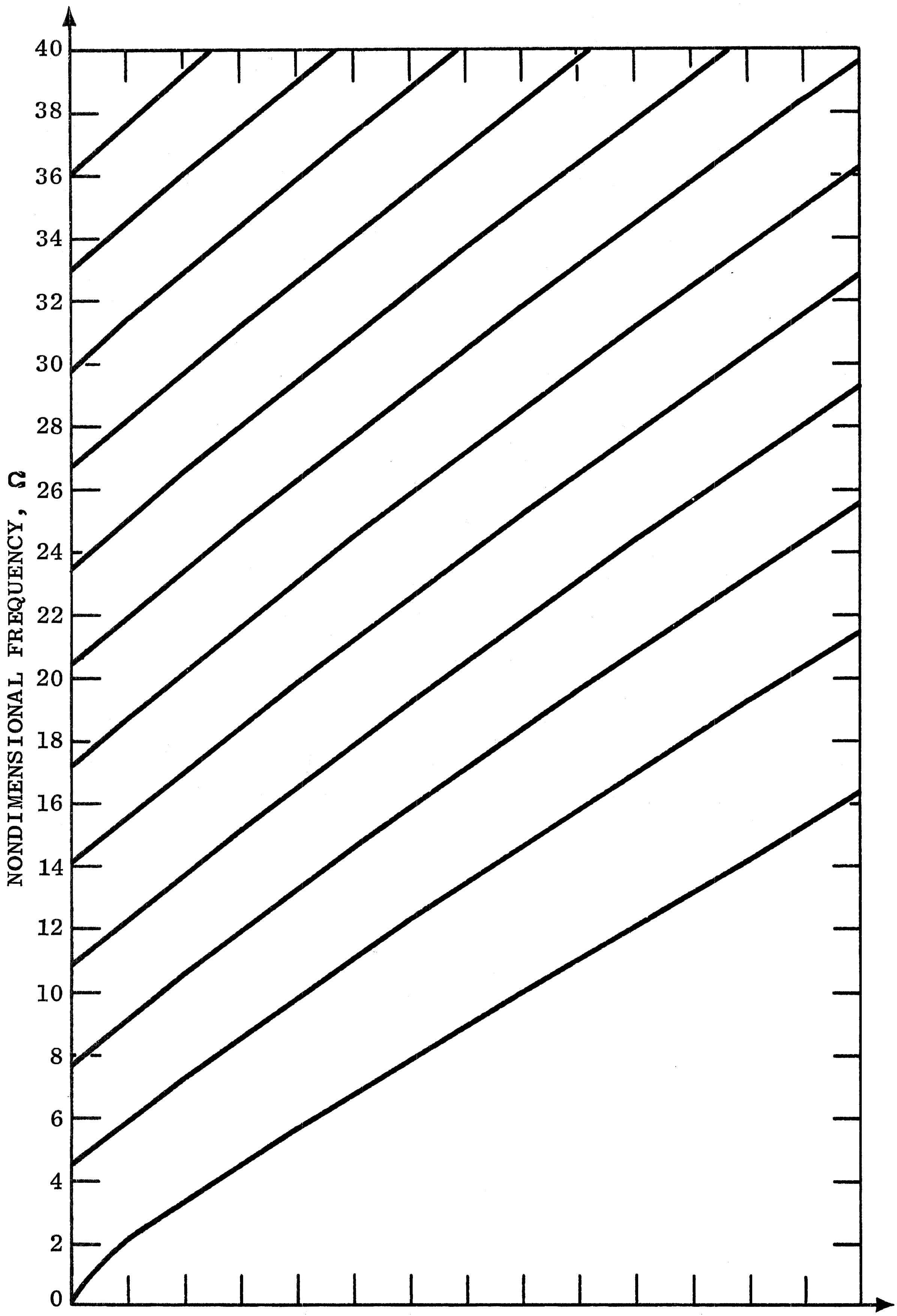

Figure 3. Frequency spectrum for a rigid fluid-filled spherical shell.

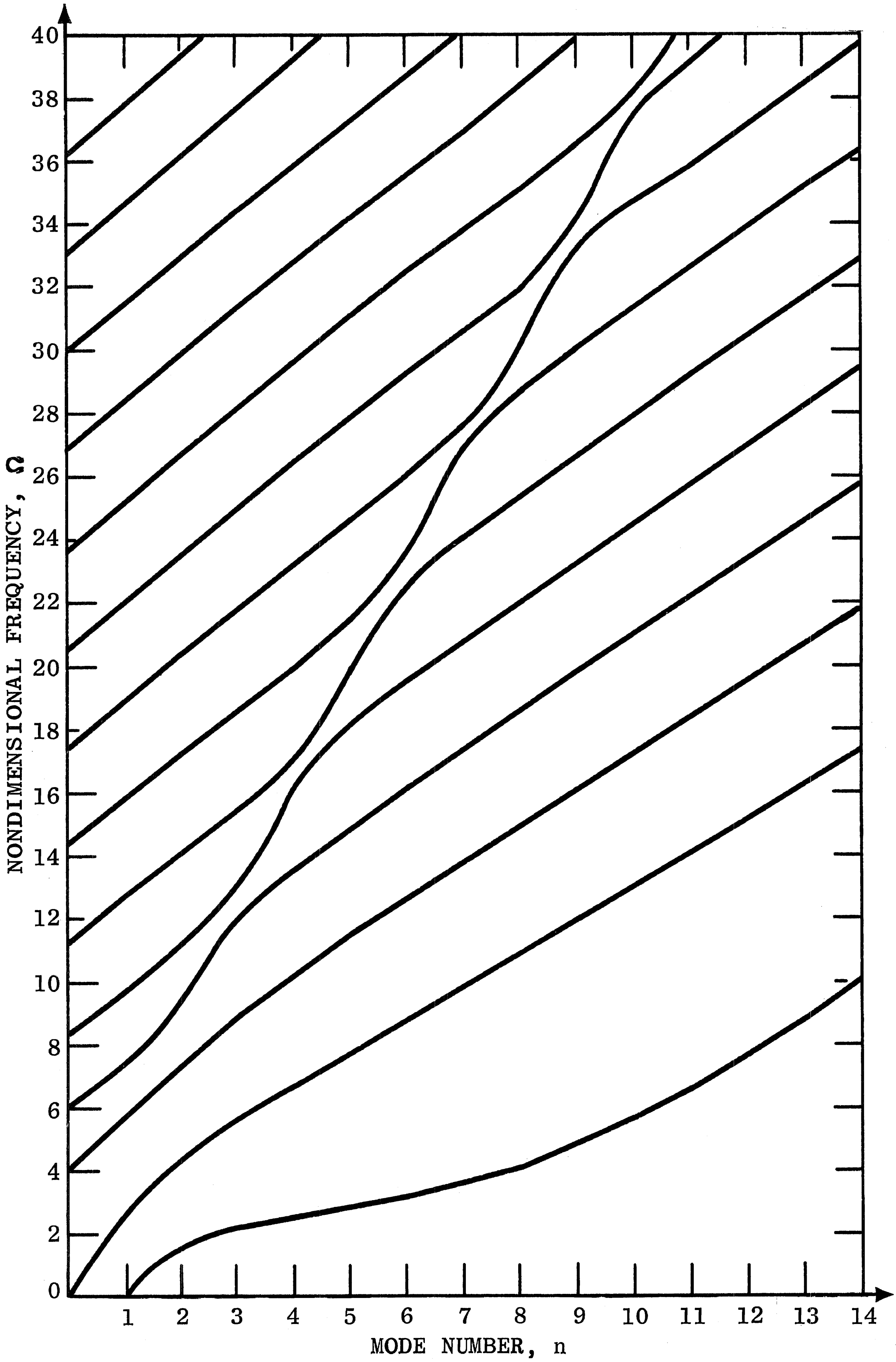

Figure 4. Frequency spectrum for an elastic fluid-filled spherical shell.

behavior of the shell.

(c) Comparison of Figures 3 and 4 exhibits a branch of frequencies which does not exist in the spectrum of Figure 3, but shows itself in the spectrum of Figure 4. This is the lowest branch of frequencies displayed in Figure 4. The existence of this branch in the frequency spectrum for an elastic fluid-filled shell is due to the existence of the "lower branch" of frequencies corresponding to a composite mode behavior of the empty shell. The composite mode behavior in the empty shell case is explained in Ref. 17 to have the effects of both membrane and bending; membrane behavior for small n and bending behavior for large.

CHAPTER 3

RESPONSE TO A LOCAL RADIAL IMPULSE

In this chapter, the response of a fluid-filled spherical shell subjected to a local, radial impulsive load will be determined. The equations of motion derived in Section 2.3 are solved by means of Laplace transformation.

3.1. PRELIMINARY REMARKS

The external load, designated by $F_e(\varphi,t)$ in equation (2.3.7), is assumed to be axisymmetric and its impulsive nature is expressed by means of the Dirac delta function, $\delta(t)$, the properties of which are accepted here in the usual sense seen in applied mathematics. When the external load, $F_e = F(\varphi)\ \delta(t)$, is applied to the fluid-filled shell which is initially at rest relative to the inertial reference XYZ, as shown in Figure 5, the mass center of the sphere will experience a rigid body velocity, V_c, with a step function H(t) behavior due to the impulsive nature of the external load. Since the resultant force

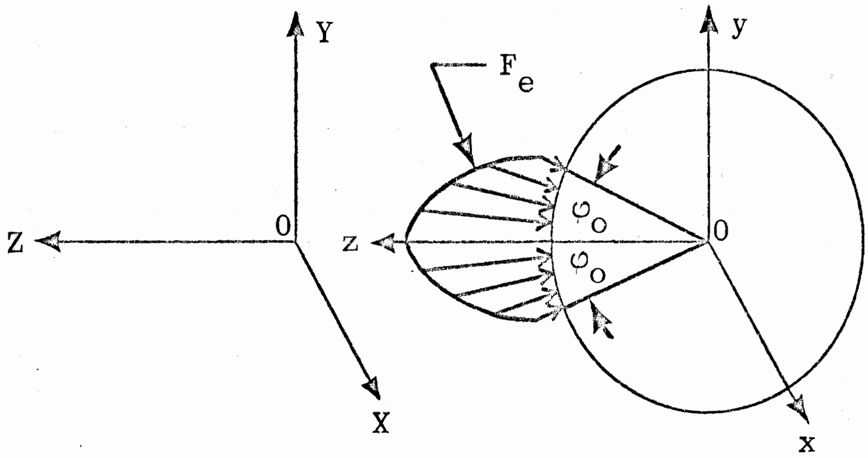

Figure 5. Axisymmetric, external load application.

of the external load passes through the mass center of the sphere, V_c can be calculated from

$$\int_S F(\varphi)\ \delta(t)dS = M\frac{dV_c}{dt} \quad , \tag{3.1.1}$$

where $M = m_s + m_o$ is the total mass of the system

$F(\varphi)$ = external load intensity per unit mid-surface area of the shell

$dS = 2\pi a^2 \sin\varphi \ d\varphi$

Integration of (3.1.1) with respect to time yields the velocity, V_c, imparted to the mass center of the system in the -Z direction

$$V_c = \frac{H(t)}{M}\int_S F(\varphi)dS \quad , \tag{3.1.2}$$

where $H(t)$ is Heaviside unit step function.

If desired, the equations of motion which were obtained in Section 2.3 with respect to a coordinate system moving with the sphere can be written with respect to the inertial reference XYZ by defining a nondimensional displacement vector $\bar{D}$ for the mid-surface of the shell and a nondimensional velocity potential Φ_2 for the fluid. In Figure 6, at $t = 0$, XYZ and xyz are assumed to coincide and this figure is helpful for the definitions of $\bar{D}$ and Φ_2. Let the radial and tangential components of $\bar{D}$ be W and U respectively, then

$$\left.\begin{aligned} W(\varphi,\tau) &= \zeta(\varphi,\tau) - \frac{V_c\tau}{c_s}\cos\varphi \quad , \\ U(\varphi,\tau) &= \psi(\varphi,\tau) + \frac{V_c\tau}{c_s}\sin\varphi \quad , \\ \Phi_2(r_1,\varphi,\tau) &= \Phi_1(r_1,\varphi,\tau) - \frac{V_c r_1}{c_s}\cos\varphi \quad , \end{aligned}\right\} \tag{3.1.3}$$

In (3.1.3), $\zeta(\varphi,\tau)$, $\psi(\varphi,\tau)$, and $\Phi_1(r_1,\varphi,\tau)$ are as defined in Chapter 2.

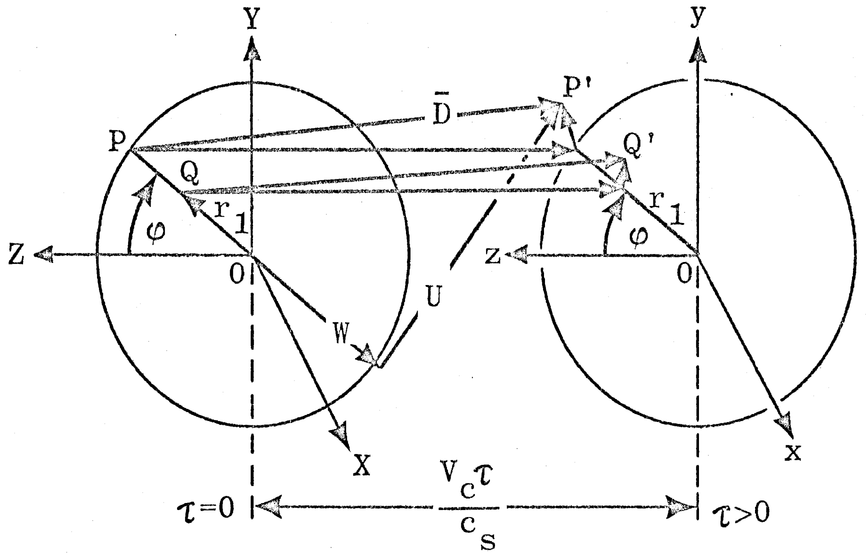

Figure 6. Displacement vectors referred to inertial reference XYZ.

3.2. TRANSFORMS OF EQUATIONS OF MOTION

The nondimensional forms of equations (2.3.6), (2.3.7), and (2.3.11) are rewritten here for convenience, they are respectively:

$$\alpha^2\left[\frac{\partial^2\psi}{\partial\varphi^2} + \cot\varphi \frac{\partial\psi}{\partial\varphi} - (\nu+\cot^2\varphi)\psi - \frac{\partial^3\zeta}{\partial\varphi^3} - \cot\varphi \frac{\partial^2\zeta}{\partial\varphi^2} + (\nu+\cot^2\varphi)\frac{\partial\zeta}{\partial\varphi}\right] + \frac{\partial^2\psi}{\partial\varphi^2}$$

$$+ \cot\varphi \frac{\partial\psi}{\partial\varphi} - (\nu+\cot^2\varphi)\psi + (1+\nu)\frac{\partial\zeta}{\partial\varphi} - \frac{\partial^2\psi}{\partial\tau^2} = 0 \quad , \qquad (3.2.1)$$

$$\alpha^2\left[\frac{\partial^3\psi}{\partial\varphi^3} + 2\cot\varphi \frac{\partial^2\psi}{\partial\varphi^2} - (1+\nu+\cot^2\varphi)\frac{\partial\psi}{\partial\varphi} + \cot\varphi\,(2-\nu+\cot^2\varphi)\psi - \frac{\partial^4\zeta}{\partial\varphi^4} - 2\cot\varphi \frac{\partial^3\zeta}{\partial\varphi^3}\right.$$

$$\left. + (1+\nu+\cot^2\varphi)\frac{\partial^2\zeta}{\partial\varphi^2} - \cot\varphi\,(2-\nu+\cot^2\varphi)\frac{\partial\zeta}{\partial\varphi}\right] - (1+\nu)\left(\frac{\partial\psi}{\partial\varphi} + \cot\varphi\,\psi + 2\zeta\right)$$

$$- \frac{\partial^2\zeta}{\partial\tau^2} - f\,\frac{\partial\Phi_1(1,\varphi,\tau)}{\partial\tau} = - \frac{(1-\nu^2)}{Eh} a\,F(\varphi)\,\delta(\tau) \quad , \qquad (3.2.2)$$

$$\frac{1}{r_1^2}\frac{\partial}{\partial r_1}\left(r_1^2\frac{\partial\Phi_1}{\partial r_1}\right) + \frac{1}{r_1^2\sin\varphi}\frac{\partial}{\partial\varphi}\left(\sin\varphi\frac{\partial\Phi_1}{\partial\varphi}\right) - \frac{1}{s^2}\frac{\partial^2\Phi_1}{\partial\tau^2} = 0 \quad , \qquad (3.2.3)$$

where

$$\psi = \frac{u}{a} \;, \quad \zeta = \frac{w}{a} \;, \quad \tau = \frac{c_s}{a}t \;, \quad c_s = \left[\frac{E}{\rho_s(1-\nu^2)}\right]^{1/2}$$

$$s = \frac{c}{c_s} \;, \quad r_1 = \frac{r}{a} \;, \quad \Phi_1 = \frac{\Phi}{ac_s} \;, \quad f = \frac{\rho_o a}{\rho_s h} \;.$$

Since the fluid-filled shell is assumed to be at rest prior to the application of the radial impulsive load, all the initial conditions relevant to the differential equations (3.2.1), (3.2.2), and (3.2.3) are homogeneous, i.e.,

$$
\begin{aligned}
&(1)\quad \zeta(\varphi,0) = 0 \ , &&(2)\quad \frac{\partial\zeta(\varphi,0)}{\partial\tau} = 0 \ , \\
&(3)\quad \psi(\varphi,0) = 0 \ , &&(4)\quad \frac{\partial\psi(\varphi,0)}{\partial\tau} = 0 \ , \qquad\qquad (3.2.4)\\
&(5)\quad \Phi_1(r_1,\varphi,0) = 0 \ , &&(6)\quad \frac{\partial\Phi_1(r_1,\varphi,0)}{\partial\tau} = 0 \ .
\end{aligned}
$$

Let the following be the notation for the Laplace transform of a function $F(\tau)$ with respect to τ

$$
L\{F(\tau)\} = \bar{F}(p) = \int_0^\infty e^{-p\tau} F(\tau)d\tau \ ,
$$

where p is a complex variable. Since ζ, ψ, and Φ_1 are functions of more than one independent variable, let their Laplace transforms be denoted by

$$
\begin{aligned}
L_\tau\{\zeta(\varphi,\tau)\} &= \bar{\zeta}(\varphi,p) = \bar{\zeta} \ , \\
L_\tau\{\psi(\varphi,\tau)\} &= \bar{\psi}(\varphi,p) = \bar{\psi} \ , \qquad\qquad (3.2.5)\\
L_\tau\{\Phi_1(r_1,\varphi,\tau)\} &= \bar{\Phi}_1(r_1,\varphi,p) = \bar{\Phi}_1 \ .
\end{aligned}
$$

Using the notation defined in (3.2.5) and the initial conditions (3.2.4) the Laplace transforms of equations (3.2.1), (3.2.2), and (3.2.3) with respect to the nondimensional time, τ, are:

$$
\alpha^2\left[\frac{d^2\bar{\psi}}{d\varphi^2} + \cot\varphi\ \frac{d\bar{\psi}}{d\varphi} - (\nu+\cot^2\varphi)\bar{\psi} - \frac{d^3\bar{\zeta}}{d\varphi^3} - \cot\varphi\ \frac{d^2\bar{\zeta}}{d\varphi^2} + (\nu+\cot^2\varphi)\ \frac{d\bar{\zeta}}{d\varphi}\right] + \frac{d^2\bar{\psi}}{d\varphi^2}
$$

(equation continued on next page)

$$+ \cot\varphi \frac{d\bar{\psi}}{d\varphi} - (\nu+\cot^2\varphi)\bar{\psi} + (1+\nu)\frac{d\bar{\zeta}}{d\varphi} - p^2\bar{\psi} = 0 \quad , \tag{3.2.6}$$

$$\alpha^2\left[\frac{d^3\bar{\psi}}{d\varphi^3} + 2\cot\varphi \frac{d^2\bar{\psi}}{d\varphi^2} - (1+\nu+\cot^2\varphi)\frac{d\bar{\psi}}{d\varphi} + \cot\varphi\,(2-\nu+\cot^2\varphi)\bar{\psi} - \frac{d^4\bar{\zeta}}{d\varphi^4}\right.$$

$$\left. - 2\cot\varphi \frac{d^3\bar{\zeta}}{d\varphi^3} + (1+\nu+\cot^2\varphi)\frac{d^2\bar{\zeta}}{d\varphi^2} - \cot\varphi\,(2-\nu+\cot^2\varphi)\frac{d\bar{\zeta}}{d\varphi}\right]$$

$$- (1+\nu)\left(\frac{d\bar{\psi}}{d\varphi} + \cot\varphi\,\psi + 2\bar{\zeta}\right) - p^2\bar{\zeta} - pf\,\Phi_1(1,\varphi,p) = - \frac{(1-\nu^2)a\,F(\varphi)}{Eh} \quad , \tag{3.2.7}$$

$$\frac{1}{r_1^2}\frac{\partial}{\partial r_1}\left(r_1^2 \frac{\partial\bar{\Phi}_1}{\partial r_1}\right) + \frac{1}{r_1^2 \sin\varphi}\frac{\partial}{\partial\varphi}\left(\sin\varphi \frac{\partial\bar{\Phi}_1}{\partial\varphi}\right) - \frac{p^2}{s^2}\bar{\Phi}_1 = 0 \quad . \tag{3.2.8}$$

The transform of the boundary condition between fluid and shell is:

$$p\,\bar{\zeta}(\varphi, p) = \frac{\partial\bar{\Phi}_1(1,\varphi,p)}{\partial r_1} \quad . \tag{3.2.9}$$

Thus, the problem has been reduced from the solution of three partial differential equations to that of one partial differential equation and two ordinary differential equations in the transform space. From another point of view, one can picture the two ordinary differential equations, (3.2.6) and (3.2.7), along with condition (3.2.9) as rather complex boundary conditions to the partial differential equation (3.2.8).

Before proceeding with the solution of the above equations, we first expand the function

$$g(\varphi) = \begin{cases} F(\varphi) & , \ 0 < \varphi < \varphi_o \\ 0 & , \ \varphi_o < \varphi < \pi \end{cases} \tag{3.2.10}$$

in a series of Legendre polynomials of the form

$$g(\varphi) = \sum_{n=0}^{\infty} F_n P_n(\cos\varphi) \quad .$$

In particular, if $F(\varphi) = F$ = constant, then, the coefficients F_n are found, by the usual methods, to be

$$F_n = \frac{1}{2} F[P_{n-1}(\cos\varphi_o) - P_{n+1}(\cos\varphi_o)] \quad , \; n = 0,1,2,\ldots$$

it being realized of course, that $P_{-1}(\cos\varphi_o) \equiv 1$.

Next, the method of separation of variables is applied to the partial differential equation (3.2.8) to obtain two ordinary differential equations that $R(r_1)$ and $G(\varphi)$ must satisfy. When the assumed solution, $\Phi_1(r_1,\varphi) = R(r_1)\, G(\varphi)$ is substituted into equation (3.2.8) the following equations are obtained:

$$G''(\varphi) + \cot\varphi \; G'(\varphi) + n(n+1)\, G(\varphi) = 0 \quad , \tag{3.2.11}$$

$$R''(r_1) + \frac{2}{r_1} R'(r_1) + [k^2 - \frac{n(n+1)}{r_1^2}]R(r_1) = 0 \quad , \tag{3.2.12}$$

where (') denotes differentiation with respect to the argument, k is complex and its value is pi/s. The bounded solutions of (3.2.11) and (3.2.12) in the spherical region under consideration are $G(\varphi) = c_1 P_n(\cos\varphi)$ and $R(r_1) = c_2\, j_n(\frac{ip}{s} r_1)$ respectively; where c_1 and c_2 are two arbitrary constants. Since the equation (3.2.8) is linear, by superposition one can arrive at a formal solution

$$\bar{\Phi}_1(r_1,\varphi,p) = \sum_{n=0}^{\infty} c_n(p)\, j_n(\frac{ip}{s} r_1)\, P_n(\cos\varphi) \quad , \tag{3.2.13}$$

where the coefficients $c_n(p)$ will be determined later. Now, let us consider the two ordinary differential equations (3.2.6) and (3.2.7). In order to reduce these equations to a pair of equivalent algebraic equations in the "transform space" assume the following expansions for $\bar{\zeta}$ and $\bar{\psi}$:

$$\bar{\zeta}(\varphi,p) = \sum_{n=0}^{\infty} \bar{a}_n(p)\, P_n(\cos\varphi) \quad ,$$
$$\bar{\psi}(\varphi,p) = \sum_{n=1}^{\infty} \bar{b}_n(p)\, \dot{P}_n(\cos\varphi) \quad . \tag{3.2.14}$$

Substitution of (3.2.13) and the first expression of (3.2.14) into the transformed boundary condition (3.2.9) yields the coefficients $c_n(p)$. These coefficients, for each integer value of n, are

$$c_n(p) = \frac{\bar{a}_n(p)}{\frac{i}{s}\, j'_n(\frac{ip}{s})} \qquad n = 0,1,2\ldots \tag{3.2.15}$$

Thus, the unknown coefficients, $c_n(p)$, of the transformed velocity potential, $\bar{\Phi}_1(r_1,\varphi,p)$, are expressed in terms of the coefficients, $\bar{a}_n(p)$, of the radial displacement of the shell mid-surface in the transform space. Hence, (3.2.13) can now be written as

$$\bar{\Phi}_1(r_1,\varphi,p) = \sum_{n=0}^{\infty} \frac{\bar{a}_n(p)}{\frac{i}{s}\, j'_n(\frac{ip}{s})}\, j_n(\frac{ip}{s}\, r_1)\, P_n(\cos\varphi) \quad . \tag{3.2.16}$$

The reduction of the two ordinary differential equations (3.2.6) and (3.2.7) to algebraic equations in the transform space is accomplished by substituting (3.2.10), (3.2.14), and (3.2.16) into (3.2.6) and (3.2.7). The equations resulting from the substitutions, contain higher order derivatives of both Legendre and Associated Legendre polynomials. All these derivatives are eliminated by making repeated use of the differential equations satisfied by P_n and P'_n. Hence, after some manipulations one obtains the following equations that $\bar{a}_n(p)$ and $\bar{b}_n(p)$ must satisfy:

For $n = 0$
$$\left\{p^2\left[1 + f\,\frac{1}{\frac{ip}{s}}\,\frac{j_o(\frac{ip}{s})}{j_o'(\frac{ip}{s})}\right] + 2(1+\nu)\right\}\bar{a}_o(p) = \frac{(1-\nu^2)a}{Eh}\,F_o \tag{3.2.17}$$

$$p_{1n}\bar{a}_n(p) + (p^2+q_{1n})\,\bar{b}_n(p) = 0\ , \tag{3.2.18}$$

For $n \geq 1$
$$\left\{p^2\left[1 + f\,\frac{1}{\frac{ip}{s}}\,\frac{j_n(\frac{ip}{s})}{j_n'(\frac{ip}{s})}\right] + p_{2n}\right\}\bar{a}_n(p) + q_{2n}\bar{b}_n(p) = \frac{(1-\nu^2)a}{Eh}\,F_n\ , \tag{3.2.19}$$

where

$$\left.\begin{aligned} p_{1n} &= -(1+\nu) + \alpha^2(1-\nu-\lambda_n)\ , \\ q_{1n} &= -(1+\alpha^2)(1-\nu-\lambda_n)\ , \\ p_{2n} &= 2(1+\nu) + \alpha^2[\lambda_n^2 - \lambda_n(1-\nu)]\ , \\ q_{2n} &= -(1+\nu)\lambda_n - \alpha^2[\lambda_n^2 - \lambda_n(1-\nu)]\ . \end{aligned}\qquad \lambda_n = n(n+1)\right\} \tag{3.2.20}$$

From (3.2.17)

$$\bar{a}_o(p) = \frac{R_o}{p^2\left[1 + f\,\frac{1}{\frac{ip}{s}}\,\frac{j_o(\frac{ip}{s})}{j_o'(\frac{ip}{s})}\right] + 2(1+\nu)}\ , \tag{3.2.21}$$

where

$$R_o = \frac{(1-\nu^2)aF_o}{Eh} = \frac{(1-\nu^2)aF}{2Eh}(1 - \cos\varphi_o)\ .$$

Applying Cramer's rule to (3.2.18) and (3.2.19) we obtain the following expressions for $\bar{a}_n(p)$ and $\bar{b}_n(p)$, for ≥ 1,

$$\bar{a}_n(p) = \frac{R_n(p^2 + q_{1n})}{\Delta_n(p)} \quad , \tag{3.2.22}$$

$$\bar{b}_n(p) = \frac{-R_n\, p_{1n}}{\Delta_n(p)} \quad , \tag{3.2.23}$$

where

$$R_n = \frac{(1-\nu^2)aF_n}{Eh} = \frac{(1-\nu^2)aF}{2Eh}[P_{n-1}(\cos\varphi_o) - P_{n+1}(\cos\varphi_o)] \quad ,$$

$$\Delta_n(p) = \left[1 + f\,\frac{1}{\frac{ip}{s}}\,\frac{j_n(\frac{ip}{s})}{j_n'(\frac{ip}{s})}\right]p^4 + \left\{\left[1 + f\,\frac{1}{\frac{ip}{s}}\,\frac{j_n(\frac{ip}{s})}{j_n'(\frac{ip}{s})}\right]q_{1n} + p_{2n}\right\}p^2 + (q_{1n}p_{2n} - p_{1n}q_{2n}) \ . \tag{3.2.24}$$

Substitution of (3.2.21), (3.2.22), and (3.2.23) into (3.2.14) gives the final form of the transformed displacement components of the mid-surface. These are

$$\bar{\zeta}(\varphi,p) = \frac{R_o}{p^2\left[1 + f\,\frac{1}{\frac{ip}{s}}\,\frac{j_o(\frac{ip}{s})}{j_o'(\frac{ip}{s})}\right] + 2(1+\nu)} + \sum_{n=1}^{\infty} \frac{R_n(p^2 + q_{1n})}{\Delta_n(p)} P_n(\cos\varphi) \quad , \tag{3.2.25}$$

$$\bar{\psi}(\varphi,p) = \sum_{n=1}^{\infty} \frac{-R_n\, p_{1n}}{\Delta_n(p)} \dot{P}_n(\cos\varphi) \quad . \tag{3.2.26}$$

3.3. INVERSION OF $\bar{\zeta}(\varphi,p)$, $\bar{\psi}(\varphi,p)$, and $\bar{\Phi}_1(r_1,\varphi,p)$

Due to the physical nature of the problem ζ, ψ, and Φ_1 should satisfy the following conditions:

(1) $\zeta(\varphi,\tau)$, $\psi(\varphi,\tau)$, and $\Phi_1(r_1,\varphi,\tau)$ are defined for $\tau \geq 0$ and they are each $O(e^{c_o\tau})$, where c_o is a constant.

(2) $\zeta(\varphi,\tau)$, $\psi(\varphi,\tau)$, $\Phi_1(r_1,\varphi,\tau)$ and their time derivatives are sectionally continuous. Then

$$\zeta(\varphi,\tau) = \frac{1}{2\pi i} \lim_{R\to\infty} \int_{c-iR}^{c+iR} \left\{ \frac{R_o}{p^2\left[1 + f\,\dfrac{1}{\frac{ip}{s}}\,\dfrac{j_o(\frac{ip}{s})}{j_o'(\frac{ip}{s})}\right] + 2(1+\nu)} + \sum_{n=1}^{\infty} \frac{R_n(p^2+q_{1n})}{\Delta_n(p)} P_n(\cos\varphi) \right\} e^{p\tau} dp \,, \tag{3.3.1}$$

$$\psi(\varphi,\tau) = \frac{1}{2\pi i} \lim_{R\to\infty} \int_{c-iR}^{c+iR} \left\{ \sum_{n=1}^{\infty} \frac{-R_n\, p_{1n}}{\Delta_n(p)} \dot{P}_n(\cos\varphi) \right\} e^{p\tau} dp \,, \tag{3.3.2}$$

$$\Phi_1(r_1,\varphi,\tau) = \frac{1}{2\pi i} \lim_{R\to\infty} \int_{c-iR}^{c+iR} \left\{ \frac{R_o\, j_o(\frac{ip}{s} r_1)}{\frac{i}{s}\, j_o'(\frac{ip}{s}) \left\langle p^2\left[1 + f\,\dfrac{1}{\frac{ip}{s}}\,\dfrac{j_o(\frac{ip}{s})}{j_o'(\frac{ip}{s})}\right] + 2(1+\nu)\right\rangle} + \sum_{n=1}^{\infty} \frac{R_n(p^2 + q_{1n})\, j_n(\frac{ip}{s} r_1)}{\frac{i}{s}\, j_n'(\frac{ip}{s})\, \Delta_n(p)} P_n(\cos\varphi) \right\} e^{p\tau} dp \,, \tag{3.3.3}$$

where the path of integration is the line Re $p = c$ in the complex p-plane and c is any constant greater than c_o. As a consequence of a theorem in the theory of complex variables, the functions inside of the braces in (3.3.1), (3.3.2), and (3.3.3) are analytic functions in the half-plane Re$(p) > c$, i.e., they have no singularities to the right of the line Re $p = c$. This fact enables us to evaluate the integrals in (3.3.1), (3.3.2), and (3.3.3) by enclosing all the singularities to the left of the line Re $p = c$ by a suitable contour shown in Figure 7 and making use of Cauchy's residue theorem.

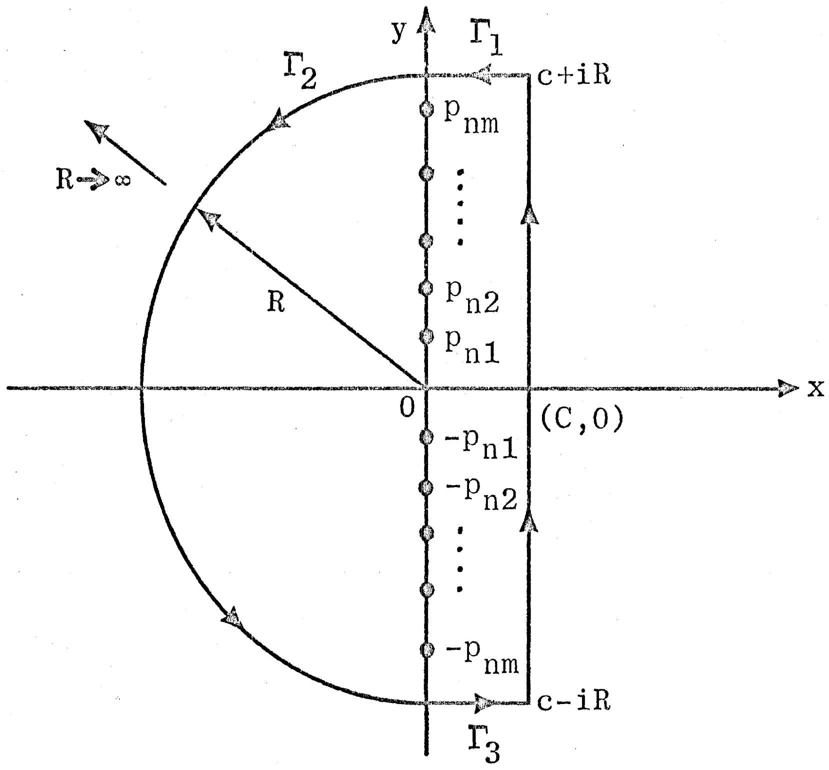

Figure 7. The path of integration for evaluations of inversion integrals.

Let any one of the terms inside of the braces in (3.3.1), (3.3.2), and (3.3.3) be denoted by $f_n(p)$, then

$$\lim_{R\to\infty}\left\{\int_{c-iR}^{c+iR} e^{p\tau} f_n(p)dp + \int_{\Gamma_1} e^{p\tau} f_n(p)dp + \int_{\Gamma_2} e^{p\tau} f_n(p)dp + \int_{\Gamma_3} e^{p\tau} f_n(p)dp\right\}$$
$$= 2\pi i \sum_{m=1}^{\infty} \operatorname{Res}_{p_{nm}} [e^{p\tau} f_n(p)] \quad . \tag{3.3.4}$$

Since $|f_n(p)| \leq M|p|^{-\kappa}$ when $|p| > R_o$, where M, κ are constants and $\kappa > 0$, then, it can be shown that (i.e., see Reference 24)

$$\lim_{R\to\infty}\left\{\int_{\Gamma_1} e^{p\tau} f_n(p)\,dp + \int_{\Gamma_2} e^{p\tau} f_n(p)dp + \int_{\Gamma_3} e^{p\tau} f_n(p)dp\right\} = 0 \quad . \tag{3.3.5}$$

Thus, in view of (3.3.4) and (3.3.5)

$$\frac{1}{2\pi i} \lim_{R\to\infty} \int_{c-iR}^{c+iR} f_n(p)e^{p\tau}dp = \sum_{m=1}^{\infty} \operatorname{Res}_{p_{nm}} [e^{p\tau} f_n(p)] \quad . \tag{3.3.6}$$

Next, let us apply (3.3.6) to each term of (3.3.1). The first term is n = 0 term and for this term

$$f_o(p) = \frac{R_o}{p^2\left[1 + f\,\dfrac{1}{\frac{ip}{s}}\,\dfrac{j_o(\frac{ip}{s})}{j_o'(\frac{ip}{s})}\right] + 2(1+\nu)} = \bar{a}_o(p) \quad . \qquad (3.3.7)$$

Since $f_o(p)$ is a single-valued function the only singularities of $f_o(p)$ are the poles. The poles of $f_o(p)$ are the zeros of the denominator. If we substitute $p = \mp is\Omega$ to the denominator of $f_o(p)$, also noting that $j_o(\Omega) = j_o(-\Omega)$ and $j_o'(\Omega) = -j_o'(-\Omega)$, we get the frequency equation (2.4.13). Denoting the zeros of (2.4.13) by Ω_{om}, we can conclude that the poles of $f_o(p)$ are pure imaginary and hence of the form $p = \mp is\Omega_{om}$. At this time a question arises concerning the possibility that $f_o(p)$ may have poles other than those on the imaginary axis. To investigate this possibility let us define $z = x + iy = ip/s$, and substitute it into denominator of $f_o(p)$. Setting the denominator equal to zero we obtain the following expression

$$\frac{z\,\cos z[-s^2z^2 + 2(1+\nu)] + \sin z[s^2z^2(1-f) - 2(1+\nu)]}{z\,\cos z - \sin z} = 0 \quad . \qquad (3.3.8)$$

Sinz and cosz are entire functions which can be written as:

$$\left.\begin{aligned} \sin z &= \sin(x+iy) = \sin x \cosh y + i \cos x \sinh y \\ \cos z &= \cos(x+iy) = \cos x \cosh y - i \sin x \sinh y \end{aligned}\right\} \qquad (3.3.9)$$

By substituting (3.3.9) into the numerator of (3.3.8) and equating the real and the imaginary parts of the resulting expression to zero we get the following two simultaneous equations which x and y must satisfy

$$\cos x \quad \cosh y\{[2(1+\nu) - s^2(x^2-y^2)]x + 2xy^2s^2\} + \sin x \quad \sinh y\{[2(1+\nu) - s^2(x^2-y^2)]y$$

$$- 2yx^2s^2\} + \sin x \quad \cosh y[s^2(1-f)(x^2-y^2) - 2(1+\nu)]$$

$$- \cos x \quad \sinh y(1-f)2xys^2 = 0 \qquad (3.3.10)$$

$$\cos x \quad \cosh y\{[2(1+\nu) - s^2(x^2-y^2)]y - 2yx^2s^2\} - \sin x \quad \sinh y\{[2(1+\nu) - s^2(x^2-y^2)]x$$

$$+ 2xy^2s^2\} + \sin x \quad \cosh y(1-f)\ 2xys^2$$

$$+ \cos x \quad \sinh y(1-f)(x^2-y^2)s^2 = 0 \qquad (3.3.11)$$

(3.3.10) and (3.3.11) have been programmed on the digital computer and no pair of (x,y) was found to satisfy both equations simultaneously. For $y = 0$ (3.3.11) is satisfied identically, and (3.3.10) reduces to

$$[-s^2x + s^2(1-f)\ \tan x]x^2 + 2(1+\nu)[x - \tan x] = 0 \qquad (3.3.12)$$

which is a different form of the frequency equation (2.4.13) corresponding to the $n = 0$ case. One can also argue from the physical point of view that $f_o(p)$ cannot have any complex poles, for if it had, this would mean that the system possesses complex frequencies. However, only systems with damping have complex frequencies and since the system under consideration does not have damping it cannot have complex frequencies. Therefore $\mp is\Omega_{om}$ are the only poles of $f_o(p)$. We also notice that all the poles are simple since all the corresponding frequencies are distinct.

In general, $e^{p\tau}f_n(p)$ has the fractional form, i.e.,

$$e^{p\tau}f_n(p) = \frac{h(p)}{g(p)} \quad . \qquad (3.3.13)$$

When $e^{p\tau} f_n(p)$ has simple pole at $p = p_{nm}$, $h(p)$ and $g(p)$ satisfy the conditions $g(p_{nm}) = 0$, $g'(p_{nm}) \neq 0$, and $h(p_{nm}) \neq 0$ then the residue of $e^{p\tau} f_n(p)$ has the value

$$\operatorname{Res}_{p_{nm}} [e^{p\tau} f_n(p)] = \frac{h(p_{nm})}{g'(p_{nm})} \quad . \tag{3.3.14}$$

Using (3.3.14) with (3.3.7) gives the residue at the pole $p = p_{om}$

$$\operatorname{Res}_{p_{om}} [e^{p} f_o(p)] = \frac{e^{p_{om}\tau} \frac{i}{s} R_o \, j_o'^2(\frac{ip_{om}}{s})}{\frac{ip_{om}}{s}(2+f)\, j_o'^2(\frac{ip_{om}}{s}) + f\, j_o(\frac{ip_{om}}{s}) \left[j_o'(\frac{ip_{om}}{s}) - \frac{ip_{om}}{s} j_o''(\frac{ip_{om}}{s}) \right]} \tag{3.3.15}$$

The poles occur at $p = 0$ and $p = \mp is\Omega_{om}$. In (3.3.15) the second derivative of the spherical Bessel function can be eliminated by utilizing the differential equation satisfied by $j_n(z)$, namely

$$z^2 j_n''(z) + 2z\, j_n'(z) + [z^2 - \lambda_n]\, j_n(z) = 0 \quad . \tag{3.3.16}$$

Substitution of the definitions of $j_o(z)$ and $j_o'(z)$ into (3.3.15) and application of L'Hospital's rule shows that the residue at $p = 0$ is zero. Evaluation of the remaining residues at the poles $p = \mp is\Omega_{om}$ gives the following relation

$$e^{is\Omega_{om}\tau} \operatorname{Res}_{-is\Omega_{om}} [e^{p\tau} f_o(p)] = - \operatorname{Res}_{is\Omega_{om}} [e^{p\tau} f_o(p)] e^{-is\Omega_{om}\tau} \tag{3.3.17}$$

In view of (3.3.17) we obtain from (3.3.6), (3.3.7), and (3.3.15)

$$a_o(\tau) = \sum_{m=1}^{\infty} \frac{\frac{i}{s} R_o [e^{-is\Omega_{om}\tau} - e^{is\Omega_{om}\tau}] \, j_o'^2(\Omega_{om})}{\Omega_{om}(2+f) \, j_o'^2(\Omega_{om}) + f \, j_o(\Omega_{om})[3j_o'(\Omega_{om}) + \Omega_{om} j_o(\Omega_{om})]}$$

or

$$a_o(\tau) = \sum_{m=1}^{\infty} \frac{\frac{2}{s} \sin(s\Omega_{om}\tau) \, R_o \, j_o'^2(\Omega_{om})}{\Omega_{om}(2+f) \, j_o'^2(\Omega_{om}) + f \, j_o(\Omega_{om})[3j_o'(\Omega_{om}) + \Omega_{om} j_o(\Omega_{om})]} \; . \tag{3.3.18}$$

For $n \geq 1$

$$a_n(\tau) = \sum_{m=1}^{\infty} \mathrm{Res}_{p_{nm}}[e^{p\tau} f_n(p)] \quad , \text{ where } f_n(p) = \frac{R_n(p^2+q_{1n})}{\Delta_n(p)} \; . \tag{3.3.19}$$

The poles of $f_n(p)$ are the zeros of $\Delta_n(p)$. Substitution of $p = \mp is\Omega$ into $\Delta_n(p)$, which was defined by (3.2.24), yields the frequency equation (2.4.15) for $n \geq 1$. Denoting the zeros of (2.4.15) by Ω_{nm}, and also following the same reasoning previously used to prove the nonexistence of poles with nonzero real parts we can conclude that all of the poles of $f_n(p)$ are located on the imaginary axis in the p-plane and that they are $p = \mp is\Omega_{nm}$. Application of (3.3.14) to (3.3.19) after some simplifications gives the residue at the pole $p = p_{nm}$

$$\mathrm{Res}_{p_{nm}}[e^{p\tau} f_n(p)] = \frac{\frac{i}{s} R_n \, e^{p_{nm}\tau}(p_{nm}^2+q_{1n}) \, j_n'^2(\frac{ip_{nm}}{s})}{d_{nm}(p_{nm})} \quad , \tag{3.3.20}$$

where

$$d_{nm}(p_{nm}) = f(p_{nm}^2+q_{1n})\left[\frac{ip_{nm}}{s} j_n'^2(\frac{ip_{nm}}{s}) - j_n(\frac{ip_{nm}}{s}) \, j_n'(\frac{ip_{nm}}{s}) - \frac{ip_{nm}}{s} \, j_n(\frac{ip_{nm}}{s}) \, j_n''(\frac{ip_{nm}}{s})\right]$$

$$+2f(2p_{nm}^2+q_{1n}) j_n(\frac{ip_{nm}}{s}) j_n'(\frac{ip_{nm}}{s}) + 2\,\frac{ip_{nm}}{s}\,(2p_{nm}^2+p_{2n}+q_{1n}) \quad j_n'^2(\frac{ip_{nm}}{s}) \; .$$

In this expression the second derivative of the spherical Bessel function can be eliminated by utilizing (3.3.16), then $d_{nm}(p_{nm})$ becomes for $p_{nm} = \pm is\Omega_{nm}$

$$
\begin{aligned}
d_{nm}(\pm is\Omega_{nm}) = {} & f(-s^2\Omega^2_{nm}+q_{1n})\{\mp \Omega_{nm}[j'^2_n(\mp \Omega_{nm}) + j^2_n(\mp \Omega_{nm})] + j_n(\mp \Omega_{nm})\, j'_n(\mp \Omega_{nm}) \\
& \pm \frac{\lambda_n}{\Omega_{nm}}\, j^2_n(\mp \Omega_{nm})\} + 2f(-2s^2\Omega^2_{nm}+q_{1n})\, j_n(\mp \Omega_{nm})\, j'_n(\mp \Omega_{nm}) \\
& \mp 2\Omega_{nm}(-2s^2\Omega^2_{nm}+p_{2n}+q_{1n})\, j'^2_n(\mp \Omega_{nm}) \quad .
\end{aligned} \tag{3.3.21}
$$

Next let us refer to the definition of spherical Bessel function

$$
j_n(z) = \frac{\sqrt{\pi}}{2}\left(\frac{1}{2}z\right)^n \sum_{k=0}^{\infty} \frac{(-\frac{1}{4}z^2)^k}{k!\,\Gamma(n+k+\frac{3}{2})} ,
$$

from this definition it is easy to verify that for any z

$$
\left.
\begin{aligned}
j_n(z) &= j_n(-z) && \text{for n even} \\
j_n(z) &= -j_n(-z) && \text{for n odd} \\
j'_n(z) &= -j'_n(-z) && \text{for n even} \\
j'_n(z) &= j'_n(-z) && \text{for n odd}
\end{aligned}
\right\} \tag{3.3.22}
$$

In view of relations (3.3.22) one can show from (3.3.21) that

$$
d_{nm}(+is\Omega_{nm}) = -\, d_{nm}(-is\Omega_{nm}) \quad . \tag{3.3.23}
$$

Hence,

$$
e^{is\Omega_{nm}\tau}\, \mathrm{Res}_{-is\Omega_{nm}}[e^{p\tau}f_n(p)] = -\, e^{-is\Omega_{nm}\tau}\, \mathrm{Res}_{is\Omega_{nm}}[e^{p\tau}f_n(p)] \quad . \tag{3.3.24}
$$

Substituting (3.3.20) into (3.3.19) and keeping in mind the relation (3.3.24) we obtain for $n \geq 1$

$$a_n(\tau) = \sum_{m=1}^{\infty} \frac{\frac{i}{s} R_n [e^{-is\Omega_{nm}\tau} - e^{is\Omega_{nm}\tau}](-s^2\Omega_{nm}^2 + q_{1n}) \, j_n'^2(\Omega_{nm})}{d_{nm}(-is\Omega_{nm})} ,$$

or

$$a_n(\tau) = \sum_{m=1}^{\infty} \frac{2R_n(-s^2\Omega_{nm}^2 + q_{1n}) \sin(s\Omega_{nm}\tau) \, j_n'^2(\Omega_{nm})}{s \, d_{nm}(-is\Omega_{nm})} , \qquad (3.3.25)$$

where $d_{nm}(-is\Omega_{nm})$ was defined in (3.3.21). Following the same steps outlined above we get from (3.2.23) for $n \geq 1$

$$b_n(\tau) = \sum_{m=1}^{\infty} \frac{-2R_n p_{1n} \sin(s\Omega_{nm}\tau) \, j_n'^2(\Omega_{nm})}{s \, d_{nm}(-is\Omega_{nm})} . \qquad (3.3.26)$$

Here, we make a note that in obtaining (3.3.25) and (3.3.26) for the case $n = 1$, $\bar{a}_1(p)$, and $\bar{b}_1(p)$ each have a simple pole at $p = 0$. Substitution of the definitions of $j_1(z)$ and $j_1'(z)$ into the residue expressions (i.e., in the case of $\bar{a}_1(p)$, equation (3.3.20)) and repeated application of L'Hospital's rule yields the value of residue to be zero at $p = 0$.

Next, let us consider (3.3.3) for the evaluation of $\Phi_1(r_1,\varphi,\tau)$. Using (3.3.7) the first term can be written

$$\frac{1}{2\pi i} \lim_{R\to\infty} \int_{c-iR}^{c+iR} \frac{j_o(\frac{ip}{s} r_1) \, f_o(p)}{\frac{i}{s} \, j_o'(\frac{ip}{s})} e^{p\tau} dp = L^{-1} \{c_o(p) \, j_o(\frac{ip}{s} r_1)\} . \qquad (3.3.27)$$

The integral of (3.3.27) has poles at the poles of $f_o(p)$ and the zeros of $j_o'(\frac{ip}{s})$. The poles of $f_o(p)$ were already found to be $p_{om} = \mp is\Omega_{om}$. Let the zeros of $j_o'(\frac{ip}{s})$ be denoted by $p_{o\ell}$. According to Lommel's theorem on the reality of the zeros of $J_\nu(z)$ (i.e., see Watson[27]), $p_{o\ell}$ must be pure imaginary.

Now, let us apply (3.3.14) to the integrand of (3.3.27)

$$\operatorname{Res}_p\left[e^{p\tau}f_o(p)\,\frac{j_o(\frac{ip}{s}r_1)}{\frac{i}{s}\,j_o'(\frac{ip}{s})}\right] = \frac{R_o\,e^{p\tau}\,j_o(\frac{ip}{s}r_1)}{\kappa_o(p)}\ , \qquad (3.3.28)$$

where

$$\kappa_o(p) = \frac{\frac{ip}{s}(2+f)\,j_o'^2(\frac{ip}{s}) + f\,j_o(\frac{ip}{s})[3j_o'(\frac{ip}{s}) + \frac{ip}{s}\,j_o(\frac{ip}{s})]}{j_o'(\frac{ip}{s})}$$

$$+ \frac{i^2}{s^2}\,j_o''(\frac{ip}{s})\left\{p^2\left[1 + f\,\frac{1}{\frac{ip}{s}}\,\frac{j_o(\frac{ip}{s})}{j_o'(\frac{ip}{s})}\right] + 2(1+\nu)\right\} .$$

We note that since $\lim_{p\to p_{o\ell}} k_o(p) = \infty$, the residue at $p = p_{o\ell}$ is zero, and for $p = p_{om} = \mp is\Omega_{om}$ the residues satisfy the following conditions

$$e^{is\Omega_{om}}\operatorname{Res}_{-is\Omega_{om}}\left[e^{p\tau}f_o(p)\,\frac{j_o(\frac{ip}{s}r_1)}{\frac{i}{s}\,j_o'(\frac{ip}{s})}\right] = e^{-is\Omega_{om}}\operatorname{Res}_{is\Omega_{om}}\left[e^{p\tau}f_o(p)\,\frac{j_o(\frac{ip}{s}r_1)}{\frac{i}{s}\,j_o'(\frac{ip}{s})}\right]$$

(3.3.29)

In view of (3.3.29), using (3.3.6) and (3.3.28), (3.3.27) becomes

$$L^{-1}\left\{c_o(p)\,j_o(\frac{ip}{s}r_1)\right\} = \sum_{m=1}^{\infty}\frac{R_o\left[e^{-is\Omega_{om}\tau} + e^{is\Omega_{om}\tau}\right]j_o(\Omega_{om}r_1)}{\kappa_o(-is\Omega_{om})}\ ,$$

(3.3.30)

or

$$L^{-1}\left\{c_o(p)\,j_o(\frac{ip}{s}r_1)\right\} =$$

$$\sum_{m=1}^{\infty}\frac{2R_o\,j_o'(\Omega_{om})j_o(\Omega_{om}r_1)\,\cos(s\Omega_{om}\tau)}{\Omega_{om}(2+f)\,j_o'^2(\Omega_{om}) + f\,j_o(\Omega_{om})[3j_o'(\Omega_{om}) + \Omega_{om}\,j_o(\Omega_{om})]} .$$

From (3.3.3), excluding $P_n(\cos\varphi)$, a typical term of $\Phi_1(r_1,\varphi,\tau)$ corresponding to $n \geq 1$, is

$$\frac{1}{2\pi i} \lim_{R\to\infty} \int_{c-iR}^{c+iR} \frac{j_n(\frac{ip}{s} r_1)\ f_n(p)}{\frac{i}{s}\ j_n'(\frac{ip}{s})}\ e^{p\tau} dp = L^{-1}\{c_n(p)\ j_n(\frac{ip}{s} r_1)\} \quad . \tag{3.3.31}$$

The poles of the integrand of (3.3.31) are those of $f_n(p)$, which are $p_{nm} = \mp is\Omega_{nm}$, and the zeros of $j_n'(\frac{ip}{s})$. Let us denote the zeros of $j_n'(\frac{ip}{s})$ by $p_{n\ell}$. Then, the application of (3.3.14) gives

$$\mathrm{Res}_p \left[e^{p\tau} f_n(p) \frac{j_n(\frac{ip}{s} r_1)}{\frac{i}{s}\ j_n'(\frac{ip}{s})} \right] = \frac{R_n(p^2+q_{1n})\ j_n(\frac{ip}{s} r_1)}{\kappa_n(p)} \quad , \tag{3.3.32}$$

where

$$\kappa_n(p) = \frac{i^2}{s^2}\ j_n''(\frac{ip}{s})\ \Delta_n(p) + \frac{d_{nm}(p)}{j_n'(\frac{ip}{s})} \quad .$$

In this expression, $\Delta_n(p)$ and $d_{nm}(p)$ are as previously defined. We again note that $\kappa_n(p) \to \infty$ as $p \to p_{n\ell}$, hence the residue at $p = p_{n\ell}$ is zero, and for $p = p_{nm} = \mp is\Omega_{nm}$ the residues satisfy the following condition

$$e^{is\Omega_{nm}}\ \mathrm{Res}_{-is\Omega_{nm}} \left[e^{p\tau} f_n(p) \frac{j_n(\frac{ip}{s} r_1)}{\frac{i}{s}\ j_n'(\frac{ip}{s})} \right] = e^{-is\Omega_{nm}}\ \mathrm{Res}_{+is\Omega_{nm}} \left[e^{p\tau} f_n(p) \frac{j_n(\frac{ip}{s} r_1)}{\frac{i}{s}\ j_n'(\frac{ip}{s})} \right] \quad . \tag{3.3.33}$$

Using (3.3.6), (3.3.32), and (3.3.33), (3.3.31) becomes

$$L^{-1}\{c_n(p)\ j_n(\frac{ip}{s} r_1)\} = \sum_{m=1}^{\infty} \frac{R_n(-s^2\Omega_{nm}^2 + q_{1n})[e^{-is\Omega_{nm}\tau} + e^{is\Omega_{nm}\tau}]\ j_n(\Omega_{nm} r_1)}{\kappa_n(-is\Omega_{nm})} \quad ,$$

or

$$L^{-1}\{c_n(p)\, j_n(\frac{ip}{s} r_1)\} = \sum_{m=1}^{\infty} \frac{2R_n(-s^2\Omega_{nm}^2 + q_{1n})\, j_n'(\Omega_{nm})\, j_n(\Omega_{nm} r_1)\, \cos(s\Omega_{nm}\tau)}{d_{nm}(-is\Omega_{nm})} \quad . \tag{3.3.34}$$

To get the complete solution for the nondimensional velocity potential we substitute (3.3.30) and (3.3.34) into (3.3.3) which results in the following expression:

$$\Phi_1(r_1,\varphi,\tau) = \sum_{m=1}^{\infty} \frac{2R_o\, j_o'(\Omega_{om})\, j_o(\Omega_{om} r_1)\, \cos(s\Omega_{om}\tau)}{\Omega_{om}(2+f)\, j_o'^2(\Omega_{om}) + f\, j_o(\Omega_{om})[3j_o'(\Omega_{om}) + \Omega_{om}\, j_o(\Omega_{om})]}$$
$$+ \sum_{n=1}^{\infty}\sum_{m=1}^{\infty} \frac{2R_n(-s^2\Omega_{nm}^2 + q_{1n})\, j_n'(\Omega_{nm})\, j_n(\Omega_{nm} r_1)\, \cos(s\Omega_{nm}\tau)\, P_n(\cos\varphi)}{d_{nm}(-is\Omega_{nm})} \quad . \tag{3.3.35}$$

We get the solution for the nondimensional radial displacement of the shell mid-surface by substituting (3.3.18) and (3.3.25) into (3.3.1),

$$\zeta(\varphi,\tau) = \sum_{m=1}^{\infty} \frac{2R_o\, j_o'^2(\Omega_{om})\, \sin(s\Omega_{om}\tau)}{s\{\Omega_{om}(2+f)\, j_o'^2(\Omega_{om}) + f\, j_o(\Omega_{om})[3j_o'(\Omega_{om}) + \Omega_{om}\, j_o(\Omega_{om})]\}}$$

$$+ \sum_{n=1}^{\infty}\sum_{m=1}^{\infty} \frac{2R_n(-s^2\Omega_{nm}^2 + q_{1n})\, j_n'^2(\Omega_{nm})\, \sin(s\Omega_{nm}\tau)\, P_n(\cos\varphi)}{s\, d_{nm}(-is\Omega_{nm})} \quad . \tag{3.3.36}$$

Finally, substitution of (3.3.26) into (3.3.2) yields the nondimensional tangential displacement of the shell mid-surface:

$$\psi(\varphi,\tau) = \sum_{n=1}^{\infty}\sum_{m=1}^{\infty} \frac{-2R_n\, p_{1n}\, j_n'^2(\Omega_{nm})\, \sin(s\Omega_{nm}\tau)\, \dot{P}_n(\cos\varphi)}{s\, d_{nm}(-is\Omega_{nm})} \quad . \tag{3.3.37}$$

From (3.3.36) and (3.3.37), the response of a closed empty shell subjected to a local radial impulsive load can be easily obtained by setting

$f = 0$. In the absence of fluid, the corresponding forms of the equations (3.3.36) and (3.3.37) are

$$\zeta(\varphi,\tau) = \frac{R_o}{\bar{\Omega}_o} \sin \bar{\Omega}_o \tau + \sum_{n=1}^{\infty} \sum_{m=1}^{2} \frac{R_n(q_{1n}-\bar{\Omega}^2_{nm}) \sin(\bar{\Omega}_{nm}\tau) P_n(\cos\varphi)}{\bar{\Omega}_{nm}(q_{1n}+p_{2n}-2\bar{\Omega}^2_{nm})} , \tag{3.3.38}$$

$$\psi(\varphi,\tau) = \sum_{n=1}^{\infty} \sum_{m=1}^{2} \frac{-R_n\, p_{1n} \sin(\bar{\Omega}_{nm}\tau) \dot{P}_n(\cos\varphi)}{\bar{\Omega}_{nm}(q_{1n}+p_{2n}-2\bar{\Omega}^2_{nm})} , \tag{3.3.39}$$

where $\bar{\Omega}_o = \frac{\omega_o a}{c_s}$ is the nondimensional breathing mode frequency and the value of ω_o was given by (2.4.16); $\bar{\Omega}_{nm}$ are the two distinct roots of the frequency equation, (2.4.17), for the empty shell.

Since the external load was assumed to be of the form $F(\varphi)\ \delta(\tau)$ the solutions obtained thus far represent the impulse response of the system. In general, a small, but finite length of time elapses during the application of the external load. This means the external pressure should be denoted by $F(\varphi)\ T(\tau)$, where $F(\varphi)$ has again the same meaning, namely, external load intensity per unit mid-surface area of the shell, and $T(\tau)$ represents any arbitrary pressure time function one desires to choose. According to Borel's theorem the response of a linear system to an excitation function $T(\tau)$ is the convolution of its impulse response and the excitation function. Hence, the response of a fluid-filled spherical shell to an external load $F(\varphi)\ T(\tau)$ is obtained by applying this theorem to (3.3.35), (3.3.36), and (3.3.37); denoting the resulting expressions by $\tilde{\Phi}_1$, $\tilde{\zeta}$, and $\tilde{\psi}$ we get

$$\tilde{\Phi}_1(r_1,\varphi,\tau) = \int_0^{\tau} \Phi_1(r_1,\varphi,\xi)\ T(\tau-\xi)d\xi \quad , \tag{3.3.40}$$

$$\tilde{\zeta}(\varphi,\tau) = \int_0^\tau \zeta(\varphi,\xi)\ T(\tau-\xi)d\xi \quad , \tag{3.3.41}$$

$$\tilde{\psi}(\varphi,\tau) = \int_0^\tau \psi(\varphi,\xi)\ T(\tau-\xi)d\xi \quad . \tag{3.3.42}$$

Since the external load has a finite duration the expression, (3.1.2), which gives the velocity imparted to the mass center of the system should be modified to

$$V_c = \frac{1}{M} \int_S \int_0^{t_1} F(\varphi)\ T(t)\ dSdt \tag{3.3.43}$$

where t_1 is the time duration of the external load.

CHAPTER 4

NUMERICAL RESULTS

In this chapter the solutions obtained in the previous chapter will be utilized in getting some numerical results for the idealized model representing the human head when subjected to the impulsive external load. The possible locations of brain damage and skull injury will be indicated on the basis of the numerical computations.

4.1. PRELIMINARY REMARKS

In order to use the solutions obtained so far, some ideal conditions must be assumed. In the first place, we assume a spherical form of the brain substance enclosed by the inner layer of the skull cap which is approximately spherical. Furthermore, the brain substance is taken to be homogeneous and as it was pointed out by Goldsmith,[4] since the physical properties of the brain resemble those of a fluid and, in particular, the intercranial-fluid shows some resemblence to water, water is chosen to be the fluid occupying the interior space of the spherical shell. The skull cap which is idealized by the thin shell is also taken to be homogeneous and isotropic. Under these assumptions we arrive at the following data:

$$\left.\begin{aligned} \rho_s &= 0.0772 \text{ lbm/in.}^3 \\ E &= 2 \times 10^6 \text{ lbf/in.}^2 \\ \nu &= .25 \\ a &= 3 \text{ in.} \\ h &= .15 \text{ in.} \end{aligned}\right\} \text{For the shell}$$

$$\left.\begin{array}{l} \rho_o = 0.0362 \text{ lbm/in.}^3 \\ c = 57{,}100 \text{ in./sec} \end{array}\right\} \text{ For the fluid}$$

From the shell data we note that a/h is within the justifiable thin shell theory limits; also the calculated value for c_s is 103,280 in./sec which is in close agreement with the wave speed of 106,000 in./sec through the skull mentioned in Goldsmith's paper.[4] The axisymmetric external impulsive load is considered to be applied on the shell with a constant magnitude of 546.5 lbf/in.^{2} on a polar cap of 15° angle. Thus, the addition of $F_o = 546.5$ lbf/in.^{2} and $\varphi_o = 15°$ to the above completes the necessary data.

The nondimensional velocity potential for the fluid and the components of the displacement vector of the shell mid-surface are given by (3.3.35), (3.3.36), and (3.3.37). In these expressions Ω_{om} and Ω_{nm} represent the roots of the frequency equations (2.4.15) and (2.4.17), respectively. 420 of these roots were first determined on the computer by an interval-halving technique; later on their accuracy was increased considerably by means of Mueller's iteration scheme of successive bisections and inverse parabolic interpolation. Mueller's iteration method was chosen since it does not require the derivative of the function. All the calculations were done with double precision accuracy and the maximum value of the function at any one of the 420 roots is less than 10^{-6}. In the determination of poles ($\mp is\Omega_{nm}$) and corresponding residues the spherical Bessel functions play an important role. Unavailability of the spherical Bessel function subroutine compelled us to write a subroutine by using a recursion formula and the series representation given on page 40. Since for the small arguments the recursion formula gives unstable results for the values of the spherical Bessel function, the series representation which exhibits strong convergence for the small arguments is substituted. For each order, n, of the spherical Bessel function and its first derivative an argument was determined for which both recursion and the series representation gave the same result to within the desired accuracy. Thus, the subroutine was designed to call for the series representation when the arguments are less than a particular number and the recursion formula otherwise.

The nondimensional excess pressure, p_1, is equal to $-\partial\Phi_1/\partial\tau$ and it is obtainable directly from (3.3.35). If we consider one to one correspondence between the natural frequencies and the modes of the system, for $n = 0,\ldots,20$ and $m = 1,\ldots,20$ there are 420 modes which were partly computed as residues to get the shell mid-surface displacement components ζ, ψ, and the excess pressure p_1. For ζ and ψ less than half of these modes give sufficient convergence; but for the fluid pressure it was necessary to use all of the modes. For comparison purposes the response of the empty shell subjected to the same impulsive load was also determined from (3.3.38) and (3.3.39) which are the special cases of (3.3.36) and (3.3.37).

4.2. DISCUSSION OF THE RESULTS

On Figures 8 through 15 the numbers enclosed by small circles designate the multiples of the time increment. The time increment chosen represents 1/10 of the calculated time which the stress wave on the shell takes to arrive at the opposite pole. Thus, 1 refers to actual time of $t = 9.125 \times 10^{-6}$ sec or nondimensional time $\tau = 0.3141$ and 10 refers to actual time of $t = 9.125 \times 10^{-5}$ or nondimensional time $\tau = 3.141$. We can make the following remarks based on a close study of the numerical results and the graphs shown on Figures 8 through 15:

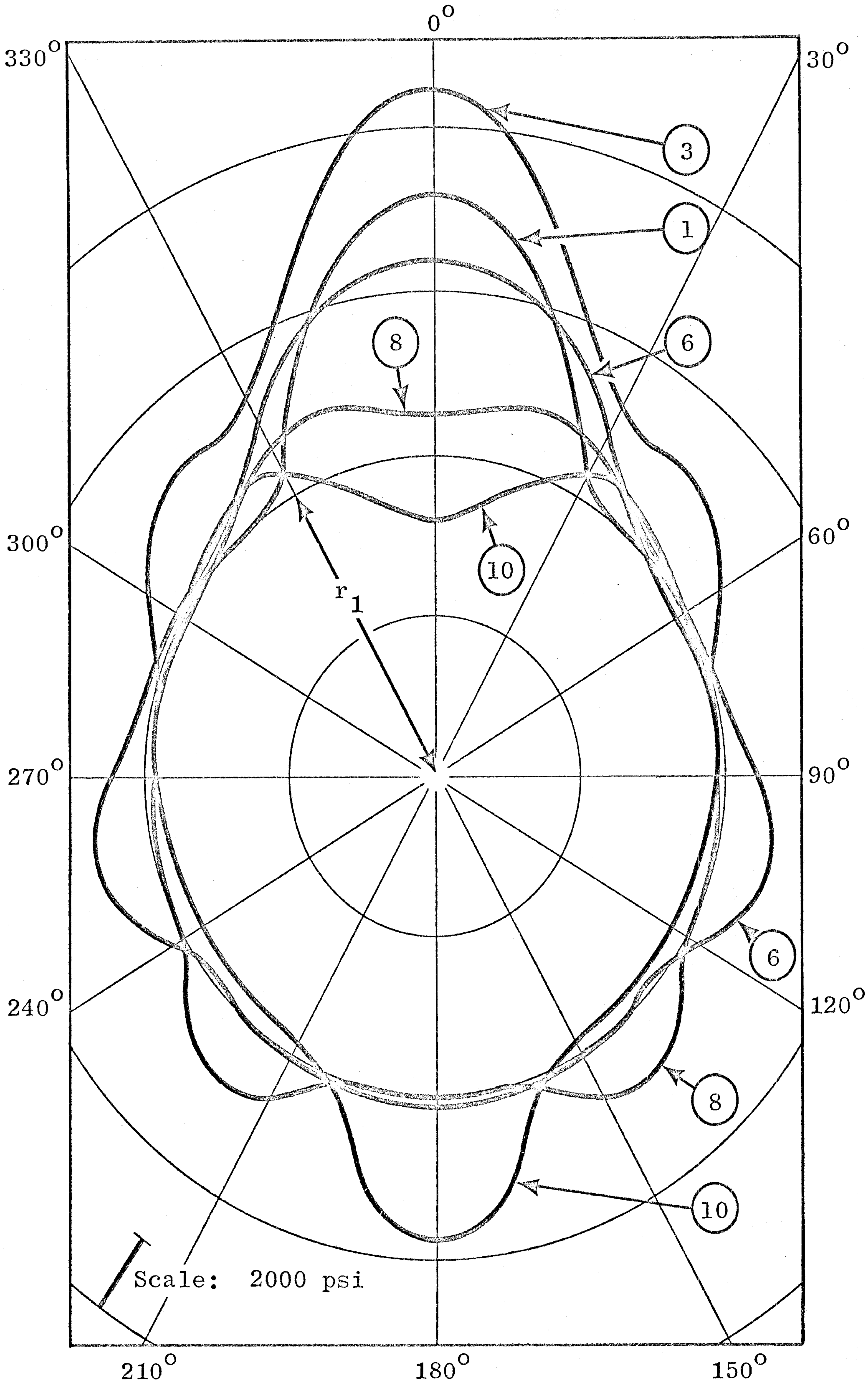

Figure 8. Normal stress in the φ-direction as a function of the polar angle, φ, at various times (in vacuo case), z = 0.

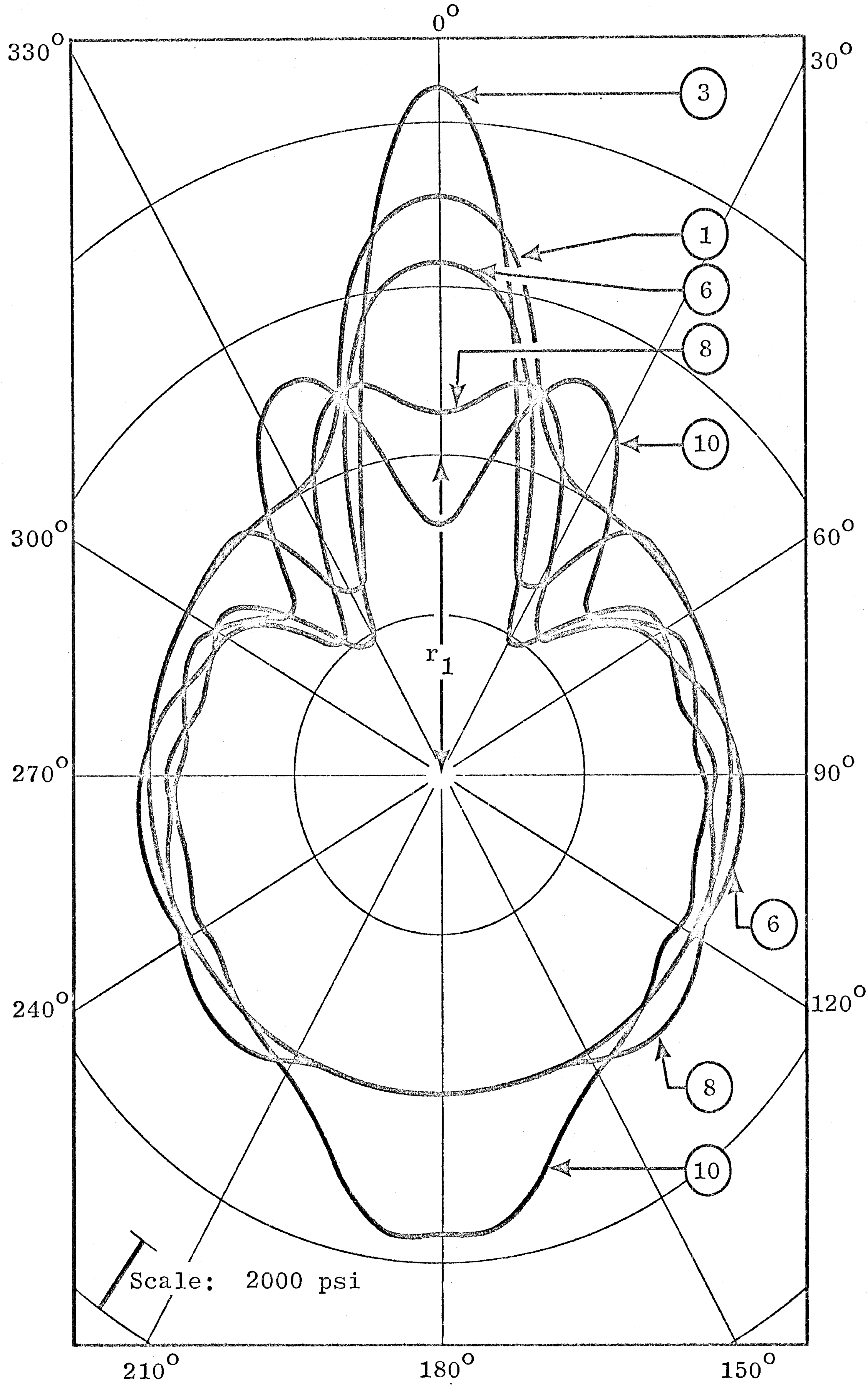

Figure 9. Normal stress in the Θ-direction as a function of the polar angle, φ at various times (in vacuo case), z = 0.

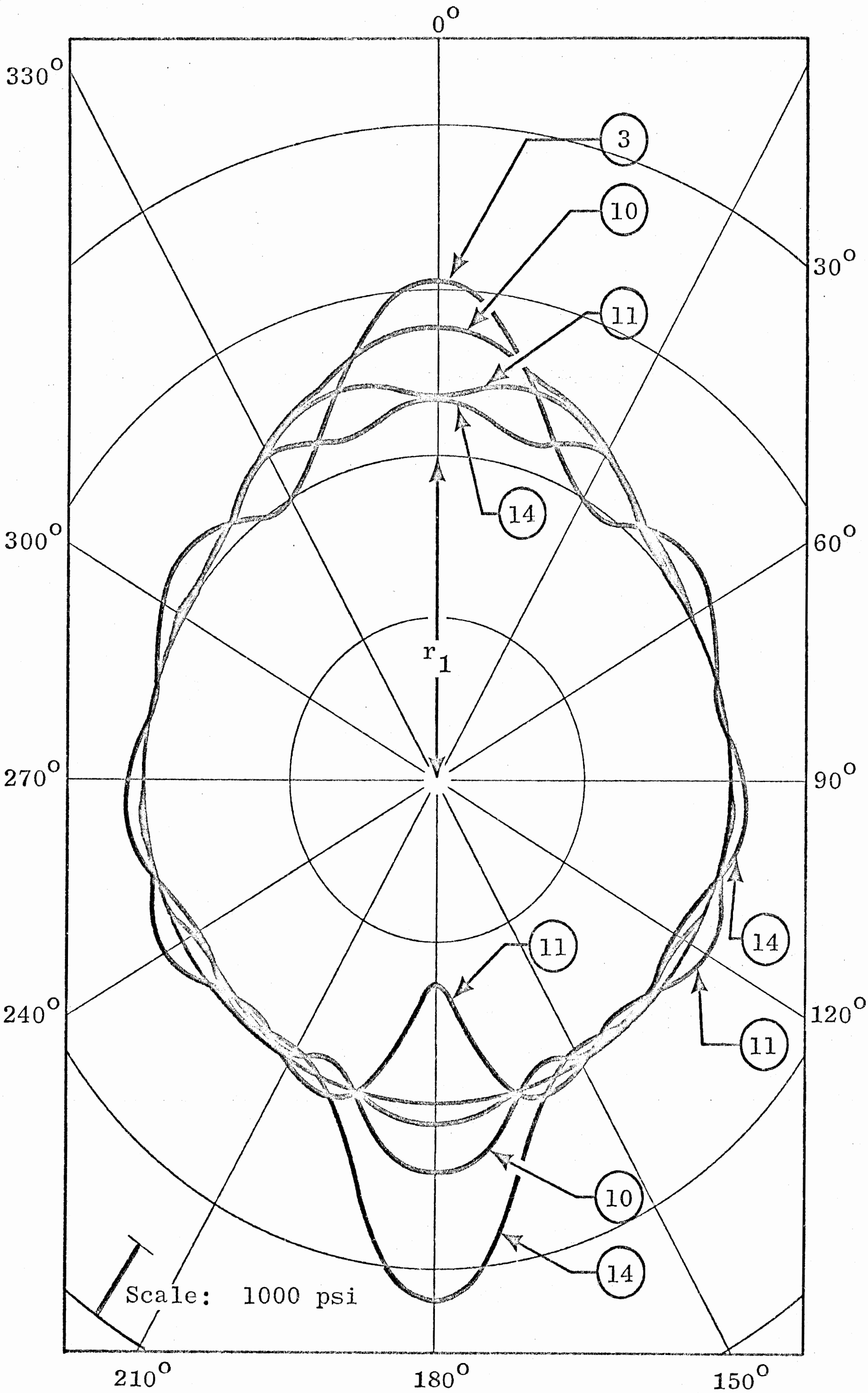

Figure 10. Normal stress in the φ-direction as a function of the polar angle, φ, at various times (fluid-filled case), z = 0.

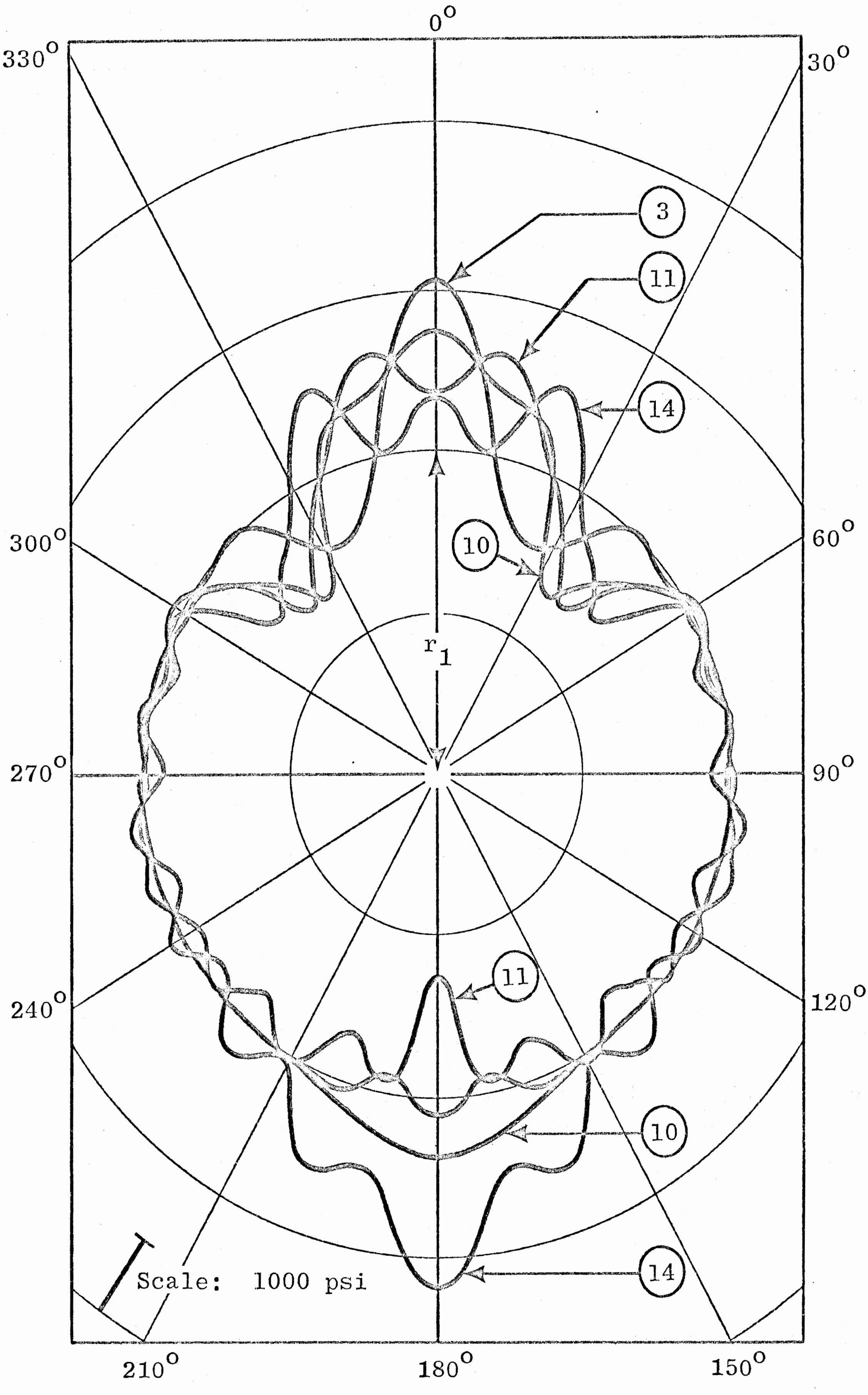

Figure 11. Normal stress in the Θ-direction as a function of the polar angle, φ, at various times (fluid-filled case), z = 0.

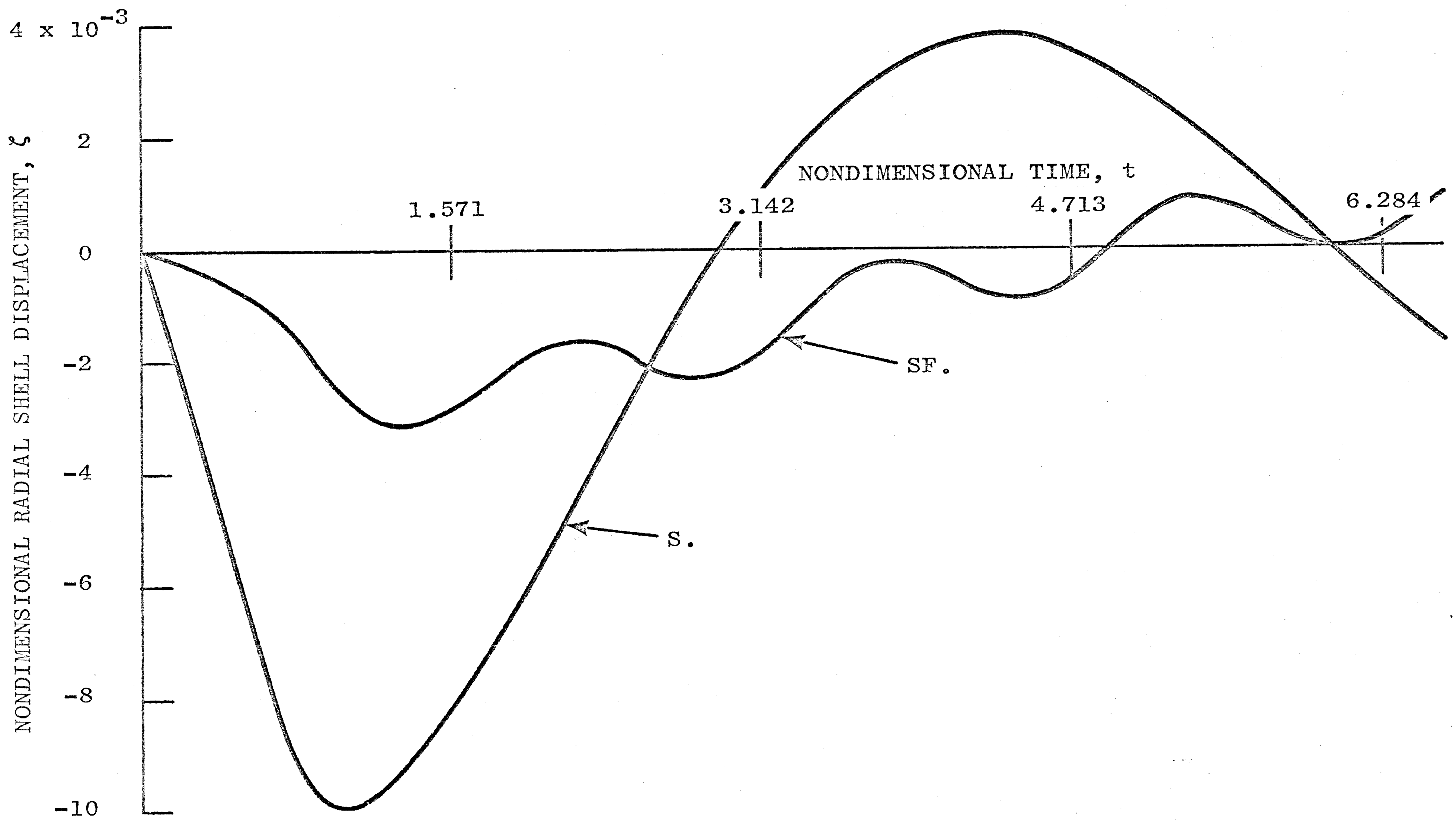

Figure 12. Nondimensional radial shell displacement vs. time, $\varphi = 0$.

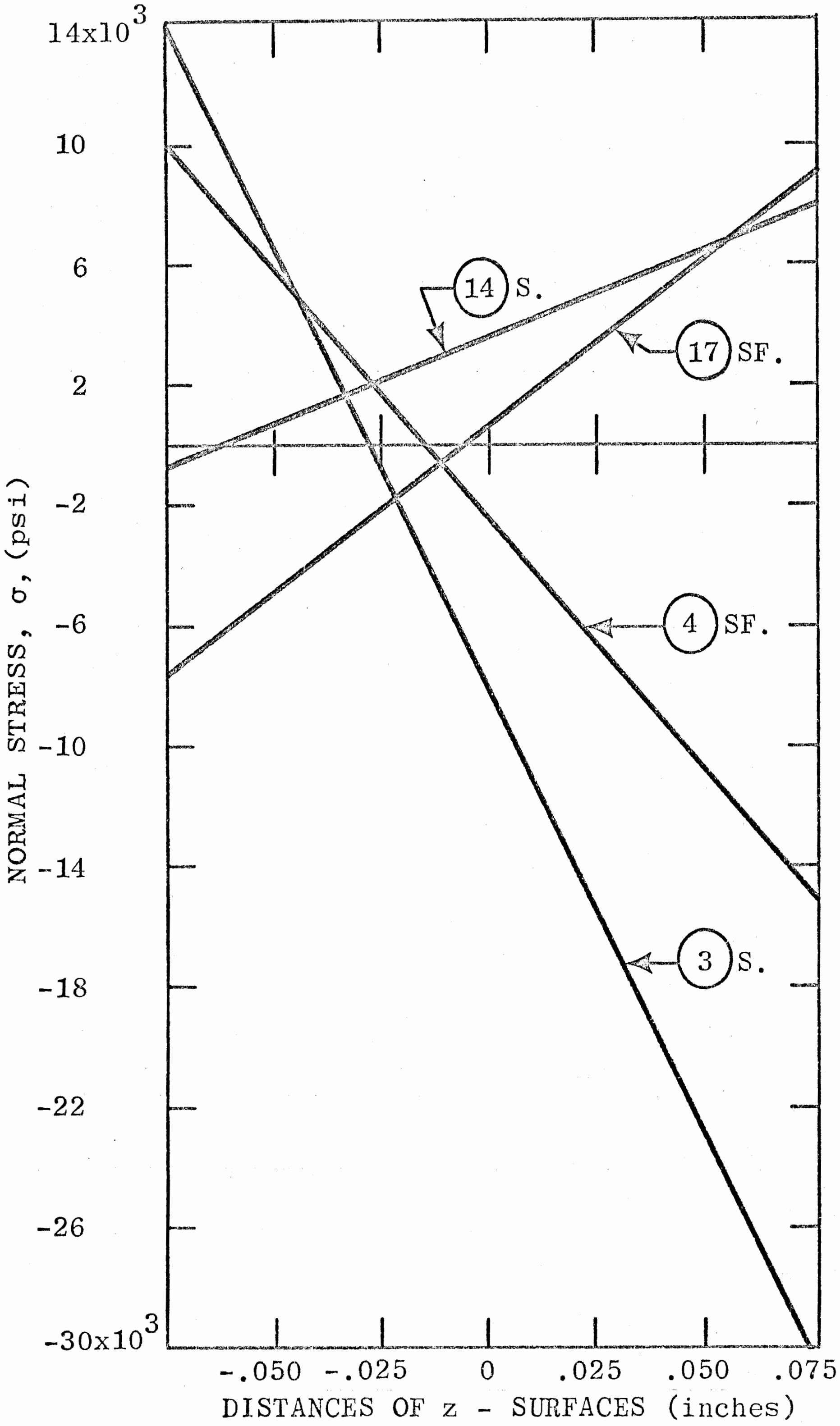

Figure 13. Normal stress vs. distance of z-surfaces, $\varphi = 0$.

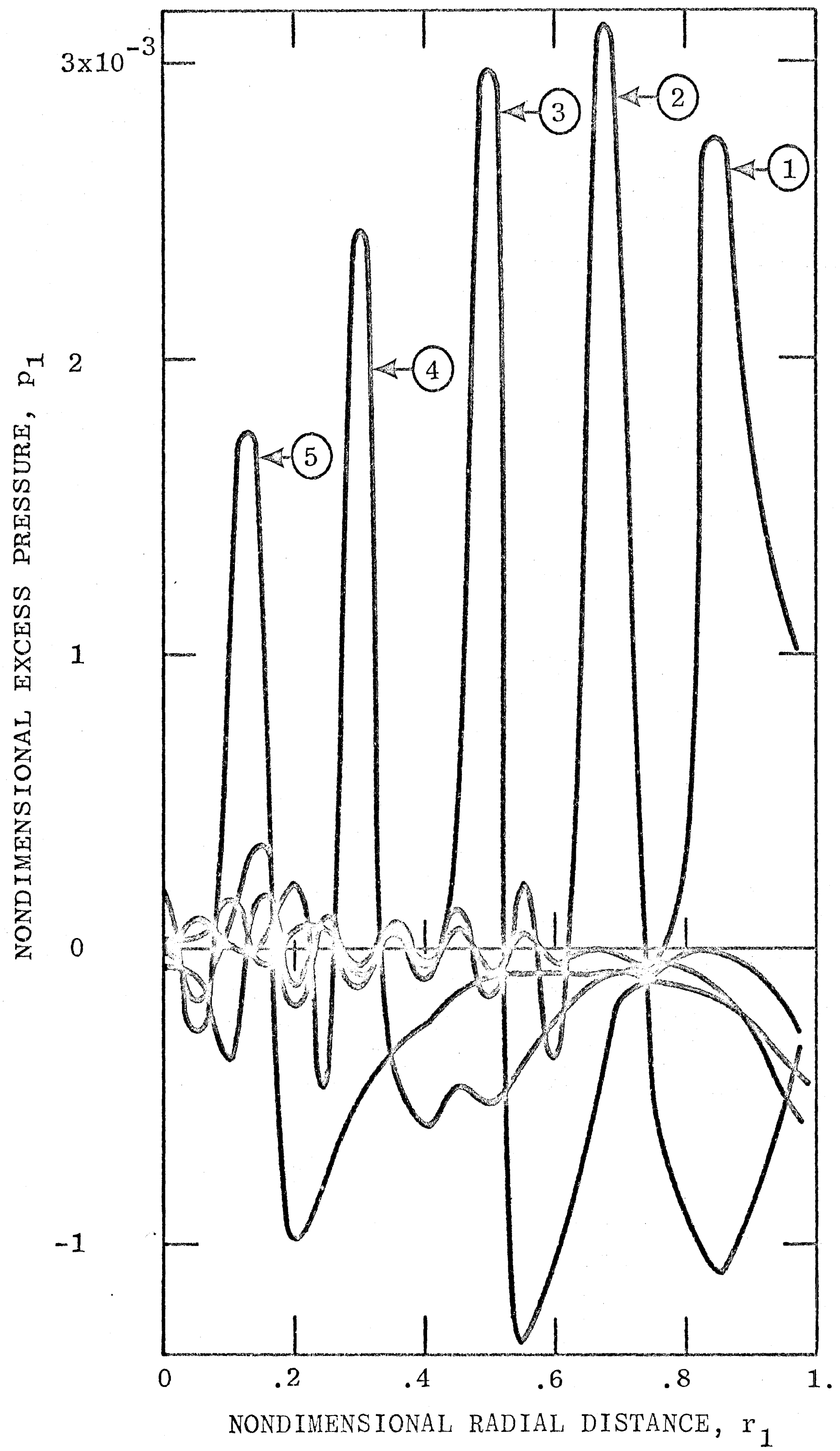

Figure 14. Nondimensional pressure, p_1, vs. nondimensional radial distance, r_1.

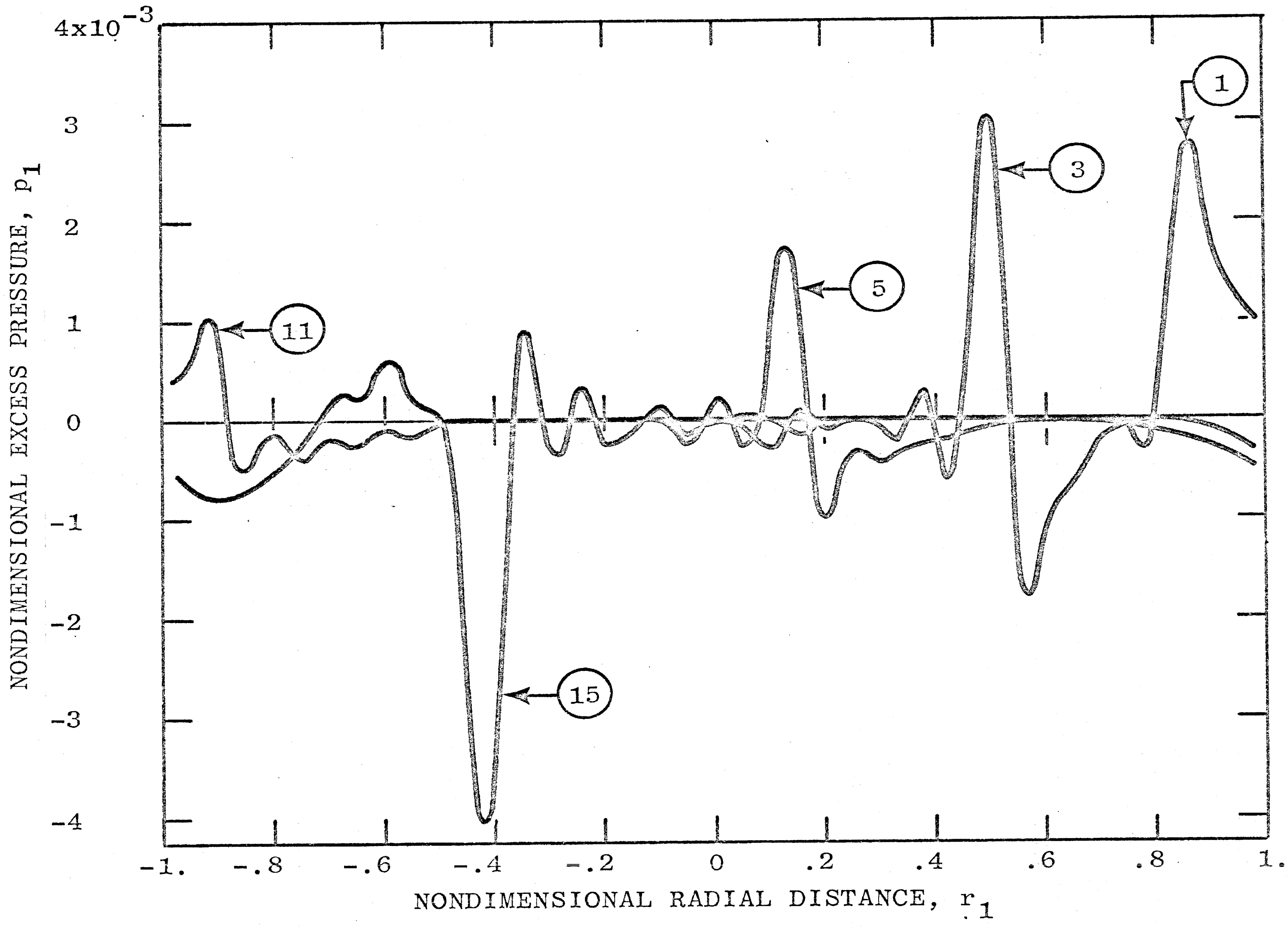

Figure 15. Nondimensional pressure, p_1, vs. nondimensional radial distance, r_1.

(1) The magnitudes of stress components σ_φ and σ_Θ acting on the mid-surface of the shell ($z = 0$) in the fluid-filled case are considerably less than those of the in vacuo case. The obvious reason for this is the presence of the high density fluid which absorbs a large portion of the initial energy input from the shell material whose modulus of elasticity is quite low.

(2) In the fluid-filled case the maximum compressional stress on the mid-surface of the shell at the opposite pole occurs at a later time, namely, at time 14 whereas in the invacuo case this time is 10.

(3) Time 11 corresponds approximately to the arrival of the compressional fluid pulse at the opposite pole. The magnitude of the tensile stress on the mid-surface of the shell at this time is higher than the magnitude of the compressive stress at time 10. This increase is caused by the reflection of the compressional fluid pulse at the opposite pole.

(4) Figure 12 shows for both the fluid-filled and in vacuo cases, the occurrence of the maximum inward and outward radial shell displacements at the pole where the impulsive load is applied. Figure 13 is a plot of the stress distribution throughout the shell thickness at those times when the radial displacements are maximal for each of the two cases.

(5) In Figure 14, the nondimensional excess pressure is plotted as a function of the nondimensional radial distance. From this plot we can see the propagation of the compressional pulse toward the center of the fluid. There is a decrease in magnitude of the pulse as it progresses toward the center of the sphere. We keep in mind that this pulse represents a rather complex superposition of pulses generated on, and reflected, with varying strengths from the shell surface as the compressional disturbance on the shell propagates

from the pole of loading toward the opposite pole.

(6) Figure 15 shows a similar plot, but the radial distance is taken from one pole to the other. The purpose of this plot is to show the occurrence, location, and magnitude of the maximum negative excess pressure. The magnitude of this negative excess pressure is indeed higher than the magnitude of the maximum positive excess pressure.

4.3. CONCLUSION

In view of Figures 10, 11, and 13 we can state that the possible locations on the skull susceptible to severe damage are; the pole where the impulsive load is applied, a neighborhood of $\varphi = 35°$ where tensile stresses develop repeatedly, and at the opposite pole where high values of tensile stress are generated after the reflection of both types of waves one after the other. If we feel that brain damage occurs at the points of rarefaction of the fluid, then Figure 15 indicates that this situation arises at time 3 and location $r_1 = .55$ and much more severely at time 15 and location $r_1 = -.43$. This fact clearly establishes the difference between the present and rigid shell analysis where it was inferred that maximal brain damage occurs at the center.

In conclusion, the immediate extension of this numerical work can be the consideration of different pulse shapes and durations by utilization of the formulas derived at the end of Chapter 3. In my opinion, both the pulse shapes and their durations can be important factors on the location of damage in the brain as well as on the skull. The further extension of this thesis for different head injury models may possibly be the application of the correspondence principle in order to obtain solutions for a linear viscoelastic material.

BIBLIOGRAPHY

1. Anzelius, A., "The Effect of an Impact on a Spherical Liquid Mass," Acta Path. et Microbio. Scand., Supplement 48, 1943.

2. Baker, W. E., "Axisymmetric Modes of Vibration of Thin Spherical Shell" The Journal of the Acoustical Society of America 33 (1961) p. 1749.

3. Bateman, H., "Partial Differential Equations of Mathematical Physics" Cambridge, at the University Press, 1932, p. 152.

4. Goldsmith, W., "The Physical Processes Producing Head Injury" Proceedings of the Head Injury Conference, J. P. Lippincott Co., 1966, pp. 350-382.

5. Goodman, R. R. and Stern, K., "Reflection and Transmission of Sound by Elastic Spherical Shells" The Journal of the Acoustical Society of America, Vol. 34, No. 3, March, 1962, pp. 338-344.

6. Greenspon, J. E., "Vibration of Thick and Thin Cylindrical Shells Surrounded by Water" The Journal of the Acoustical Society of America, Vol. 33, No. 3, October, 1961, pp. 1321-1328.

7. Güttinger, W., "Der Stosseffekt auf eine Flüssigkeitskugel als Grundlage einer Physikalischen Theorie der Entstehung von Gehirnverletzungen", Zeit. F. Naturforschung, Teil A, Vol. 5, 1950, pp. 622-628.

8. Hildebrand, F. B., Methods of Applied Mathematics, 2nd Edition, Prentice-Hall, Inc., 1965, pp. 119-181.

9. Humphreys, J. S. and Winter, R., "Dynamic Response of a Cylinder to a Side Pressure Pulse" AIAA Journal, Vol. 3, January, 1965, pp. 27-32.

10. Junger, M. C., "Vibration of Elastic Shells in a Fluid Medium and Associated Radiation of Sound" Journal of Applied Mech., Vol. 74, 1952, pp. 439-445.

11. Kalnins, A., "Effect of Bending on Vibrations of Spherical Shells" The Journal of the Acoustical Society of America, Vol. 36, 1964, p. 74.

12. Klein, S., "Vibration of Multilayer Shells of Revolution under Dynamic and Impulsive Loading" U.S. Naval Res. Lab., Shock and Vibration Bulletin 35, pt. 3, January 1966, pp. 27-44.

13. Lamb, H., "On the Vibrations of Spherical Shell" Proceedings of the London Mathematical Society" Vol. XIV, p. 50.

14. Long, C. F., "Vibrations of Radially Loaded Shell" ASCE Proceedings, Vol. 92, April, 1966, pp. 235-250.

15. Love, A.E.H., "The Small Free Vibrations and Deformation of a Thin Elastic Shell" Philosophical Transactions of the Royal Society, 179A 1888, p. 491.

16. Love, A.E.H., The Mathematical Theory of Elasticity, Dover Publications, New York, 1944.

17. McIvor, I. K. and Sonstegard, D. A., "Axisymmetric Response of a Closed Spherical Shell to a nearly Uniform Radial Impulse" Journal of the Acoustical Society of America, Vol. 40, No. 6, December, 1966, pp. 1540-1547.

18. Medick, M. A., "On the Initial Response of a Spherical Shell to a Concentrated Force" Journal of Applied Mech., Vol. 29, 1962, pp. 689-695.

19. Morse, P. M. and Feshbach, H., "Methods of Theoretical Physics" McGraw-Hill, New York, Part II, 1953, pp. 1469-1472.

20. Naghdi, P. M. and Kalnins, A., "On Vibrations of Elastic Spherical Shells" Journal of Applied Mechanics, Vol. 29, 1962, p. 65.

21. Novozhilov, V. V., "Thin Shell Theory" 2nd. Ed., Noordhoff Ltd., Groninger, Holland, 1964.

22. Rand, R. and Dimaggio, F., "Vibrations of Fluid-Filled Spherical and Spheroidal Shells" The Journal of the Acoustical Society of America, Vol. 42, No. 6, December, 1967, pp. 1278-1286.

23. Rayleigh, Lord, "On the Infinitesimal Bending of Surfaces of Revolution" Proceedings of the London Mathematical Society, XIII, 1888, p. 4.

24. Scott, E. J., Transform Calculus with an Introduction to Complex Variables Harper and Brothers, 1955, pp. 56-60.

25. Shklyarchuk, F. N., "Approximate Calculation of Axisymmetric Oscillations of Liquid-Filled Shells of Revolution" Akademia Nauk, Izvestia, Mekhanika No. 6, November-December, 1965, pp. 123-129.

26. Silbiger, A., "Free and Forced Vibrations of a Spherical Shell" ONR Report U-106-48, December, 1960.

27. Watson, G. N., A Treatise on the Theory of Bessel Functions, 2nd. Ed., Cambridge University Press, 1958, p. 482.

APPENDIX D

SOFT TISSUE BIBLIOGRAPHY

BIBLIOGRAPHY
ON
THE PROPERTIES OF THE SOFT TISSUE

D. E. Bendure, M. R. Berg, P. M. Fuller, D. H. Robbins, H. J. Siegel, and J. L. Wood

Highway Safety Research Institute
The University of Michigan

Abrahams, M. 1967 Mechanical Behaviour of Tendon in Vitro; A Preliminary Report. Medical and Biological Engineering, 5: 433-443.

Abrahams, M. 1967 The Mechanical Behavior of Tendon Collagen Fibers Under Tension in Vitro. 7th International Conference on Medical Electronics and Biological Engineering, Stockholm.

Abrahams, M. and T. C. Duggan 1965 The Mechanical Characteristics of Costal Cartilage. Biomechanics and Related Bio-Engineering Topics. Ed. by R. M. Kenedi. Pergamon Press, London., Chap. 24, 285-300.

Agostini and G. Graziati 1966 Presentation of a New Apparatus for the Measurement of Certain Physical Properties of Articular Cartilage. (In Italian). Atti Della S. Medico-Chirurgica Di Padova E Della Facoltà Di Medicina Di Padova (1963), Vol. XXXIX; also reported in: Advances in Bioengineering and Instrumation I, Fred Alt, Instrument Society of America, Plenum Press, New York.

Alexander, R. S. 1957 Elasticity of Muscular Organs. Tissue Elasticity. Ed. by J. W. Remington. Am. Physiol. Soc., 111-122.

Apter, J. T. 1966 Correlation of Visco-Elastic Properties of Large Arteries with Microscopic Structure. Circulation Research, 19: 104-121.

Apter, J. T. 1960 Distribution of Contractile Forces in the Iris of Cats and Dogs. American Journal of Physiology, 199 . 377-380.

Apter, J. T. 1964 Mathematical Development of a Physical Model of Some Visco-Elastic Properties of the Aorta. Bull. Math. Biophys., 26: 367-388.

A.S.M.E. 1966 Biomechanics. Ed. by Y. C. Fung.

Asmussen, E. and K. Heeboll-Nielsen 1961 Isometric Muscle Strength of Adult Men and Women. Danish Nat'n Assn. Infantile Paralysis, Communication 11.

Aubert, X. 1955 Intervention d'un Element Elastiane Pur Dans La Contraction Du Muscle Strie. Archives Internationales de Physiologie et de Biochemie, 63 : 197-202.

Auburt, X., M. L. Roquet, and J. van der Elst 1951 The Tension-Length Diagram of the Frog's Sartorius Muscle. Arch. Intern. Physio., 59: 239-241.

Backhouse, K. M. and W. T. Calton 1954 An Experimental Study of the Functions of the Lambrical Muscles in the Human Hand. J. Anat., 88: 133-141.

Bader, H. 1967 Dependence of Wall Stress in the Human Thoracic Aorta on Age and Pressure. Circul. Res., 20: 354-361.

Banus, M. G., and A. M. Zetlin 1938 The Relation of Isometric Tension to Length of Skeletal Muscle. Jr. Cellular and Com. Physiol., 12(3): 403-421.

Balasubramaniam, E. and K. J. Whiteley Stress Relaxation of Animal Fibres. Biorheology, 5(3): 215-225.

Beckwith, T. G., G. S. Brody, A. A. Glaser, T. Prevenslik and W. L. White 1963 Standardization of Methods of Measuring the Mechanical Properties of Wounds. Am. Soc. of Mec. Eng., Paper No. 63-WA-276.

Benedict, J. V., L. B. Walker, and E. H. Harris 1968 Stress-Strain Characteristics and Tensile Strength of Unembalmed Human Tendon. J. Biomechanics, 1(1): 53-63.

Benis, A. M. 1967 Rotational Viscometry by Torque Relaxation at Low Shear Rates with Application to Biological Systems. Biorheology, 4: 33-40.

Bergel, D. H. 1958 A Photo-Electric Method for the Determination of the Elastoviscous Behaviour of the Arterial Wall. Jr. Physiol., 141: 22-23.

__________ 1961 The Static Elastic Properties of the Arterial Wall. Jr. Physiol., 156: 445-457.

__________ 1961 The Dynamic Elastic Properties of the Arterial Wall. Jr. Physiol., 156: 458-469.

Biomedical Fluid Mechanics Symposium 1966 Am. Soc. Mech. Eng., New York.

Biomechanical and Human Factors Symposium 1967 Am. Soc. Mech. Eng., New York.

Biomechanics Monograph 1967 Am. Soc. Mech. Eng., New York.

Biggs, N. L. 1960 Tensile Strength of Various Rat Tissue. Anat. Rec., 136: 164-165.

Bird, F., H. Becker, J. Healer and M. Messer 1968 Experimental Determination of the Mechanical Properties of Bone. Aerospace Medicine, 1:44-48/

Blanton, P. 1964 Tensile Strength of Fetal and Adult Human Tendons. M. S. Thesis, Dept. of Anat., Baylor University, Dallas, 1-47.

Bohr, D. F. 1964 Contraction of Vascular Smooth Muscle. Canadian Medical Association Journal 90, 174-179.

1964 Electrolytes and Smooth Muscle Contractions, Pharmacological Reviews 16: 85-108.

Bohr, D. F., D. C. Brodie, and D. H. Chen 1958 Effects of Electrolytes on Arterial Muscle Contraction. Circulation, 17: 746-749.

Bohr, D. F. and R. C. Zuberbuhkr 1965 Response of Coronary Smooth Muscle to Catecholamines. Circulation Research 16.

Bozler, V. 1936 An Analysis of Properties of Smooth Muscle. Cold Spring Harbor Symposia on Quantitative Biology 4, 260.

Braams, R. 1960 The Effect of Electron Radiation on the Tensile Strength of Tendon. Int. J. of Rad. Biol., 41: 27-31.

Brady, A. J. 1967 The Three Element Model of Muscle Mechanics: Its Applicability to Cardiac Muscle. The Physiologist, 75-86.

Bramwell, J. C., A. C. Downing and A. V. Hill 1923 The Effect of Blood Pressure on the Extensibility of the Human Artery. Heart, 10: 289-300.

Breig, A. 1960 Biomechanics of the Central Nervous System. Year Book, Stockholm.

Brocas, J. and F. Verzar 1961 Measurement of Isometric Tension During Thermic Contraction as Criterion of the Biological Age of Collagen Fibres. Gerontologia, 5: 223-227.

Buchthal, F. 1942 Mechanical Properties of Single Striated Muscle Fiber at Rest and During Contraction and Their Structural Interpretation. Kgl. Danske Videnskabernes Selskab, Copenhagen. Biologiske Meddelelser, 17: 2.

Buchthal, F., E. Kaiser, and G. G. Knappeis 1944 Elasticity, Viscosity and Plasticity in the Cross Striated Muscle Fibre. Acta Physiol. Scand., 8: 16-37.

Buchthal, F. and P. Rosenfalck, 1957 Elastic Properties of Striated Muscle. Tissue Elasticity. Ed. by J. W. Remington. Am. Physiol. Soc., 73-97.

Bull, H. B. 1957 Protein Structure and Elasticity. Tissue Elasticity. Ed. by J. W. Remington. Am. Physiol. Soc, 33-42.

Burstein, A. and U. H. Frankel 1945 The Elastic Element of Skeletal Muscle. Am. Chem. Soc. J., 67: 2047-2048.

________ 1965 Viscoelasticity of Biological Materials. Presented at 1st ASME Human Factors Conference.

Caldwell, F. T., P. Donohue, and B. Rosenberg 1962 Rate Gain of Tensile Strength of Abdominal Wounds in Rats (Effect of Environmental Temperature). J.A.M.A., 179(10): 129-131.

Cammack, K., R. L. Rapport, J. Paul, and W. C. Baird 1959 Deceleration Injuries of the Thoracic Aorta. AMA Arch. of Surg., 79: 244-251.

Carlson, F. D. 1957 Kinematic Studies on Mechanical Properties of Muscle. Tissue Elasticity. Ed. by J. W. Remington. Am. Physiol. Soc., 55-72.

Carstensen, E. L. 1960 The Mechanism of the Absorption of Ultrasound in Biological Materials IRET Rans. on Med. Elec., 158.

Causey, G. 1948 The Effect of Pressure on Nerve Fibres. J. Anat., 82: 262-270.

Charney, J., M. B. Williamson, and F. W. Bernhart 1947 An Apparatus for the Determination of Tensile Strength in Healing Wounds. Science, 105: 396-397.

Clark, J. H. 1932 A Method for Measuring Elasticity in Vivo and Results Obtained on the Eyeball at Different Intraocular Pressures. Am. Jr. Physiol., 101: 474-481.

_________ 1933 The Elasticity of Veins. Am. Jr. Physiol., 105: 418-427.

Coermann, R. R., G. H. Ziegenrbecker, A. L. Wittiver, and H. E. von Gierke 1968 The Passive Dynamic Mechanical Properties of the Human Thorax-Abdomen System and of the Whole Body. Aerospace Med., 36: 443-445. 445.

Combs, R. G. 1966 Equilibrium in Thick Walled Blood Vessels. Proceedings, 19th ACEMB, 8:180.

Conrad, J. T., W. L. Johnson, W. K. Kuhn and C. A. Hunter 1966 Passive Stretch Relationships in Human Uterine Muscle. American Journal of Obstetrics and Gynecology, 96: 1055-1059.

Conrad, J. T. and W. Kuhn 1967 The Active Length-Tension Relationship in Human Uterine Muscle. American Journal of Obstetrics and Gynecology 97: 154-160.

Conrad, J. T., W. K. Kuhn and W. L. Johnson 1966 Stress Relaxation in Human Uterine Muscle. American Journal of Obstetrics and Gynecology, 95: 254-265.

Coulson, W. F., N. Weissman, and W. H. Carnes 1965 Cardiovascular Studies on Copper-Deficient Swine; VII. Mechanical Properties of Aortic and Dermal Collagen. Lab. Invest. 14(3): 303-309.

Cox, H. T. 1941 The Cleavage Lines of the Skin. British Jr. of Surg., 29: 234-240.

Craik, J. E. and I. R. R. McNeil 1966 Micro-Architecture of Skin and its Behaviour Under Stress. Nature. 209(5026): 931-932.

_________ 1965 Histological Studies of Stressed Skin. Biomechanics and Related Bio-Engineering Topics. Ed. by R. M. Kenedi, Pergamon Press, London. 159-164.

Cronkite, A. E. 1936 The Tensile Strength of Human Tendons. Anat. Rec., 64: 173-186.

Daly, C. H. 1966 The Biomechanical Charcteristics of Human Skin. Ph.D. Thesis, Univ. of Strathclyde.

Davidsson, L. 19 4 Tensile Strength, Rupture, and Regeneration of Tendons. Ann Chir. Gynaec. Fenn., Suppl. 5. 43: 62-66.

____________ 1956 Uber die subkutanen sehnenrupturen und die regeneration der schne eine experimentelle, klinische und patologish-anatomische untersuchung. Ann. Chir. Gynaec. Fenn., Suppl.6: 1-113.

Denney-Brown, D. and C. Brenner 1944 Lesion in Peripheral Nerve Resulting From Compression by Spring Clip. Arch. Neurol. Psychiat., 52: 1-19.

Dick, J. C. 1951 The Tension and Resistance to Stretching of Human Skin and Other Membranes, with Results from a Series of Normal and Oedematous Cases. Jr. Physiol., 112: 102-113.

Dill, J. C. and R. W. Stacy 1964 Dynamics of Stress Relaxation in Smooth Muscle. The Physiologist, 7:117.

Dodgson, M. C. H. 1962 Colloidal Structure of Brain. Biorheology, 1: 21-30.

____________ 1948 Physical Nature of Mouse Brain. Nature, 162(4111):253.

Doi, Y. 1920 Studies on Muscular Contraction. Jr. Physiol., 54: 218-226.

Dubuisson, M. and A. M. Monnier 1943 Sur Les Proprietes Elestiques Des Fils De Myosine. Archives Internationales de Physiologie, 53: 230.

Dunn, F. 1963 Temperature and Amplitude Dependence of Acoustic Absorptions in Tissue. JASA, 34 : 1545.

________ 1965 Ultrasonic Absorption in Biological Materials. Ultrasonic Energy, 64.

Edwards, J. 1967 Physical Characteristics of Articular Cartilage. The Inst. of Mech. Eng.

Elden, H. R. 1963 The Interaction of Connective Tissue with Aqueous Urea; I. Reversible and Irreversible Effects. Biochim. Biophys. Acta, 75: 37-47.

__________ 1963 The Interaction of Connective Tissue with Aqueous Urea; II. Rate Analysis of Influence of Urea Concentration, Temperature and pH. Biochim. Biophys. Acta, 75: 48-58.

__________ 1964 Aging of Rat Tail Tendons Jr. Gerontology, 19: 173-178.

Elden, H. R. and R. J. Boucek 1960 A Reaction of Water with Rat Tail Tendons (Hydration-Elongation). Biochim. Biophys. Acta, 38: 205-211.

Elden, H. R. and B. Cassac 1962 Urea-Induced Contraction-Relaxation of Rat Tail Tendons. Jr. Poly. Sci., 59: 283-292.

Elden, H. R. and M. Feldman 1963 A Kinetic Analysis of Swelling of Rat Tail Tendon. Jr. Poly. Sci., Part A, 1: 23-35.

Ellis, D. G. 1969 Cross-Sectional Area Measurements for Tendon Specimens: A Comparison of Several Methods. Biomechanics, II (2).

Elmore, S. M., L. Sokoloff, G. Norris, and P. Carmeci 1963 Nature of "Imperfect" Elasticity of Articular Cartilage. Jr. Appl. Physiol., 18(2): 393-396.

Evans, C. L. and A. V. Hill 1914 The Relation of Length to Tension Development and Heat Production on Contraction in Muscle. Jr. Physiol., 49: 10-16.

Evans, J. H. and W. W. Siesennop 1967 Controlled Quasi-Static Testing of Human Skin in Vivo. Digest of the 7th International Conference on Medical Electronics and Biological Engineering; Stockholm, 371.

Evans, R. L., K. D. Bearman, G. W. Modin and Guenemoen 1967 Mechanical Behavior of the Aortas of Anesthetized Dogs. Digest of the 7th International Conference on Medical and Biological Engineering; Stockholm,

Fantuzzo, D. and G. Graziati 1967 A Mathematical Model for Articular Cartilage. Digest of the 7th Int. Conf. on Medical and Biological Eng.; Stockholm, 506.

Feigl, E. O. 1967 Effects of Stimulation Frequency on Myocardial Extensibility. Circulation Research, 20: 447-458.

Feng, T. P. 1932 The Thermo Elastic Properties of Muscle. Jr. of Physiol., 74: 455-470.

Fenn, W. O. and B. S. Marsh 1935 Muscular Force at Different Speeds of Shortening. Journal of Physiology 85: 277-297.

Fenn, W. O. 1957 Some Elasticity Problems in the Human Body. Tissue Elasticity. Ed. by J. W. Remington, Am. Physiol. Soc., 98-101.

__________ 1957 Changes in Length of Blood Vessels on Inflation. Tissue Elasticity. Ed. by J. W. Remington, Am. Physiol. Soc., 154-167.

Fick, R. 1904 Handbuch der Anatomie und Mechanik der Gelenke. Verlag G. Fischer, Jena.

Fischer, G. M. and J. G. Llaurado 1966 Collagen and Elastic Content in Canine Arteries Selected from Functionally Different Vascular Beds. Circulation Research, 19: 394-399.

Flexner, L. B., J. H. Clark and L. H. Weed 1932 The Elasticity of the Dural Sac and Its Contents. Am. Jr. Physiol., 101: 292-303.

Flory, P. J. 1956 Role of Crystallization in Polymers and Proteins. Science, 124(3211): 53-60.

Franke, E. 1949 The Mechanical Impedance of the Surface of the Human Body. JASA, 21: 55.

Franke, E. K. 1951 Mechanical Impedance of the Surface of the Human Body. Journal of Applied Physiol., 3: 582-590.

Frankel, V. H. and A. H. Burstein 19 Viscoelasticity of Biological Materials.

Fraser, T. M. 1968 Storage of Biological Samples. Aerospace Medicine, 39(2): 146-152.

Fraser, W. G. 1966 What is Known About the Physiology of Large Blood Vessels. ASME, Biomechanics Sýmposium, New York.

Fríesen, M., M. Mägi, L. Sonnerup and A. Viidik 1969 Rheological Analysis of Soft Collagenous Tissue, Part I: Theoretical Considerations. J. Biomechanics, II(1).

Fry, D. L., D. M. Griggs, and J. C. Greenfield 1964 Myocardial Mechanics; Tension-Velocity-Length Relationships of Heart Muscle. Circulation Research, 14: 73-85.

Fry, P., M. L. R. Harkness and R. D. Harkness 1964 Mechanical Properties of the Collagenous Framework of Skin in Rats of Different Ages. Am. Jr. Physiol., 206: 1425-1429.

Fry, P., M. L. R. Harkness, R. D. Harkness and M. Nightingale 1962 Mechanical Properties of Tissue and of Lathyritic Animals. Jr. Physiol., 164: 77-89.

Fukada, E. 1968 Mechanical Deformation and Electrical Polarization in Biological Substances. Biorheology, 5(3): 199-208.

Fukada, E. and M. Date 1963 Viscoelastic Properties of Collagen Solutions in Dilute Hydrocholoric Acid. Biorheology, 1: 101-109.

Fung, Y. C., B. W. Zweifach and M. Intaglietta 1966 Elastic Environment of the Capillary Bed. Circulation Research, 19: 441-461.

Gadd, C. W., W. A. Lange and F. J. Peterson 1967 Strength of Skin and Its Measurement. Biomechanics Monograph. ASME,184.

Gadd, C. W., F. J. Peterson, and W. A. Lange 1965 Strength of Skin and Its Measurement. ASME Paper 65-WA/HUF-8.

Galante, J. O. 1967 Tensile Properties of Human Lumbar Annulus Fibrosus, Acta Orthop. Scand. Suppl. 100, Kipenhamn.

Gerstenkorn, G. F., A. S. Kobayashi, C. A. Weiderhielm, and R. F. Rushmer 1966 Structural Analysis of an Arteriole by the Direct Stiffness Method. ASME Paper 66-HUF-6, and also in J. Engineering Ind. 88 (Series B), 363-368.

Gibson, F. and R. M. Kenedi 1963 Biomechanics in Plastic Surgery. Am. Col. of Surg. Forum., 14: 478.

Gibson, T., H. Stark and J.H. Evans 1969 Directional Variation in Extensibility of Human Skin in Vivo. J. Biomechanics, II(2).

von Gierke, H. E. 1949 Sound Absorption at the Surface of the Body of Man and Animals, JASA, 21: 55.

von Gierke, H. E., L. Oestreicher, E. K. Franke, H. O. Parrack, and W. W. von Wittern 1952 Physics of Vibrations in Living Tissue. Jr. Appl. Physiol., 4: 886-900.

Glaser, A. A., R. D. Marangoni, J. S. Must, T. G. Beckwith, G. S. Brody, G. R. Walker, and W. L. White 1965 Refinements in the Methods for the Measurement of the Mechanical Properties of Unwounded and Wounded Skin. Med. Ele. Biol. Engng., 3: 411-419.

Goldacre, R. J. 1958 Surface Films, Their Collapse on Compression, the Shapes and Sizes of Cells and the Origin of Life. Surface Phenomena in Chemistry and Biology. Danielli, Pankhurst, and Riddiford eds., Pergamon Press.

Grahams, M. 1967 Mechanical Behavior of Tendon in Vitro. Med. and Biol. Engng. 5: 433-443.

Gratz, C. M. 1931 Tensile Strength and Elasticity Tests on Human Fascia Lata. Jr. Bone and Joint Surg., 13: 334-340.

Gratz, C. M. and S. N. Blackberg 1935 Engineering Methods in Medical Research. Mech. Engineering, 57: 217-220.

Gray, J. A. B. and J. M. Ritchie 1954 Effects of Stretch on Single Myelinated Nerve Fibers. J. Physiol., 124: 84-89.

Gray, W. A. and E. A. Johnson 1967 An Anatomical Evaluation of the Myocardial Length-Tension Diagram. Circulation Research, 21: 33-43.

Gundfest, H. 1936 Effects of Hydrostatic Pressures Upon the Excitability, the Recovery and the Potential Sequence of Frog Nerve. Cold Spring Harbor Symp. Quant. Biol., 5: 179-187.

Guth, E. 1947 Muscular Contraction and Rubber-like Elasticity. N. Y. Academy of Sciences Annals, 47: 738-750.

Gutstein, W. H. 1956 A Generalization of Hooke's Law in Muscle Elasticity. Bulletin of Math. Biophysics, 18: 151-170.

Hallock, P. 1934 Arterial Elasticity in Man in Relation to Age as Evaluated by the Pulse Wave Velocity Method. Arc. Int. Med., 54: 770-798.

Hallock, P. and I. C. Benson 1937 Studies on the Elastic Properties of Human Isolated Aorta. Jr. of Clin. Invest., 16: 595-602.

Hamilton, W. F., J. W. Remington, and P. Dow 1945 The Determination of the Propagation Velocity of the Arterial Pulse Wave. Am. Jr. of Physiol., 144: 521-535.

Hardung, V. 1953 Vergleichende Messungen Der Dynamischen Elastizitat und Uiskositat von Blutgefässen, Kautschuk, und Synthetischen Elastomeren. Helvetica Physiologica et Pharmacologica Acta, 11: 194.

Hardy, R. H. 1951 Observations on the Structure and Properties of the Plantar Calcaneo-Navicular Ligament in Man. Jr. of Anat., 85: 135-139.

Harkness, R. D. 1961 Biological Functions of Collagen, Part VIII. Mechanical Properties of Collagenous Frameworks. Biol. Rev. Camb. Phil. Soc., 36: 427-438.

Harkness, R. D. and M. A. Nightingale 1962 The Extensibility of the Cervix Uteri of the Rat at Different Times of Pregnancy. Jr. Physiol., 160: 214-220.

Harris, E. H., B. R. Bass, and L. B. Walker 1964 Tensile Strength and Stress-Strain Relationships in Cadaveric Human Tendon. Anat. Rec., 148: 289.

Harris, E. H., L. B. Walker, and B. R. Bass 1966 Stress-Strain Studies in Cadaveric Human Tendon and an Anomaly in the Young's Modulus Thereof. Med. and Biol. Engng., 4: 253-259.

Hartree, W. and A. V. Hill 1922 The Heat-Production and the Mechanism of the Veratrine Contraction. Jr. Physiol., 56: 294-300.

________ 1922 The Recovery Heat-Production in Muscle. Jr. Physiol., 56: 367-381.

Hass, G. M. 1942 Elastic Tissue: I. Description of a Method for the Isolation of Elastic Tissue. Arch. of Path., 34: 807-819.

________ 1943 Elastic Tissue: III. Relations Between the Structure of the Aging Aorta and the Properties of the Isolated Aortic Elastic Tissue. Arch. of Path., 35: 29-45.

________ 1944 Types of Internal Injuries of Personnel Involved in Aircraft Accidents. Jr. of Aviation Medicine, 15: 77-84.

________ 1942 Elastic Tissue: II. A Study of the Elasticity and Tensile Strength of Elastic Tissue Isolated from the Human Aorta. Arch. of Path., 34: 971-981.

Herrick, E. H. 1945 Tensile Strength of Tissues as Influenced by Male Sex Hormone. Anat. Rec., 93: 145-149.

Hickman, K. E., et al. 1963 Rheological Behavior of Tissues Subjected to External Pressure. Proc. of the San Diego Symposium for Biomedical Engng., 3: 133-140.

Hiertonn, T. E. and P. Jordan 1956 The Tensile Strength of Canine Aortic Segments. Angiology, 7: 21-26.

Highberger, J. A. 1947 The Structural Stability of the Collagen Fiber in Relation to the Mechanism of Tanning. J. Am. Leather Chemists Assoc., 43: 493-510.

Hildebrandt, J., H. Fukaya, and C. J. Martin Completing the Length-Tension Curve of Tissue. (To be published in J. Biomechanics).

Hill, A. V. 1938 Heat of Shortening and Dynamic Constants of Muscle. Proc. Roy. Soc. Lon., B. 126: 136.

_________ 1953 The 'Instantaneous' Elasticity of Active Muscle, Proc. Roy. Soc. Lon., B, 141: 171-178.

_________ 1922 The Maximum Work and Mechanical Efficiency of Human Muscles, and Their Most Economical Speed. Jr. Physiol., 56: 19-41.

_________ 1926 Muscular Activity. Williams & Wilkins Co., Baltimore.

_________ 1948 The Pressure Developed in Muscle During Contraction, Jr. Physiol., 107: 518-526.

_________ 1950 Mechanics of the Contractile Element of Muscle. Nature, 166(4219): 415-419.

_________ 1949 The Heat of Activation and the Heat of Shortening in a Muscle Twitch. Proc. Roy. Soc. Lon., B, 136: 195-211.

_________ 1949 The Energetics of Relaxation in a Muscle Twitch. Proc. Roy. Soc. Lon. B., 136: 211-219.

_________ 1949 Work and Heat in a Muscle Twitch. Proc. Roy. Soc. Lon., B, 136: 220-228.

_________ 1949 Myothermic Methods. Proc. Roy. Soc. Lon., B, 136: 228-241.

_________ 1953 Chemical Change and Mechanical Response in Stimulated Muscle. Proc. Roy. Soc. Lon., B, 141: 314-320.

_________ 1953 The 'Plateau' of Full Activity During a Muscle Twitch. Proc. Roy. Soc. Lon., B, 141: 498-503.

_________ 1953 A Reinvestigation of Two Critical Points in the Energetics of Muscular Contraction. Proc. Roy. Soc. Lon., B, 141: 503-510.

_________ 1952 The Mechanics of Active Muscle, Proc. Roy. Soc. Lon., B, 141: 104-117.

_________ 1950 The Development of the Active State of Muscle during the Latent Period. Proc. Soc. Lon., B, 137: 320-329.

_________ 1950 A Note on the Heat of Activation in a Muscle Twitch. Proc. Roy. Soc. Lon., B, 137: 330-331.

_________ 1950 The Series Elastic Component of Muscle. Proc. Roy. Soc. Lon., B, 137: 273-280.

Hill, A. V. 1950 Does Heat Production Precede Mechanical Response in Muscular Contraction? Proc. Roy. Soc. Lon., B, 137: 268-273.

_________ 1957 A Discussion on Muscular Contraction and Relaxation: Their Physical and Chemical Basis. Proc. Roy. Soc. Lon., B, 137: 40-87.

_________ 1949 The Onset of Contraction. Proc. Roy. Soc. Lon., B, 136: 242-254.

_________ 1949 The Abrupt Transition from Rest to Activity in Muscle. Proc. Roy. Soc. Lon., B, 136: 399-420.

_________ 1949 Is Relaxation an Active Process? Proc. Roy. Soc. Lon., B, 136: 420-435.

Hill, A. V. and W. Hartree 1937 Thermoelastic Properties of Muscle. Philosophical Transactions of the Roy. Soc. Lon., B, 210: 153.

Hill, T. L. 1957 Statistical Mechanical Models of Elastic Element in Muscle. Tissue Elasticity. Ed. by J. W. Remington, Am. Physiol. Soc., 43-54.

Hinke, J. A. M. 1965 In Vitro Demonstration of Vascular Hyper-Responsiveness in Experimental Hypertension. Circulation Research, 17: 359-371.

Hinke, J. A. M. and M. L. Wilson 1962 Effect of Electrolytes on Contractability of Artery Segments in Vitro. Amer. Journ. of Physiol., 203: 1161-1166.

_________ 1962 A Study of Elastic Properties of a 550-μ Artery in Vitro. Am. Jr. of Physiol., 203: 1153-1160.

Hirsch, C. 1955 The Use of Some Electric Measurements on Biomechanical Phenomena. Acta Orthop. Scand., 24: 184-194.

Hirsch, C. and J. Galante 1967 Laboratory Conditions for Tensile Tests in Annulus Fibrosus from Human Intervertebral Discs. Acta Orthop. Scand., 38: 148-162.

Hirsch, C. and L. Sonnerup 1968 Macroscopic Rheology in Collagen Material. J. Biomechanics, 1(1): 13-18.

Hirsch, W. 1955 Reaction of Intervertebral Discs to Compression Forces. J. Bone Joint Surg., 37A: 1188

Holladay, A. and I. G.Bowen 1963 A Mathematical Model of the Lung for Studies of Mechanical Stress. San Diego Symp. for Bio-Med. Engrg.

Howes, E. L., J. W. Sooy, and S. G. Harvey 1929 The Healing of Wounds as Determined by Their Tensile Strength. JAMA, 92(1): 42-45.

Hsu, F. H. 1968 The Influences of Mechanical Loads on the Form of a Growing Elastic Body. J. Biomechanics, 1(4): 303-311.

Husian, T. 1953 An Experimental Study of Some Pressure Effects on Tissues, with Reference to the Bed-Sore Problem. Jr. of Path. and Bacteriol., 66: 347-358.

Jacobs, H. R. 1963 An Improved Microviscometer for Viscous Biological Liquids. Biorheology, 1: 225-228.

________ 1963 The "Viscosity" of Red Cell Packs. Biorheology, 1: 129-138.

________ 1963 The Deformability of Red Cell Packs. Biorheology, 1: 233-238.

Jacobson, K. H. and R. M. Lollar 1951 Wet Tension Testing Studies as Influenced by Chemical Modifications of Collagen. J. Am. Leather Chemists' Assoc., 46:7-19.

Jamison, C. E., R. D. Marangoni and A. A. Glaser 1967 Viscoelastic Properties of Soft Tissue by Discrete Model Characterization. Amer. Soc. Mech. Engr., Paper No. 67-WA/BHF-1.

________ 1968 Viscoelastic Properties of Soft Tissue by Discrete Model Characterization, J. Biomechanics, 1(1): 33-46.

Janicki, J. S. and D. J. Patel 1968 A Force Gauge for Measurement of Longitudinal Stresses in a Blood Vessel In Situ. J. Biomechanics, 1(1): 19-21.

Jansson, F. and E. Sundmark 1961 Determination of the Velocity of Ultrasound in Ocular Tissues at Different Temperatures. Acta Ophtal., 39: 899.

Jewell, B. R. and D. R. Wilkie 1958 An Analysis of the Mechanical Components in Frog's Striated Muscle. Jr. Physiol., 143: 515-540.

Johns, R. J. and V. Wright 1962 Relative Importance of Various Tissues in Joint Stiffness. Jr. Appl. Physiol., 17: 824-828.

________ 1964 An Analytical Description of Joint Stiffness. Biorheology, 2: 87-95.

Jokinen, T. 1958 Tensile Strength of the Wholethickness Skin Graft Used as Replacement of Tendon and Ligament Defects. Acta Orth. Scand. Suppl. 36, 1-84.

Jordan, H. J. 1938 Viscosity Effects in the Living Protoplasm and in Muscles. Ch. 6 in Second Report on Viscosity and Plasticity; Amsterdam, Noord-Hollandsche Uit, 214-256.

Katake, K. 1961 Studies on the Strength of Human Skeletal Muscles. JKPMU, 69: 463-483.

Keatinge, W. R. 1966 Electrical and Mechanical Response of Vascular Smooth Muscle to Vasodilator Agents and Vasoactive Polypeptides. Circulation Research, 18: 641-649.

Kenedi, R. M. 1964 Bio-engineering Studies of the Structural Components of the Human Body. The Structural Engineer, 43(3): 101-109.

Kenedi, R. M., T. Gibson and M. Abrahams 1963 Mechanical Characteristics of Skin and Cartilage. Human Factors, 5: 525-529.

Kenedi, R. M., T. Gibson and C. H. Daly 1965 Bioengineering Studies of the Human Skin - II. Proc., Symp. on Biomechanics and Related Bioengineering Topics ,Ed. by R.M. Kenedi, 147-158.

_________ 1965 The Determination of Significance and Application of Biomechanical Characteristics of Human Skin. Digest of the 6th Int. Conf. on Med. Elec. and Biol. Eng., Tokyo, 531-534.

Kerry, R. L. 1961 Mobility of the Skin and Subcutaneous Tissue of the Face; Their Anatomy and Surgical Importance. Dept. of Anat., The University of Michigan, 1-58.

Kesson, J. E. 1913 The Elasticity of the Hollow Viscera. Quart. Jr. of Exp. Physiol., 6: 355-372.

King, A. L. 1946 Pressure-Volume Relation for Cylindrical Tubes with Elastomeric Walls: The Human Aorta. Jr. Appl. Phys., 17: 501.

King, A. L. 1957 Some Studies in Tissue Elasticity. Tissue Elasticity. Ed. by J. W. Remington, Am. Physiol. Soc., 123-130.

King, A. L. and R. W. Lawton 1948 Elasticity of Body Tissues. Ed. by H. A. Robinson, High-Polymer Physics: A Symp., Brooklyn, Chemical Publishing Co., Inc., 303-316.

_________ 1950 Elasticity of Body Tissues. Medical Physics, II: 303,

_________ 1950 Elasticity of Body Tissues. Med. Phys., III: 234-237.

Kirk, E. and S. A. Kvorning 1949 Quantitative Measurements of the Elastic Properties of the Skin and Subcutaneous Tissue in Young and Old Individuals. Jr. of Gerontol., 4(4): 273-284.

Kjosnes, N. I. 1967 A Technique for the Rapid Determination of Ultrasonic Propagation Velocity in Mammalion Tissues Solids and Liquids. Master's Thesis, Wake Forest College.

Koeneman, J. B. 1966 Viscoelastic Properties of Brain Tissue. MSE Thesis, Case Inst. of Tech., 1-83.

Koeneman, J. B., O. Lindan, J. B. Reswick, and R. H. Scanlan 1967 Viscoelastic Properties of Brain Tissue. Seventh International Conf. on Medical and Biological Engineering; Stockholm.

Krause, H. W. and K. O. Langs 1963 The Non-Linear Behavior of Bio-Medical Systems. ASME Paper No. 63-WA-278.

Krogman, W. M. 1941 The Nervous System. A Bibliography of Human Morphology, 1914-1939, U. of Chicago Press, 185-197.

Kubo, K., K. Nose, and K. Shono 1959 Study on the Tear Test of the Soft Tissues. JKPMU, 66(3): 466-469.

LaBan, M. M. 1962 Collagen Tissue: Implications of Its Response to Stress In Vitro. Arch. Phys. Med. Rehabil., 43: 461-466.

Landowne, M. 1951 A New Method for the Study of Vessel Characteristics; Pressure-Distensibility Relationship of Human Arteries. Fed. Proc. 10: 78.

__________ 1957 Pulse Wave Velocity as an Index of Arterial Elastic Characteristics. Tissue Elasticity. Ed. by J. W. Remington. Am. Physiol. Soc., 168-176.

Landsineer, J. M. F. 1955 Anatomical and Functional Investigations on the Articulation of the Human Finger. Acta Anat., Suppl. 24, 2 ad., 25: 1-69.

Landsineer, J. M. F. and C. Long 1965 The Mechanism of Finger Control Based on Electromyograms and Location Analysis. Acta Anat., 60: 330-347.

Lawton, R. W. 1955 Measurements on the Elasticity and Damping of Isolated Aortic Strips of the Dog. Cir. Res., 3: 403-408.

__________ 1957 Some Aspects of Research in Biological Elasticity. Tissue Elasticity. Ed. by J. W. Remington. Am. Physiol. Soc., 1-11.

Learoyd, B. M. and M. G. Taylor 1966 Alterations with Age in the Viscoelastic Properties of Human Arterial Walls. Cir. Res., 18: 278-292.

Lee, J. S., W. G. Frasher, and Y. C. Fung 1967 Two-Dimensional Finite Deformation Experiments on Dog's Arteries and Veins. Rept. No. AFOSR 67-1980, Bioengineering, Univ. Calif. San Diego.

LeGros, C. W. E. 1965 The Tissues of the Body. Oxford Claredon Press, 5th Ed.

Lindsay, W. K. and H. G. Thomson 1960 Digital Flexor Tendons: An Experimental Study Part I. Br. Jr. of Plas. Surg., 12: 289-316.

Lissner, H. R. 1965 The Response of the Human Body to Impact. Biomechanics and Related Bio-Engineering Topics. Ed. by R. M. Kenedi. Pergamon Press, London, 135-144.

Lissner, H. R. and E. S. Guidjian 1966 A Study of the Mechanical Behavior of the Skull and Its Contents when Subjected to Injuring Blows. SESA 3:40.

Long, C. and M. E. Brown 1964 Electromyographic Kinesiology of the Hand: Muscles Moving the Middle Finger. J. Bone Jt. Surg., 46A: 1683-1706.

Long, C., D. Thomas, and W. J. Crochetiere 1964 Viscoelastic Factors in Hand Control. Proc. 4th Int. Cong. Phys. Med. Excerpta Medica International Congress, Series No. 107, 440-445.

Lorkovic, H. 1966 Influence of Change in pH on the Mechanical Activity of Cardiac Muscle. Cir. Res., 19: 711-720.

Lowy, J. and B. M. Millman 1962 Mechanical Properties of Smooth Muscles of Cephalopod Molluscs. Jr. Physiol., 160: 353-363.

Ludwig, G. 1950 The Velocity of Sound Through Tissues and the Acoustic Impedance of Tissues. JASA, 22: 862.

Lundevall, J. 1964 Traumatic Rupture of the Aorta. Acta Path. et Microbiol. Scand., 62: 29-33.

_________ 1964 The Mechanism of Traumatic Rupture of the Aorta. Acta Path. et Microbiol. Scand., 62: 34-36.

Mac Conail, M. A. 1951 The Mechanical Structure of Articulating Cartilage. J. of Bone and Joint Surgery, 33-B(2).

McCutchen, C. W. 1965 A Note Upon Tensile Stresses in the Collagen Fibers of Articular Cartilage. Med. Electron, Biol. Eng., 3: 447.

McElhaney, J. H. 1966 Dynamic Response of Bone and Muscle Tissue, Jr. Appl. Physiol., 21: 1231-1236.

McElhaney, J. H. and E. F. Byars 1965 Dynamic Response of Biological Materials. ASME Paper 65-WA/HUF-9.

McMaster, P. E. 1933 Tendon and Muscle Ruptures. Jr. Bone and Joint Surg., 15: 705-722.

Mao, T. J. and W. T. Roddy 1950 The Dry Strength of Collagen Fiber Aggregates as Influenced by Tanney Processes, J.Am.Leather Chemists'Assoc., 45:131-138.

Marangoni, R. D., A. A. Glaser, J. S. Must, G. S. Brody, T. G. Beckwith, G. R. Walker, and W. L. White 1966 Effect of Storage and Handling Techniques on Skin Tissue Properties. N. Y. Academy of Sciences, Annals, 136(16): 439-454.

Marangoni, R. D., J. S. Must, G. S. Brody, et. al. 1965 Apparatus Designed to Produce Uniform Experimental Wounds. Med. Elect. Biol. Engng., 3: 407-409.

Mathur, P. D., J. R. McDonald, and R. K. Ghormley 1949 A Study of the Tensile Strength of the Menisci of the Knee. Jr. Bone and Joint Surg., 31A(3): 650-654.

Matsuo, Y., T. Uehira, and K. Kubo 1963 Study on the Partial Differences of Mechanical Strength of Aortic Wall in Dog. JKPMU, 63:417-420.

Matthews, L. S. and D. Ellis 1968 Viscoelastic Properties of Cat Tendon: Effects of Time After Death and Preservation by Freezing. J. Biomech., 1: 65-71.

Mela, M. J. 1967 Elastic-Mathematical Theory of Cells and Mitochondria in Swelling Process. I. The Membranous Stresses and Modulus of Elasticity of the Egg Cell to Sea Urchin. Biophys. Jour., 7: 95-110.

Mendoza, S. A. and R. A. Milch 1964 Tensile Strength of Skin Collagen. Surg. Forum, 15: 433-434.

Merrill, E. W. and G. A. Pelletier 1967 Viscosity of Human Blood: Transition from Newtonian to Non-Newtonian. J. of Appl. Physiol., 23(2): 178-182.

Meryman, H. T. 1956 Mechanics of Freezing in Living Cells and Tissues. Science, 124(3221): 515-521.

Meyer, V. H. 1873 Statik Und Mechanik des Menschlichen Knochengeruitez. Leipzig, 222.

Milch, R. A. 1966 Some Topological Properties of Carbohydrate-Plasticized Collagen Matrices. Biorheology, 3: 107-116.

________ 1966 Polymer-Diluent and Certain Other Effects of Solvent Environment on the Thermal Shrinkage (Contraction) and Tensile Strength Properties of Native Calfskins. Biorheology, 3: 97-106.

Milch, R. A., L. J. Frisco, and E. A. Szymkowiak 1966 Solid State Dielectric Properties of Aldehydetrated Goatskin Collagen. Biorheology, 3: 9-20.

Mochizuki, T. 1958 On the Tension Test Made Upon the Wall of the Thoracic Aorta in Animals. JKPMU, 63: 103-106.

Nachemson, A. 1963 The Influence of Spinal Movements on the Lumbar Intradiscal Pressure and on the Tensile Stresses in the Annulus Fibrosus. Acta Orthop. Scand., 33: 183-207.

________ 1966 The Load on Lumbar Discs in Different Positions of the Body. Clin. Orthop., 45: 107-122.

________ 1968 Some Mechanical Properties of the Third Human Lumbar Interlaminar Ligament (Ligamentum flavum). J. Biomech., 1(3): 211-220.

Narumiya, S. and I. Asami 1960 Strength of Human Spinal Dura Mater. JKPMU, 68: 1371-1376.

Nickerson, J. L. and M. Drazic 1964 Young's Modulus and Breaking Strength of Body Tissues. Aerospace Medical Research Labs. Tech. Doc. Rpt., 64-23: 1-11.

Nubar, Y. 1962 Stress-Strain Relationship in Skeletal Muscle. Annals, N. Y. Academy of Sciences, 93: 857-876.

Nunley, R. L. 1958 The Ligamenta Flava of the Dog. A Study of Tensile and Physical Properties. Am. J. Phys. Med., 37: 256-268.

Oda, K. 1952 Study on the Bursting Test of a Rabbit's Viscera and Tissues. JKPMU, 50: 447-464.

Ogawa, Y. and S. Narumiya 1959 Examination on the Shearing Strength of Various Organs and Tissues. JKPMU, 66: 800-806.

Ohara, T. 1953 On the Comparison of Strengths of the Various Organ-Tissues. JKPMU, 53: 577-597.

Ohnishi, T. 1963 Rheology of Glycerinated Muscle Fibers. Biorheology, 1: 83-90.

Okamoto, T. 1955 Study on Strength of Peripheral Nerve Tissue of Human Beings and Various Animals. JKPMU, 58: 1007-1029.

Ommaya, A. K. 1968 Mechanical Properties of Tissues of the Nervous Systems. Jr. of Biomech., 1(2): 127-138.

Opatowski, I. 1967 Elastic Deformations of Arteries. J. of Appl. Physiol., 23(5): 772-778.

Oya, H. 1960 Examination on the Effects of the Conditions of Materials to the Strength Test of Tissues. JKPMU, 67: 1337-1338.

Papazian, H. S. The Response of Linear Viscoelastic Materials in the Frequency Domain. Eng. Exp. Sta. Bulletin 192, Ohio St. Univ., Columbus, Ohio.

Parmley, W. W. and E. H. Sonnenblick 1967 Series Elasticity in Heart Muscle: Its Relation to Contractile Element Velocity and Proposed Muscle Models. Cir. Res., 20: 112-123.

Parrack, H. O., H. von Gierke, H. Oestreicher, and W. W. von Wiltern 1950 Absorption of Vibratory Energy by Human Body Surface. Amer. Physiol. Soc., 4: 97-98.

Partington, F. R. 1964 Studies on Physical Properties of Tendon Fibres. PhD Thesis, U. of Manchester.

Patel, D. J. and D. L. Fry 1966 Longitudinal Tethering of Arteries in Dogs. Cir. Res., 19: 1011-1021.

__________ 1968 Static Anisothropic Elastic Properties of Large Blood Vessels in Living Dogs. Brit. Soc. of Rheol. Mtg., London. With technical assistance of J. S. Janicki.

Peerless, S. J. and N. B. Rewcastle 1967 Shear Injuries of the Brain. Canadian Med. Assoc., Jr., 96(10): 577-582.

Peterson, L. H. 1962 Properties and Behavior of the Living Vascular Wall. Physiol. Reviews, Suppl. 5. 42: 309.

Peterson, L. H., R. E. Jensen and J. Parnell 1960 Mechanical Properties of Arteries In Vivo. Circul. Res., 8: 622-639.

Peterson, L. H. and R. B. Shepard 1955 In Vivo Determination of Arterial Distensibility and Viscous Resistance in Dogs. Fed. Proc., 14: 114.

Pfeiffer, H. H. 1963 Zur Analyse der Fliess-Elastizitat Durch Spinnversuche am Corpus Vitreus. Biorheology, 1: 111-117.

Pick, J. C. 1951 The Tension and Resistance to Stretching of Human Skin and Other Membranes with Results from a Series of Normal and Oedermatous Cases. J. Physiol., 112: 102-113.

Plazek, D. J., M. N. Vrandsen, and J. W. Berge 1958 A Torsion Pendulum for Dynamic and Creep Measurements of Soft Viscoelastic Materials. Trans. of the Soc. of Rheology, II: 39-51.

Pryor, M. G. M. 1950 Mechanical Properties of Fibers and Muscles. Prog. Biophys. and Biophys. Chem., I: 216-268.

Radford, E. P. 1957 Recent Studies of Mechanical Properties of Mammalian Lungs. Tissue Elasticity. Ed. by J. W. Remington. Am. Physiol. Soc., 177-190.

Ramsey, R. W. and S. F. Street 1940 The Isometric Length-Tension Diagram of Isolated Skeletal Muscle Fibers of the Frog. Jr. of Cellular and Comparative Physiol., 15: 11-34.

Reichel, H. 1952 Muscle Elasticity. Ergebnisse Der Physiologie, 47: 469.

Remington, J. W. 1955 Hysteresis Loop Behavior of the Aorta and Other Extensible Tissues. Am. Jr. Physiol., 180: 83-95.

________ 1957 Extensibility Behavior and Hysteresis Phenomena in Smooth Muscle Tissue. Tissue Elasticity. Ed. by J. W. Remington. Am. Physiol. Soc., 138-153.

Renk, F. and E. Wohlisch 1939 The Thermoelastic Anomaly of Skeletal Musculature and the Static Kinetic Theory of Rubber-Like Elasticity. Pflüger's Arch. für. Physiologie, 243: 110.

Reutervall, O. P. P. 1921 Ober die Elastizitat der Gefabwande und die Methoden Ihrer Nahren Prufung. (On the Elasticity of Vessel Walls and the Methods of Their More Detailed Explanation). Acta Med. Scand., Suppl. 2.

Rhodin, J. A. G. 1967 The Ultrastructure of Mammalian Arterioles and Precapillary Sphincters. Jr. of Ultrastructure Res., 17.

Rich, A. 1961 The Molecular Structure of Collagen. Jr. Mol. Biol., 3: 483-506.

Richard, K. 1962 Determination of the Mechanical Properties of High Polymers at High Speeds of Testing. Jr. of Polymer Science, 58: 71-84.

Ridge, M. D. and V. Wright 1964 The Description of Skin Stiffness. Biorheology, 2: 67-74.

________ 1966 The Directional Effects of Skin. Jr. of Investigative Dermatology, 46(4): 341-346.

________ 1965 An Engineering Study of Human Skin. Engineering, 199: 363-364.

________ 1966 An Extensometer for Skin; Its Construction and Application. Med. and Biol. Engng., 4: 533-542.

________ 1966 Mechanical Properties of Skin: A Bioengineering Study of Skin Structure. Jr. Appl. Physiol., 21: 1602-1606.

Ridge, M. D. and V. Wright 1965 A Rheological Study of Skin. Biomechanics and Related Bio-Engineering Topics, Ed. by R. M. Kenedi. Pergamon Press, London. 165-175.

_________ 1965 The Rheology of Skin (A bio-engineering study of the mechanical properties of skin in relation to its structure). Brit. Jr. of Dermatol., 77: 639-649.

Rigby, B. J. 1964 Effect of Cyclic Extension on the Physical Properties of Tendon Collagen and Its Possible Relation to Biological Aging of Collagen. Nature, 202: B-2.

Rigby, B. J., N. Hirai, J. D. Spikes and H. Eyring 1959 The Mechanical Properties of Rat Tail Tendon. Jr. Gen. Physiol., 43: 265-283.

Roach, M. R. and A. C. Burton 1957 The Reason for the Shape of the Distensibility Curves of Arteries. Canadian Jr. Biochem. and Physiol., 35: 681-690.

Rosenblueth, A., B. R. Alvarez and R. J. Garcia 1953 The Response of Axons to Mechanical Stimuli. Acta Physiol. Latinoam., 3: 204-215.

Rosenflack, P. and F. Buchthal 1955 Contraction Disappearance in Muscle in Light of Transmutation Theory. Pflüger's Arch., 260: 197-209.

Roy, C. S. 1880 The Elastic Properties of the Arterial Wall. Jr. of Physiol., 3: 125-159.

Sandblom, P. 1944 The Tensile Strength of Healing Wounds. Acta Chirurgica Scandinavia, Suppl. 89, 1-108.

Sandblom, P., P. Peterson, and A. Muren 1953 Determination of the Tensile Strength of the Healing Wound as a Clinical Test. Acta Chirurgica Scandinavia, 105: 253.

Saunders, D. W. 1965 Large Deformations in Amorphous Polymers. Biomechanics and Related Bioengineering Topics. Ed. by R. M. Kenedi. Pergamon Press, London.

Schneider, D. 1952 Die Dehnbarkeit der Markhaltigen Nervenfoser des Frosches in Abhangigkeit von Funklion und Struktar. Z. Naturf., 76: 38-48.

Schottelius, B. A. Stiffness and Stretch Relocation in Shortened Skeletal Muscle. Am. J. Phys. Med., 36-57.

Shim, S. S., D. H. Copp and F. P. Patterson 1967 An Indirect Method of Bone Blood-Flow Measurement Based on the Bone Clearance of Circulating Bone-Seeking Radioisotope. Reprint from J. of Bone and Joint Surg., 49-A(4): 693-702.

Sichel, F. J. M. 1934 The Elasticity of Isolated Resting Skeletal Muscle Fibers. Jr. of Cellular and Comparative Physiol., 5(1): 21-42.

Silver, P. H. S. 1954 Direct Observations of Changes in Tension in the Supraspinous and Spinous Ligaments During Flexion and Extension of the Vertebral Column in Man. J. Anat., 88: 550.

Simonson, E., A. Snowden, A. Kerp, and J. Brozek 1948 Measurement of Elastic Properties of Skeletal Muscle In Situ. J. Appl. Physiol., 1: 512-525.

Smith, J. W. 1954 The Elastic Properties of the Anterior Cruciate Ligament of the Rabbit. Jr. of Anat., 88: 369-379.

Snyder, R. D. (To Be Published) The Thermo-Mechanical Structure of Constitutive Equations for Rate-Sensitive Materials. Jr. of Biomechanics, 1-15.

Sokoloff, L. 1966 Elasticity of Aging Cartilage. Fed. Proc., 25(3).

________ 1963 Elasticity of Articular Cartilage: Effects of Ions and Viscous Solutions. Science, 141: 1055-1057.

Sonnenblick, E. H. 1962 Force-Velocity Relations in Mammalian Heart Muscle. Amer. Jr. Physiol., 202: 931.

________ 1962 Implications of Muscle Mechanics in the Heart. Fed. Proc., 21: 975.

________ 1964 Series Elastic and Contractile Elements in Heart Muscle: Change in Muscle Length. Am. Jr. Physiol., 207: 1330-1338.

Sonoda, T., K. Yoshikawa, and S. Ibuki 1962 Examination of the Shearing and Punching Strength of Human Cerebral and Spinal Dura Mater. JKPMU, 71: 703-709.

Speckmann, E. W. and R. K. Ringer 1966 Volume-Pressure Relationships of the Turkey Aorta. Canadian Jr. of Physiol. and Pharmacol., 44: 901-907.

Stacy, R. W. 1957 Reaction Rate Kinetics and Some Tissue Mechanical Properties. Tissue Elasticity. Ed. by J. W. Remington. Am. Physiol. Soc., 131-137.

Stacy, R. W., D. T. Williams, R. E. Worden, R. O. McMorris, and O. Glasser 1955 Essentials of Biological and Medical Physics. McGraw-Hill, N. Y.

Strasser, H. 1908 Lehrbuch der Muskel, und Gelenkmechanik. Springer, Berlin.

Stuke, K. 1950 The Elasticity of the Achilles Tendon in Loading Experiments. Langebeck Arch. Klin. Chir., 265(5): 579-599.

________ 1951 Tendon Loads and Rupture in Animal Experiments. Chirurg., 22: 16.

Sunderland, S. and K. C. Bradley 1961 Stress-Strain Phenomena in Human Peripheral Nerve Trunks. Brain, 84: 102-119, 120-124, 125-217.

________ 1961 Stress-Strain Phenomena in Human Spinal Nerve Roots. Brain, 84: 120-124.

Supnik, R. H. 1962 Rate Sensitivity: Its Measurement and Significance. Mat. Res. Stand., 2: 498-500.

Takigawa, M. 1953 Study Upon Strength of Human and Animal Tendons. JKPMU, 53: 1-19.

Tannenbaum, I. and J. A. Ferguson 1948 Rapid Deceleration and Rupture of the Aorta. Arch. Path., 45: 504-506.

Tasaki, I. and C. S. Spyropoulos 1957 Influence of Changes in Temperature and Pressure on the Nerve Fiber. The Influence of Temperature on Biological Systems. Ed. by S. S. Johnson. Waverly Press, Baltimore 201-220.

Taylor, M. G. 1966 Use of Random Excitation and Spectral Analysis in the Study of Frequency-Dependent Parameters of the Cardiovascular System. Cir. Res., 18: 585-595.

Thomas, D. H., C. Long and J. M. F. Landsineer 1968 Biomechanical Considerations of Lumbricalis Behavior in the Human Finger. J. Biomech., 1(2): 107-115.

Thurlow, S. J. 1963 Impact Tests on Human Occipital Scalp Material. Brit. Jr. of Exper. Pathol., 64(5): 538-545.

Tickner, E. G. and A. H. Sach 1964 Theoretical and Experimental Study of the Elastic Behavior of the Human Brachial and Other Human and Canine Arteries. Vidya Rpt., Palo Alto., 162.

Toridis, T. S., R. S. Ledley and H. K. Huang 1967 Mechanical Effects. National Biomedical Research Foundation, Silver Springs, Maryland. Annual. Conf., Bioengineering in Medicine and Biology.

Tregear, R. T. 1966 Physical Functions of Skin. London, Academic Press.

Triepel, H. 1902 Einführung in die Physikalische Anatomie. I. Teil: Allgemeine Elasticitäts - und Festigkeitslehre in Elementarer Darstellung. II.Teil: Die Elasticität und Festigkeit der Menshlichers Gervebe und Organe. Wiesbaden, Bergmann Verlag.

Troup, J. D. G. and A. F. Chapman 1969 The Strength of the Flexor and Extensor Muscles of the Trunk. J. Biomechanics, II(1).

Van Brocklin, J. D. and D. G. Ellis 1965 A Study of the Mechanical Behavior of Toe Extensor Tendons Under Applied Stress. Arch. of Physical Medicine and Rehabilitation, 46: 369-373.

Von Hardung, V. 1952 Über eine Methode zur Messung der dynamischen Elastizitat und Viskosität Kautschukahnlicher Korper, insbesondere von Blutgefaben und anderen elastischen Gewebeteilen. Helv. Physiol. Acta, 10: 482-498.

Veronda, D. R. and R. A. Westmann (To Be Published) Mechanical Characterization of Skin - Finite Deformations. J. Biomechanics.

Viidik, A. 1966 Biomechanics and Functional Adaption of Tendons and Joint Ligaments. Studies on the Anatomy and Function of Bone and Joints. Ed. by F. G. Evans. Heidleberg, 17-35.

________ 1968 Elasticity and Tensile Strength of the Anterior Cruciate Ligament in Rabbits as Influenced by Training. Acta Physiol. Scand. In Press.

________ 1967 Experimental Evaluation of the Tensile Strength of Isolated Rabbit Tendons. Biomedical Engineering, 2: 64-67.

________ 1968 A Rheological Model for Uncalcified Parallel-Fibred Collagenous Tissue. J. Biomechanics, 1: 3-11.

Viidik, A. and T. Lewin 1966 Changes in Tensile Strength Characteristics and Histology of Rabbit Ligaments Induced by Different Modes of Postmortal Storage. Acta Orthop. Scand., 37: 141-155.

Viidik, A. and M. Mägi 1967 Visco-Elastic Properties of Ligaments. Digest, 7th Int. Conf. Med. Biol. Engng. Ed. by B. Jacobson. Almqvist-Wiksell, Stockholm. 507.

Viidik, A., L. Sandquist and M. Mägi 1965 Influence of Postmortal Storage on Tensile Strength Characteristics and Histology of Rabbit Ligaments. Acta Orthop. Scand., Suppl. 79, 1-38

Walker, L. B. and E. H. Harris 1964 An Instrument for the Measurement of Cross-sectional Area of Small, Flaccid, Moist Fibrous Bundles (e.g. tendon). Anat. Rec., 148: 407-408.

Walker, L. B., E. H. Harris and J. V. Benedict 1964 Stress-Strain Relationship in Human Cadaveric Plantaris Tendon: A Preliminary Study. Med. Electron. Biol. Engng., 2: 31-38.

Wertheim, M. G. 1847 Mémoire sur l'Elastiaté et le Adhesion des Principaux Tissues de Corps Humain. Annls. Chim. Phys., 21: 385-414.

White, W. L. and N. L. Buck 1965 The Standardization of Testing Methods in Wound Healing. Terminal Prog. Rept., NIH Grant No. GM-11066-01-02.

Wiederhielm, C. A. 1965 Distensibility Characteristics of Small Blood Vessels. Fed. Proc., 24(5): Part I, 1075-1084.

Wiederhelm, C. A., A. S. Kobayashi, D. D. Stromberg, and S. L. Y. Woo 1968 Structural Response of Relaxed and Constricted Arterioles. J. Biomech., 1(4).

Wilkie, D. R. 1956 The Mechanical Properties of Muscle. Brit. Med. Bull., 12(3): 177-182.

________ 1950 The Relation Between Force and Velocity in Human Muscle. Jr. Physiol., 110: 249-280.

Wood, G. C. 1954 Some Tensile Properties of Elastic Tissue. Biochem. Biophys., 15: 331.

Wright, D. G. and D. C. Rennels 1964 A Study of the Elastic Properties of Plantar Fascia. Jr. of Bone and Joint Surg., 46-A(3): 482-492.

Wright, V. and R. J. Johns 1960 Physical Factors Concerned with Stiffness of Normal and Diseased Joints. Bull. Johns Hopkins Hospt., 106: 215-231.

Wylie, E. B. 1966 Flow Through Tapered Tubes with Nonlinear Wall Properties. Civil Engineering Department, The University of Michigan, Ann Arbor, Michigan. 82-95.

Yamada, H. 1963 Human Biomechanics. Kyoto Press, Kyoto, Japan.

Yamaguchi, T. 1960 Study on the Strength of Human Skin. JKPMU, 67: 347-379.

Yorra, A. J. 1963 The Investigation of the Structural Behavior of the Intervertebral Disc. Master's Thesis, MIT.

Yoshida, T. and I. Bessho 1959 Comparison of the Strength of the Organs Composed of the Different Kinds of Principal Tissue. JKPMU, 66: 836.

Yuganov, E. M. et al. 1963 Muscle Tonus Under Conditions of Weightlessness. NASA, TT F-131.

Zarek, J. M. 1966 Dynamic Considerations in Load Bearing Bones with Special Reference to Osteosynthesis and Articular Cartilage. Heidelberg. 40-51.

__________ 1965 Dynamics Considerations of the Human Skeletal System. Biomechanics and Related Bio-Engineering Topics. Ed. by R. M. Kenedi. Pergamon Press, London. 187-203.

Zarek, J. M. and J. Edwards 1963 The Stress-Structure Relationship in Articular Cartilage. Med. Electron. Biol. Engng., 1: 497-507.

__________ 1965 A Note on the Stress-Structure Relationship in Articular Cartilage. Med. Electron. Biol. Engng., 3: 449-450.

Zatzman, M., R. W. Stacy, J. Randall and A. Eberstein 1954 Time Course of Stress Relaxation in Isolated Arterial Segments. Am. Jr. Physiol., 117: 299-302.